FT-IR and MAS NMR Analysis of Montmorillonite K10 Supported MF_2 reagents and their Activity as Catalysts

BY

FATHI M. ASSEID (BSc. Hons.)

A thesis
submitted to the Department of Chemistry
in partial fulfillment of the requirements
of the degree of Master of Science

October 1991
Brock University
St.Catharines, Ontario

Abstract

ZnF_2, CdF_2, and CuF_2 have been adsorbed onto the surface of montmorillonite K10, and the infrared and ^{19}F, ^{27}Al, and ^{29}Si MAS NMR spectra of the reagents over a range of loadings have been obtained. CuF_2 was observed to attack the SiO_2 layer and form the complex $CuSiF_6$, ZnF_2 tends to attack the aluminium oxide layer, in which Zn isomorphously replaces Al, and forms AlF_3 and AlF_4^- complexes. All the spectroscopic evidence ruled out the formation of any Al-F and/or Si-F free species as CdF_2 is adsorbed on the surface of montmorillonite K10. The reactivity of MF_2-K10 reagents towards Friedel-Crafts benzylation of benzene with benzyl chloride varied from one reagent to another. ZnF_2-K10 was observed to be the most reactive and CuF_2 was the least reactive.

Acknowledgements

The author of this work would like to thank his supervisor, Dr. Jack M. Miller for all of his advice and patience throughout the program. The author would also like to thank Dr. J. S. Hartman and Dr. E.A. Cherniak for their help and advice whenever needed. Thanks go to Dr. J.H. Clark and Dr. A.P. Kybett for their attention and advice regarding this project. The author is also grateful to T.R.B Jones and D. Vukmanic for their technical assistance with the NMR and IR instrument, and Dr. B. Sayer for his assistance with the Bruker AM-500 NMR instrument.

The author would like to thank his parents for their continued support and encouragement throughout his years of study. Thanks also go to the colleagues in the inorganic and analytical chemistry laboratory who made it possible for this project to proceed undisturbed.

Table of Contents

Page

INTRODUCTION.....1

I. Catalytic Metal Oxides.....1

I-1. Alumina and alumina supported reagents.....1

a. Alumina supported reagents.....2

b. Alumina supported alkali metal fluorides.....3

I.2. Silica and silica supported reagents.....4

a. Silica supported reagents.....5

b. Silica supported fluorides.....5

I-3. Aluminosilicates.....7

a. Zeolites.....7

a-1. Fluorinated zeolites.....10

b. Clays.....11

II. Montmorillonite K10.....12

II-1. Structural analysis.....12

II-2. Supported montmorillonite catalysts.....13

II-3. Montmorillonite K10 supported alkali metal fluorides.....16

II-4. Reactivity of montmorillonite K10 17

a. Reactivity due to Lewis acid

centres on mont. K10.....18

b. Reactivity due to Bronsted acid

centres on mont. K10.....23

III. Characterization of metal oxide and metal oxide supported reagents.....23

a. Infrared spectroscopy.....24

b. NMR spectroscopy.....25

IV. Magic-Angle Spinning (MAS) NMR.....27

a. Theoretical aspects.....28

b. ^{19}F MAS NMR spectral features.....31

V. Aim of this work.....35

EXPERIMENTAL.....36

I. Reagent preparation.....36

a. ZnF_2-montmorillonite K10.....36

b. CuF_2-montmorillonite K10.....37

c. CdF_2-montmorillonite K10.....37

II. Instrumentation.....38

a. Nuclear Magnetic Resonance (NMR) Spectroscopy.....38

b. Fourier Transform Infrared (FT-IR) Spectroscopy.....41

III. Friedel-Crafts Alkylation.....41

a. Benzylation of benzene with benzyl chloride.....41

b. Benzylation of benzene with paraformaldehyde.....42

RESULTS AND DISCUSSION......43

I.1. ZnF_2 supported montmorillonite K10.(ZnF_2-K10).....43

a. FT-IR Spectroscopy.....43

b. ^{19}F MAS NMR Spectroscopy.....44

c. ^{29}Si MAS NMR Spectroscopy.....45

d. ^{27}Al MAS NMR Spectroscopy.....46

e. Friedel-Crafts alkylation.....47

f. Discussion.....49

I.2. CdF_2 supported montmorillonite K10.(CdF_2-K10).....63

a. FT-IR Spectroscopy.....63

b. ^{19}F MAS NMR Spectroscopy.....64

c. ^{29}Si MAS NMR Spectroscopy.....65

d. ^{27}Al MAS NMR Spectroscopy.....66

e. Friedel-Crafts alkylation.....67

f. Discussion.....68

I.3. CuF_2 supported montmorillonite K10.(CuF_2-K10).....81

a. FT-IR Spectroscopy.....81

b. ^{19}F MAS NMR Spectroscopy.....82

c. ^{29}Si MAS NMR Spectroscopy.....83

d. ^{27}Al MAS NMR Spectroscopy.....84

e. Friedel-Crafts alkylation.....85

f. Discussion.....86

I.4. MF_2-silica reagents (M=Zn, Cd, and Cu).....98

a. Infrared spectroscopy.....98

b. 19F MAS NMR spectroscopy.....98

c. Discussion.....99

CONCLUSIONS.....103

REFERENCES.....108

APPENDIX. I.....116

APPENDIX. II.....132

List of Figures Page

(1.1) The layer structure of montmorillonite K10.....14

(1.2a) Elements of the chemical shift tensor.....30

(1.2b) Effect of MAS.....30

(1.2c) Variation of θ from 54°44'.....30

(2.1) MAS NMR probe 40

(3.1) Infrared spectra of ZnF2-K10 reagents dried at 573K.....56

(3.2) Infrared spectra of 6.5 mmol/g ZnF_2-K10 reagents compared to spectra of mixed AlF_6^{3-}andAlF_4^-.....57

(3.3) ^{19}F MAS NMR spectrum of ZnF_2-K10 reagent compared to spectrum of mixed AlF_6^{3-} and AlF_4^-....58

(3.4) 19F MAS NMR spectra of ZnF2-K10 reagents.....59

(3.5) ^{29}Si MAS NMR spectra of ZnF_2-K10 reagents dried at 573K.....60

(3.6) ^{27}Al MAS NMR spectra of ZnF_2-K10 reagents dried at 573K.....61

(3.7) 27Al MAS NMR spectra of ZnF2-K10 dried at 873K.....62

(3.8) Infrared spectra of CdF_2-K10 reagents dried at 573K.....75

(3.9) ^{19}F MAS NMR spectra of 1.0 mmol/g of CdF_2-K10 reagents 76

(3.10) ^{19}F MAS NMR spectra of CdF_2-K10 reagents dried at 873K.....77

(3.11) ^{29}Si MAS NMR spectra Of CdF_2-K10 reagents dried at 573K....78

(3.12) ^{27}Al MAS NMR spectra of 1.0 mmol/g of CdF_2-K10 reagent dried at....79

(3.13) ^{27}Al MAS NMR spectra of 5.0 mmol/g of CdF_2-K10 reagents 80

(3.14) Infrared spectra of CuF_2-K10 reagents dried at 573K....92

(3.15) ^{19}F MAS NMR spectra of CuF_2-K10 reagents....93

(3.16) ^{19}F MAS NMR spectra of 3.5 mmol/g CuF_2-K10 reagents 94

(3.17) ^{29}Si MAS NMR spectra of CuF_2-K10 reagents dried at 573K....95

(3.18) ^{27}Al MAS NMR spectra of 1.0 mmol/g of CuF_2-K10 96

(3.19) ^{27}Al MAS NMR spectra of 5.0 mmol/g of CuF_2-K10 97

(3.20) Infrared spectra of MF_2-silica reagents dried at 373K....100

(3.21) ^{19}F MAS NMR spectra of MF_2-silica reagents dried at 373K....101

(3.22) Infrared spectra of 5.0 mmol/g of MF_2-K10 reagents dried at 573K....102

(AI-1) Infrared spectra of ZnF_2-K10 reagents dried at 873K....117

(AI-2) ^{19}F MAS NMR spectrum of ZnF_2-K10 compared to spectrum of mixed AlF_6^{3-} and AlF_4^-.....118

(AI-3) ^{19}F MAS NMR spectrum of ZnF_2-K10 compared to spectrum of mixed AlF_6^{3-} and AlF_4^-.....119

(AI-4) ^{29}Si MAS NMR spectra of ZnF_2-K10 reagents dried at 873K.....120

(AI-5) ^{29}Si MAS NMR spectra of montmorillonite K10.....121

(AI-6) ^{27}Al MAS NMR spectra of 5.0 mmol/g reagents of ZnF_2-K10 dried at.....122

(AI-7) Infrared spectra of CdF_2-K10 reagents dried at 873K.....123

(AI-8) Infrared spectra of 6.5 mmol/g of CdF2- K10 reagents.....124

(AI-9) ^{19}F MAS NMR spectra of CdF_2-K10 reagents dried at 573K.....125

(AI-10) ^{19}F MAS NMR spectrum of CdF_2-K10 reagent compared to spectrum of CdF_2.....126

(AI-11) ^{29}Si MAS NMR spectra of CdF_2-K10 reagents.....127

(AI-12) Infrared spectra of CuF_2-K10 reagents dried at 873K.....128

(AI-13) Infrared spectra of 6.5 mmol/g of CuF_2-K10 reagents.....129

(AI-14) ^{29}Si MAS NMR spectra of CuF_2-K10 reagents dried at 873K.....130

List of Tables

(2.1) Aquisition parameters used for MAS NMR spectroscopy.....39

(3.1) ^{19}F MAS NMR chemical shifts for ZnF_2-K10 reagents, ZnF_2,and some Al-F species.....53

(3.2) Friedel-Crafts benzylation of benzyl chloride using ZnF2-K10 reagents.....54

(3.3) ^{19}F MAS NMR chemical shifts for CdF_2-K10 reagents, and CdF_2. 72

(3.4) Friedel-Crafts benzylation of benzyl chloride using CdF2-K10 reagents.....73

(3.5) ^{19}F MAS NMR chemical shifts for CuF_2-K10 reagents.....89

(3.6) Friedel-Crafts benzylation of benzyl chloride using CuF2-K10 reagents.....90

(4.1) Electronegativities and Atomic Radii of Zn, Al, Cu,and Cd.....106

(4.2) Friedel-Crafts benzylation of benzene using the following montmorillonite K10 supported reagents.....107

CHAPTER ONE
INTRODUCTION

INTRODUCTION.

I. Catalytic Metal Oxides.

Solid metal oxides are very commonly used as heterogeneous catalysts by organic chemists, because of certain advantages such as reactivity, selectivity, safety and ease of work up. Several common metal oxides such as Na_2O, MgO, SiO_2, and Al_2O_3 have different structural features and defects that help in understanding the reactivity of these oxides[1]. In this section of this chapter I will be discussing some of the structural features of silica gel, alumina, and aluminosilicates. Additionally I will discuss their suitability as solid supports for many inorganic reagents. Further analysis and characterizations of these solid supports and supported reagents improves the understanding of the molecular ingredients of heterogeneous catalysts, thereby allowing us to proceed rationally in the design of new technologies [2,3].

I-1. Alumina and alumina supported reagents

A brief consideration of the structure of Al_2O_3 is in order. Both α- and β-Al_2O_3 are well known. α-alumina (corundum) is in an anhydrous form, it is arranged in a hexagonal close-packed oxygen lattice, whereas β-alumina is believed to have an alternating close-packed lattice and contains sodium, and has the composition $Na_2O.6Al_2O_3$. β-Al_2O_3 is particularly interesting because the oxide layers are close packed, stacked in three dimensions, but every fifth layer has three quarters of its oxygens missing, and so tunnels exist through which

alkali metal ions such as Li^+, Na^+, and K^+ can easily move [1]. The activity of this porous inorganic solid has recently been realized by the general chemical community as useful not only for industrial operations such as petroleum cracking, but also for the many small, laboratory scale, hetrogeneous reactions involving milder conditions, more specific (chemospecific, regiospecific, and stereospecific) transformations, and easier isolation.

Several spectroscopic studies have been performed, for example, infrared studies by Evans and Gracey[7], and Riseman et. al, [8], nuclear magnetic resonance studies by Ripmeester [9], and transmission electron microscopy studies by Miller and Majda [10]. All of these spectroscopic studies of the surface properties of alumina have revealed interesting structural details and a more accurate picture of the interactions between acidic and basic sites on the surface. Several examples have appeared [1], which involve deliberate and planned use of alumina to achieve mild, selective, and convenient organic transformations which are of significant preparative value.

a. Alumina Supported Reagents.

Supported reagents formed by the adsorption of reagent molecules or ions onto the surface of alumina have been successfully applied to a wide variety of organic reactions, and have been shown to have many advantages over unsupported reagents. A number of alkylation reactions such as C-alkylation, O-alkylation , S-alkylation, and N-alkylation have been accomplished using newly developed alumina

supported reagents. Alumina supported KCN was found to be quite useful in the cyanation of benzyl bromide in the presence of ultrasonic irradiation, and in inducing the Friedel-Crafts reaction of benzyl bromide with toluene under mechanical ignitation [11]. Duke and Clark [12] have used infrared analysis to investigate the activity of this supporting reagent, as this study indicated a slight shift in the υ(CN) band, which confirms its strong nucleophlicity.

b. Alumina Supported Alkali Metal Fluorides.

Alkali metal fluorides can behave as strong bases which have found a wide range of applications in organic syntheses [13]. The nucleophilicity of protic compounds can be greatly enhanced by formation of strong hydrogen bonds with the fluoride anion. Miller and Clark [14,15], have reported nucleophilic substitution via hydrogen-bond assistance with alkali metal fluorides. Alkali metal fluoride-alumina reagents have received much attention recently as supported reagents to promote both base-catalyzed and non-catalytic reactions. KF-alumina`s role in base-catalyzed reactions is especially important, for example, in Knoevenagel condensations [16], and the methylation of phenol [17]. The O-methylation of phenol in the presence of alkali metal fluorides impregnated on alumina has been studied by Ando and co-workers [17], who observed that the reactivity of these supported reagents depends on the size of the alkali metal cation and that the reactivity was found to increase in the sequence CsF>KF>>NaF>LiF.

Various studies have been reported recently, aimed at observing and monitoring the activity that take place on the surface of alumina

supported HF-reagents. Different kinds of fluorine species were formed and seemed to be highly dependent on the fluoride ion concentration and on the pretreatment of the supporting reagents. Miller and co-workers [18] compared the adsorption of KF and CsF onto alumina, Ando and co-workers [17], compared the adsorption of KF and NaF onto alumina, by reaction studies and a series of spectroscopic techniques. Results of both works led to the conclusion that the effectiveness of supported reagents is highly dependent on which alkali metal fluoride is used , reagent loading, and on the calcining temperature. Very recently Miller and co-workers [6], also investigated the adsorption of the series NaF, KF, RbF, and CsF onto alumina. The results showed that MF reacts with the alumina surface to form AlF_6^{3-}, with CO_3^{2-} being formed as a by-products due to the adsorption and reaction of atmospheric CO_2 with MOH produced on the surface.

I.2. Silica And Silica Supported Reagents

Silica is one of the common metal oxides which is useful for carrying out a variety of catalytic and stoichiometric transformations of small molecules and organic compounds. It is also known to be a complex oxide. SiO_2 can be regarded as a three dimensional polymeric structure. In silica the coordination of silicon is four while that of oxygen is two. Silica gel has been used whenever a highly hydrated support or a solid Lewis acid catalyst was needed.

a. Silica Supported Reagents.

Silica gel is known to be very useful in conjunction with a number of redox reagents, which can be adsorbed onto the surface of this metal oxide. An example of dichromate coated on silica gel has been reported by Fischer and Henderson [19] who described a mild and efficient method for the preparation of quinones from hydroquinones employing either cerium(IV)/SiO_2 or chromium(VI)/SiO_2 reagents. An amazing increase in selectivity was observed to have arisen from the adsorption of zinc permanganate on silica gel [20]. This zinc salt appeared to be more reactive than the corresponding magnesium salt, while the potassium salt was virtually inactive. Recent approaches to generating Brønsted and Lewis acid sites in the silica structure have involved the addition of dopant cations such as Sc^{3+}, Mg^{2+}, Fe^{3+}, Zn^{2+}, Al^{3+}, and Ga^{3+} [21]. Lewis acid sites were found to increase in strength with the increasing electronegativity of the cation. This was confirmed by i.r studies focussing on changes in the frequency of adsorbed pyridine on the surface of the site. Brønsted acidity has been shown to increase when Sc^{3+}, Al^{3+}, and Ga^{3+} are adsorbed onto silica, because these cations are bonded tetrahedrally to the silica surface,thereby generating bridging hydroxyl groups between the dopant cation and Si^{4+}.

b. Silica Supported Fluorides.

Fluorination is considered to be an important procedure in the modification and improvement of the catalytic activity of metal oxides. Fluorination of silica results in materials with catalytic properties differing from those of untreated silica, or silica gel [22]. For

example, fluorinated silica has higher cumene cracking activity than silica alone [23]. Formation of Si-F groups on the surface of fluorinated silica gel has been confirmed, and they may in fact contribute to the reactivity of the reagent [23]. The enhanced reactivity of partially fluorinated silica is due to the electronegative effect of chemisorbed fluorine on adjacent hydroxyl groups, which causes them to become more acidic. However the fully fluorinated surface is hydrophobic and therefore a much poorer catalyst. The electron withdrawing from neighbouring hydroxyls giving more acidic protons can be illustrated as following:

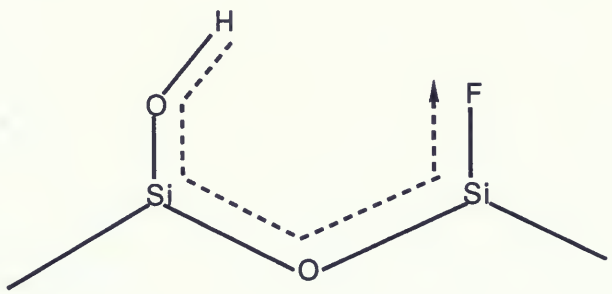

The changes which occur upon fluorination of silica can be studied by spectroscopic techniques such as MAS-NMR, and FT-IR spectroscopy. Miller and co-workers[5], have investigated the surfaces of silica gel supported potassium fluoride and ammonium fluoride. In this study ^{19}F and ^{29}Si MAS-NMR, and FT-IR spectroscopy were used to observe the formation of $(SiO)_3SiF$ groups at the surface, as well the replacement of -F with -OH and the formation of SiF_6^{2-} when silica is fluorinated with KF.

I.3. Aluminosilicates.

The framework of this material originates from the complete sharing of oxygen atoms in SiO_2 sheets with the replacement of Si^{4+} with Al^{3+} atoms, which results in a net charge that is balanced by exchangeable cations between the sheets. Among the most important framework aluminosilicates are zeolites and clays. The surfaces of both types of aluminosilicates exhibit Lewis and Brønsted acid sites. The ratio of these acid sites depends on the treatment temperature. In the following sections I will focus on both zeolites and clay and their catalytic importance in general.

I-3.a.Zeolites.

Zeolites offer useful and rather well defined solid supports for adsorption and catalysis . The three dimensional framework of zeolites is based upon the continuous linkages of all four vertices in the (SiO_4), and (AlO_4) tetrahedra. The anionic framework arises as a result of the isomorphous replacement of silicon cations by aluminum cations, and is counter balanced by a variety of cations. The diagram below illustrates the surface of zeolite structure [24].

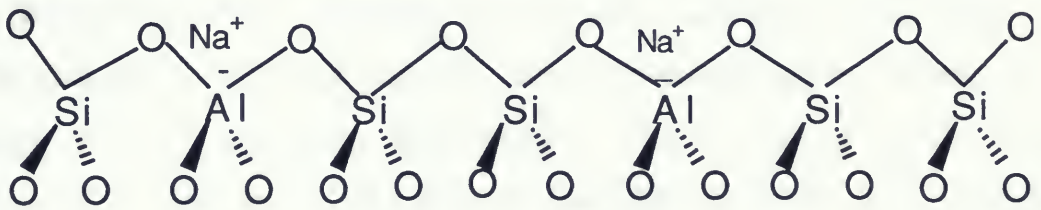

If Na+ is replaced by Ca^{2+} the structure becomes,

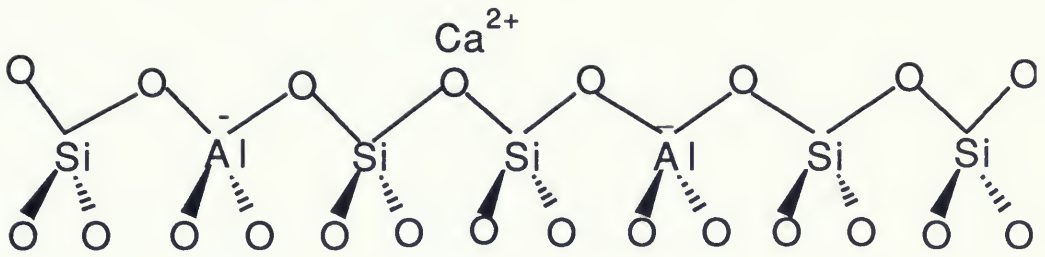

With increasing replacement of Na^+ by Ca^{2+}, the catalytic activity is enhanced [24]. Zeolitic surfaces show both Lewis acidity and Brønsted acidity. This trend was investigated using infrared spectroscopy to study pyridine and ammonia adsorbed onto the forementioned surfaces [25].

Dealumination is one of the most useful methods for modifying aluminosilicates, and it has been found to enhance the catalytic activity of zeolites [26]. The process of dealumination can be achieved by different methods such as acid-leaching [77], and thermal treatment [78]. Mordenite is one of the many zeolitic types that have the advantage that the aluminum can be removed without loss of crystallinity. Using pyridine as adsorbate the acidity of mordenites has been determined. The study showed that the number of strong acid sites increases with a decrease in the total number of acid sites. The Si-OH groups which are formed during dealumination, increase the strength of the remaining acid sites. The i.r. band observed at a frequency of 1462 cm^{-1} and at a temperature of 673K was assigned to an absorption band of pyridine adsorbed onto a strong Lewis acid site [26]. Increased dealumination renders the Brønsted acid sites accessible to pyridine at lower temperatures.

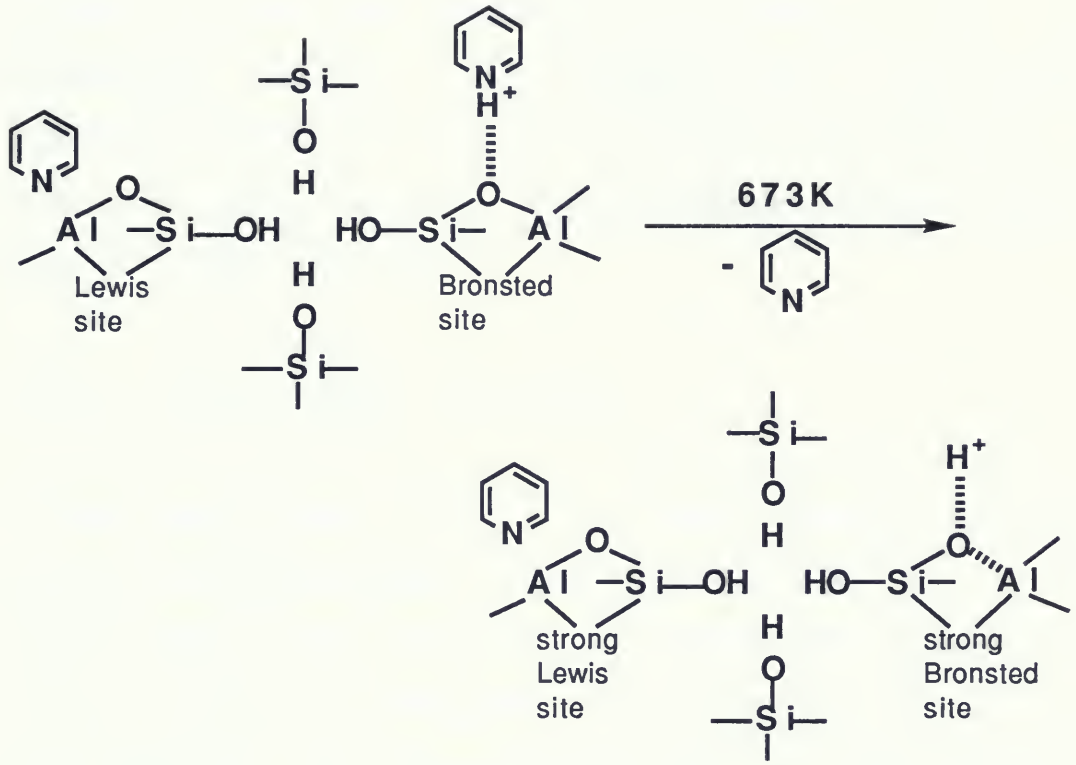

Scheme. I

The nature and number of acid sites at increasingly high temperatures and different level of Na^+-NH_4^+ exchange in mordenite were investigated by infrared analysis using pyridine as a probe [27]. It was also found that Lewis acid sites introduce a significant hindrance to pyridine uptake and required far greater thermal energy of adsorption than Brønsted acid sites. Of the pyridine that could gain access to acid sites during a given contact time, the amount adsorbing onto Brønsted sites at 773K, and onto Lewis acid sites at 823K,was

approximately linearly related to the ammonium ion content. In a different study [28], isomorphous substitution of Fe^{3+} with Al^{3+} in the framework of zeolite ZSM-23 exhibited significant ion exchange capacity and catalytic activity/shape selectivity in the metaxylene isomerization reaction. The thorough study of this isomorphous substitution process has resulted in a catalyst that possesses a weaker acidic site, that is of interest in those catalytic reactions which do not require strongly acid sites.

I-3a.1. Fluorinated Zeolites.

The incorporation of fluorine in zeolite catalysts enhances their activity for acid-catalyzed hydrocarbon reactions such as cracking reactions [29]. Upon fluorinating H-mordenite with ammonium fluoride, (NH_4F) solutions and CHF_3 [30], some of the acidic hydroxyl OH groups were replaced with fluorine atoms and the acidic strength of the remaining hydroxyl groups was enhanced because of the inductive effect of the highly electronegative fluorine. Becker and Kowalak [30], studied the infrared spectra of fluorinated mordenite covered with chemisorbed pyridine species, and they observed a decrease in the Brønsted acid site to Lewis acid site ratio with increasing fluorine content in mordenite. This provides further evidence for the replacement of OH groups (Brønsted sites) with fluorine, which in turn results in the formation of new Lewis acid sites (AlF_3 or other Al-F species). This in effect was reflected in the higher catalytic activity of the samples during cumene cracking reactions.

Kydd and Ghosh [29], infrared, elemental and X-ray analysis, and the cumene cracking reaction were used to investigate the influence of

different fluorine concentrations in mordenite. The elemental analysis showed that small amounts of fluorine are incorporated and aluminum is leached from the samples. Higher concentrations of fluorine caused silicon to be removed from the structure and decreased the size of the unit cell and the surface area. The infrared studies of these samples suggest that the incorporated small amounts of fluorine enhance strong Lewis acidity and weak Brønsted acidity.

I-3.b. Clays.

Natural clays were among the earliest solid acid catalysts used by industry to promote acid-catalyzed reactions such as cracking and isomerization [1]. Further development resulted in the synthesis of highly active clays, known as pillared clays, in which the useful surface has been increased, and shape selectivity has been created by separating the layers with large cationic clusters. Clays are classified according to the relative number of tetrahedral and octahedral layers. The two common groups known as the two-layer and three-layer clays, are important to the science of catalysis. In two-layer clays such as kaolinites the unit layer is composed of one sheet of silica and one sheet of alumina [32]. The inner-layer faces of these clays are thus half siloxane and half hydroxylated alumina. Three-layer clays such as montmorillinte and illites have a unit layer consisting of a sheet of octaredral alumina or magnesia between two sheets of tetrahedral silica [32]. Montmorillonite clay is divided into a number of homopolytypes, which may differ in either the number of layer complexes in the period of the structure, the symmetry of the overall structure, or the measure of regularity in the structure. Some of these

homopolytypes are, montmorillonite K10, montmorillonite K306, montmorillonite KP10, and montmorillonite KSF [33a]. The next section of this paper will be fully devoted to the three-layered clay, montmorillonite K10, its structure, acidity, and applications.

II. Montmorillonite K10.

II.1. Structural Analysis.

Montmorillonite K10 is classified as a semicrystalline aluminosilicate, which has the chemical composition, $Al_2O_3{:}2SiO_2$, with significant variations in the Al/Si ratio and coordination environment. Each layer consists of a two dimensional array of aluminum-oxygen octahedra sandwiched between silicon-oxygen tetrahedra. This arrangement is represented in figure (1-1). The layers consist of sheets of oxide and hydroxide groups coordinated to Si(IV) and Al(III) atoms, with hydrogen bonds between the oxide sheets and the hydroxide sheets holding the layers together [33b].

In this structure, the higher valence metal cations, typically Al^{3+}, are partially substituted by lower valence cations, such as Mg^{2+}, Zn^{2+}, Fe^{2+}, and Ni^{2+} in the octahedral sheets. Si^{4+} is partially substituted by Al^{3+}, and Fe^{3+} in the tetrahedral sheets, thereby developing a net negative charge [6,34]. The charge is balanced by exchangeable counter-cations (such as K^+, Na^+, Ca^{2+},....) within the interlayer space [35].

The structure of montmorillonite K10 undergoes slight structural changes upon calcining. A study [36] reported that on heating

montmorillonite K10, the interlayer water is driven off at 110°C to 140°C. This paper also reported a decrease in the basal spacing between the layers from 1.5nm to 1.0nm, and that most of the chemisorbed water groups are removed between 500°C and 700°C. These changes and others which are even more critical, such as changes in coordination number of Al and Si atoms, were investigated using the newly developed techniques of ^{29}Si and ^{27}Al magic-angle spinning NMR spectroscopy [36]. Montmorillonite K10 clays can be used as acidic catalysts in a number of reactions and there are clear indications that they are more efficient and selective in certain processes than other commonly used catalysts which employ Brønsted and Lewis acid sites [37].

II-2. Supported Montmorillonite Catalysts.

The introduction of catalytic reagents such as oxidizing agents or standard Lewis acids into or onto montmorillonte clays for synthetic purposes has, as yet, received little attention. However, useful advantages, in terms of modification of reactivity and selectivity, may be achieved with concomitant ease of workup and isolation of reaction products. The oxidizing reagent thallium(III)trinitrate (TTN) is a useful reagent for the oxidative rearrangement of enols and olefins [38]. In a different study Taylor and co-workers [39] have shown that the adsorption of TTN on montmorillonite K10 results in an even more powerful, selective, and convenient reagent for the oxidation of a variety of unsaturated organic substrates such as alkyl aryl ketones [39].

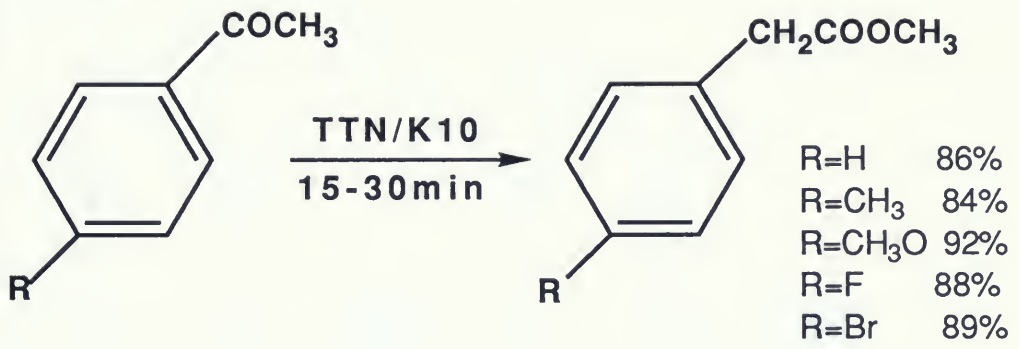

Montmorillonite supported copper(II)nitrate and iron(III)nitrate, which are refered to as claycop and clayfen respectively, have proven useful for a wide range of synthetic transformations [40,44]. In the short time since clayfen and claycop were discovered by Laszlo and co-workers, the application of these reagents toward the generation of nitrosonium ions has been illustrated by a variety of synthetic reactions [40,41]. These reagents have also proven useful when applied to a variety other reactions, including the formation of new carbon-carbon bonds in cycloaddition reactions of the Diels-Alder type[42], and the aromatization of dihydropyridines[43].

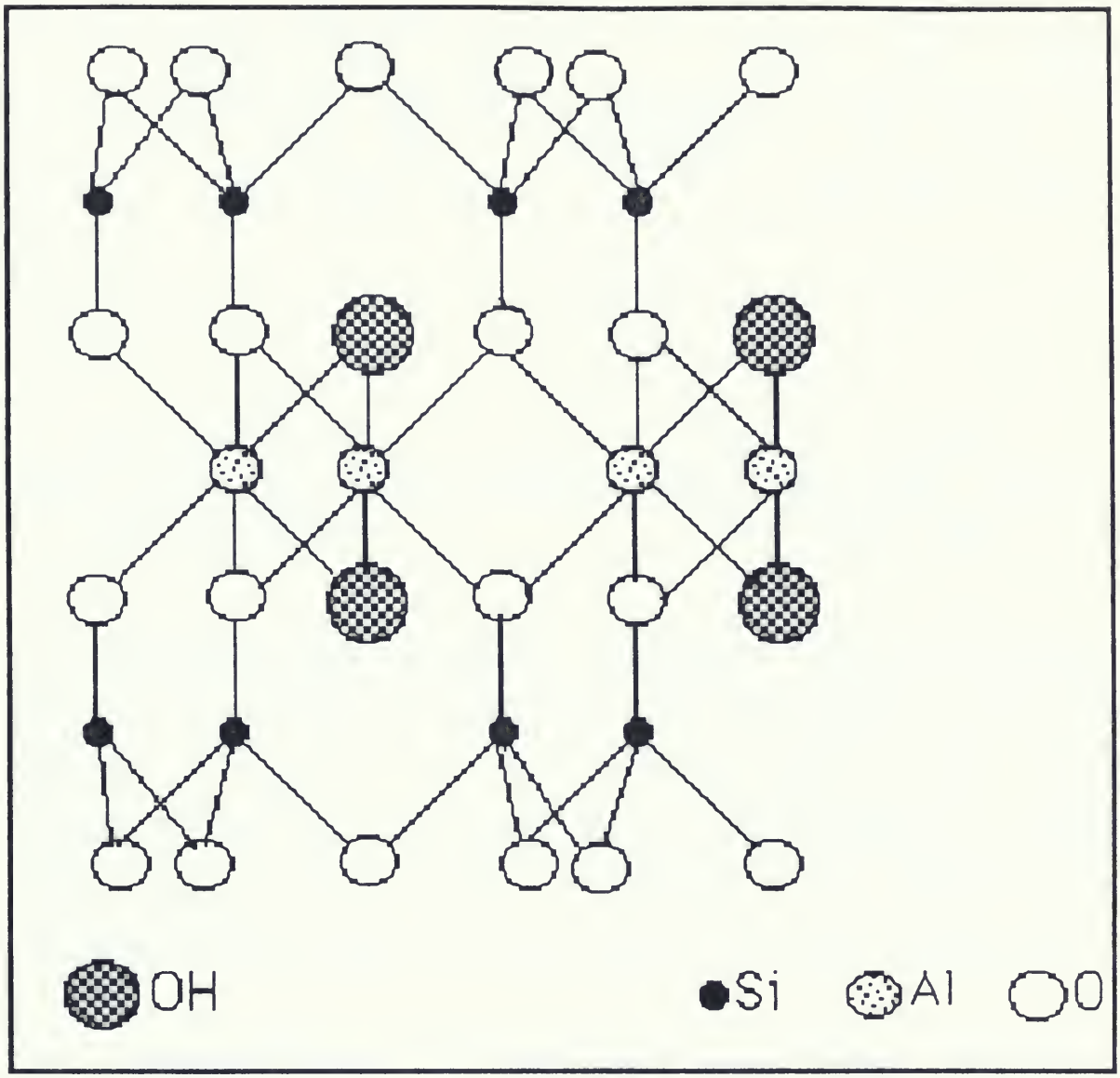

Fig. (1.1) The layer structure of montmorillonite K10

(After Laszlo and Cornelius [41])

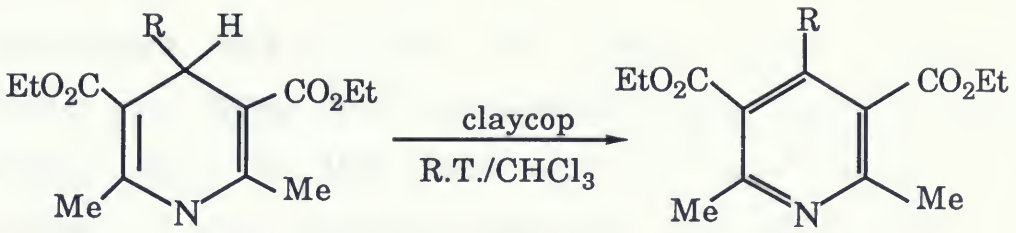

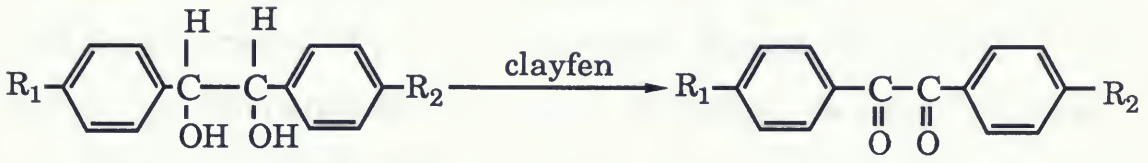

It has been suggested that the reactivity of clayfen and claycop is due to the presence of exchanged Fe(III) and Cu(II) in the spaces between the layers of the montmorillonite structure [41]. Another important effect that is encountered, is the activation of inorganic salts through total or partial dehydration. The resultant vacant coordination sites cause the metal centre to be highly reactive [34].

II-3. Montmorillonite K10 Supported Alkali Metal Fluorides.

While it is well known that fluorination of oxide catalysts causes changes in their catalytic activity, much less work has been done on fluorinated aluminosilicates, since aluminosilicates inherently exhibit a high degree of catalytic activity [22]. Takashi and Junko [45], have studied the effectiveness of various inorganic solids as supports for potassium fluoride, in the promotion of "hydrogen-bond-assisted" alkylation reactions. Among these inorganic solids, montmorillonite was found to be quite effective [45].

To investigate the activity of alkali metal supported montmorillinite clay, Miller and co-workers[4] have recently studied these reagents using ^{19}F MAS NMR and FT-IR spectroscopy. To summarize what has been observed in this study, NH_4F-K10 and MF-K10 (M=Na, K, Rb , Cs) reagents were prepared at several loadings and dried over a range of temperatures. The FT-IR and NMR spectra suggest that the silicon complexes $(NH_4)_2SiF_6$ (scheme III), K_2SiF_6, and Rb_2SiF_6.(scheme IV.) form when high fluoride concentrations and low calcination temperatures are used. Aluminum fluoride complexes such as $NaAlF_4/Na_2AlF_6$, $KAlF_4/K_2AlF_6$, and $CsAlF_4/Cs_2AlF_6$ were also characterized using FT-IR and NMR spectroscopy. These complexes tend to appear at moderate to high drying temperatures and high fluoride concentrations. This study concluded that fluoride complexes are formed when MF is adsorbed onto montmorillonite K10, the particular species formed depending on the loading of MF, the drying temperature, and the cation employed.

II-4. Reactivity of montmorillonite K10.

The reactivity of montmorillonite K10 is primarily attributable to two types of acid centers. The replacement of $Si^{4+}O_4$ tetrahedra by $Al^{3+}O_4$ tetrahedra is a fundamental factor in the generation of acid centers at the surface of montmorillonite. Brønsted acid sites and Lewis acid sites can be seen in the following illustration of the aluminosilicate lattice formation scheme(II) [46].

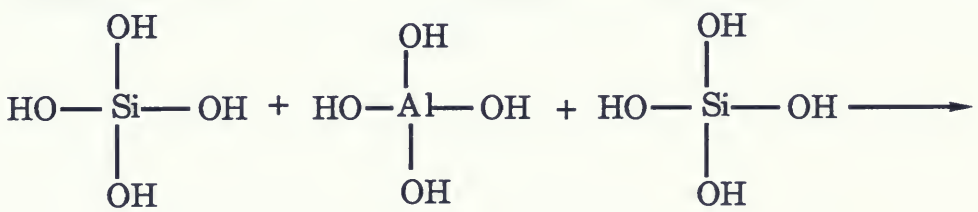

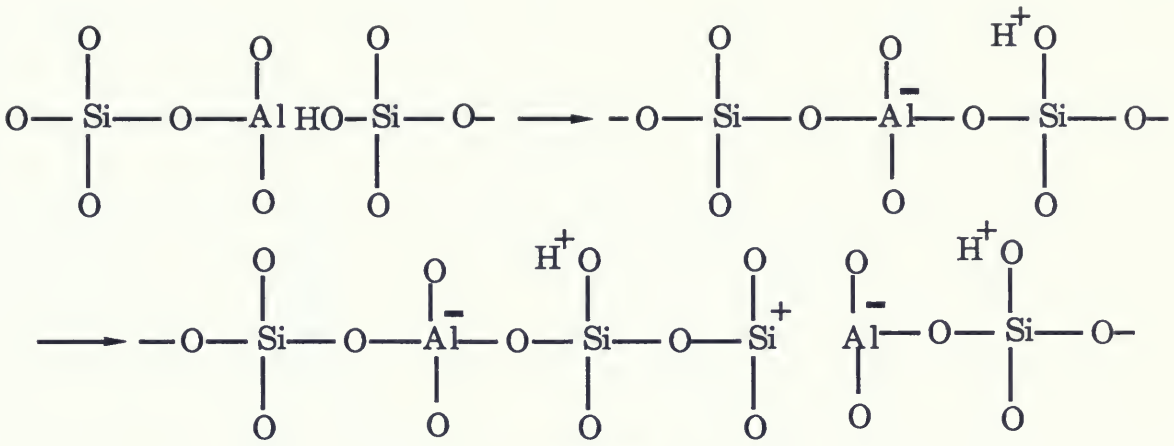

Scheme (II)

A centre containing loosely bonded protons forms, which in turn plays the role of a Brønsted acid centre. Dehydroxylation at higher temperature transforms the Brønsted centers to Lewis centers, which are characterized by a marked deficiency of electrons.

a. Reactivity Due To Lewis Acid Centres On Montmorillonite.

The general concept of the aprotic acid, or Lewis acidity, is defined in terms of capacity to accept or share pairs of electrons. Lewis acid sites are commonly derived from the coordinatively unsaturated cations found at crystal edges or adsorbed onto crystal faces; the latter results from the dehydration of hydroxylated surfaces and from dehydration of silica-alumina catalysts (or similarly treated clays having extensive tetrahedral substitution) [21]. Formation of Lewis acid sites by deamination or deamination-dehydration is dependent on the inversion of the basal oxygen of the aluminum-substituted tetrahedron away from the surface, in order to expose aluminum [47].

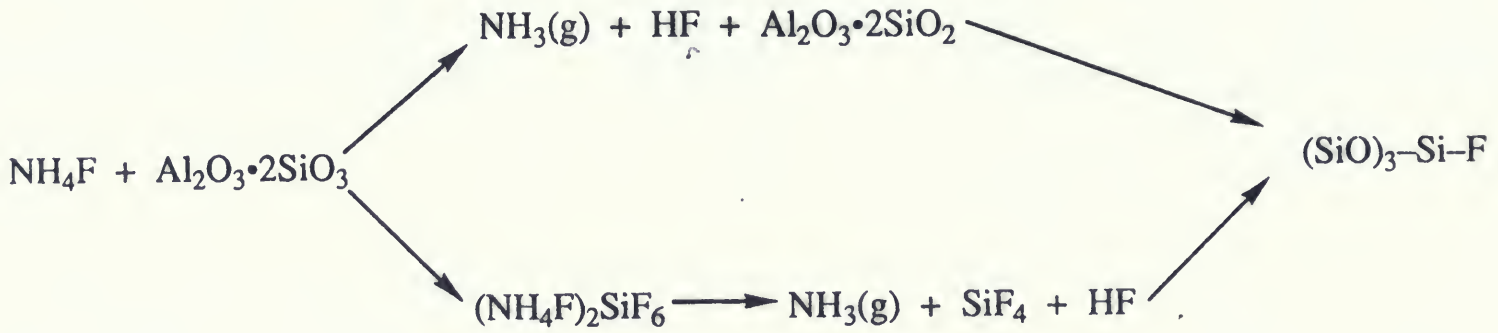
NH4F + Al2O3•2SiO3
NH3(g) + HF + Al2O3•2SiO2
(NH4F)2SiF6
NH3(g) + SiF4 + HF
(SiO)3–Si–F

Scheme III

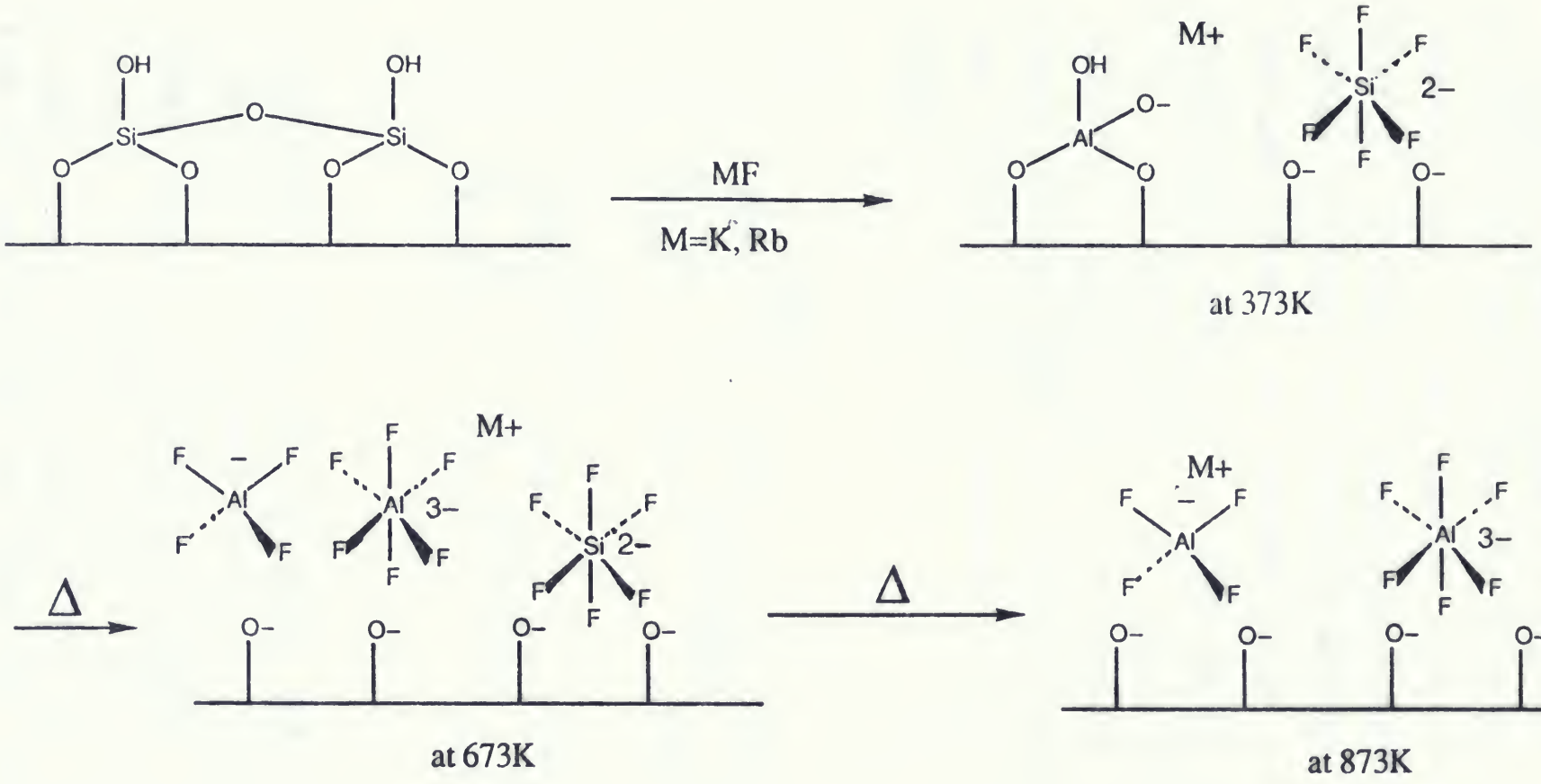
OH
OH
Si
O
Si
O
O
O
O
MF
M=K, Rb
M+
F
F
F
Si
2–
F
F
F
OH
O–
Al
O
O
O–
O–
at 373K
Δ
M+
F
F
Al
F
F
F
F
Al
3–
F
F
F
F
F
Si
2–
F
F
F
O–
O–
O–
O–
at 673K
Δ
M+
F
F
Al
F
F
F
F
Al
3–
F
F
F
O–
O–
O–
O–
at 873K

Scheme IV

Reactions subject to catalysis by Lewis acids will also be catalyzed by Lewis acidic clays. Laszlo and Mathy [48], have achieved good conversion rates by using transition metal-exchanged montmorillonite K10's as catalysts for Friedel-Crafts alkylations. Their yields improved significantly with respect to standard Lewis-acid catalysts. This study included a more systematic survey of the potency of various transition-metal cations {Ti(IV), Fe(III), Co(III), Cu(II), Zn(II), Zr(IV), Nb(V), and Ta(V)} associated with montmorillonite clay. Important Friedel-Crafts alkylations such as the benzylation of benzene by benzyl chloride and benzyl alcohol, and alkylation of toluene by 1-cyclohexene, were preformed using montmorillonite supported transition-metals cations.

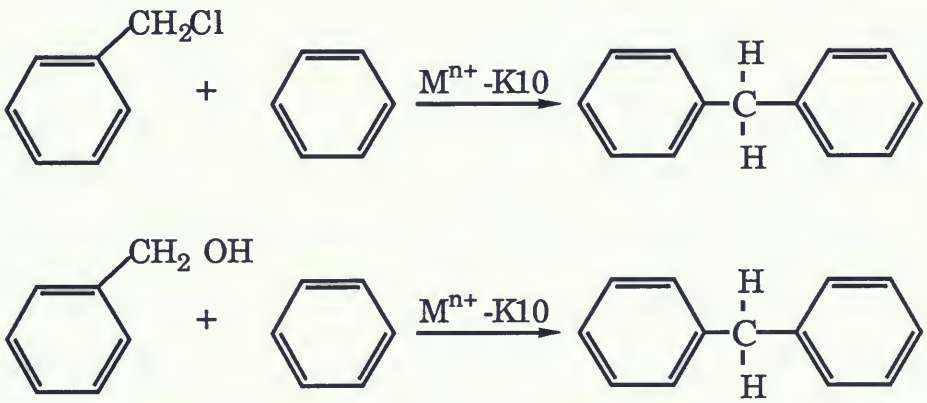

Elsewhere, Clark and co-workers [49], have studied the effectiveness of montmorillonite supported transition metal salts as catalytic reagents for Friedel-Crafts alkylations. For the purpose of this study, they included a significant number of transition metal salts. Of these transition metals they found that Zn(II), Cu(II), and Ni(II) salts have the greatest effect on Friedel-Crafts reactions, in terms of

reactivity and selectivity. The activity of these reagents was generally found to be dependent upon reagent loading and activation temperature, as well as the type of anion employed. In the benzene/benzyl chloride reaction with Zn(II) salts on montmorillonite the following order of reactivity was found :$Cl^- \approx I^- >> PO_4^{3-} > Br^- > NO_3^- > SO_4^{2-} > AcO_4^- > F^-$.

The potential Lewis acidity that exists within the montmorillonite K10 surface is believed to stem from Al(III) cations which are normally associated with the octahedral sheets but in some cases remain exposed at crystal edges where they coordinate with water molecules. If these are removed by thermal treatment, Lewis acid sites become available [41]. These clays, when further doped with standard Lewis acids, become even more effective catalysts for Friedel-Crafts reactions. Divalent cations such as Mg(II), Fe(II), Zn(II), and Ni(II), substitute for Al(III) in the octahedral layer. Ideally in montmorillonite K10, two out of three positions in the octahedral layer are occupied by Al(III) [34}. Al(III) can be replaced totally by Mg(II) to give a mineral known as saponite, by Fe(II) to give nontronite, by Cr(II) to give volkhonskoite,and by Zn(II) to give sanconite [41}. Isomorphous replacement of Si(IV) by Al(III) also takes place in montmorillonite K10 [41]. In a study [21] by Connell and Dumesic, in which they generated Lewis acid sites by doping silica with transition metal cations, it was found that the Lewis acidity increases with the increasing electronegativity of the dopant cation (Se^{3+}, Mg^{2+}, Fe^{2+}, Zn^{2+}, Al^{3+}).

b. Reactivity Due To Brønsted Acid sites On Montmorillonite.

The Brønsted acidity of tetrahedrally substituted clays has been attributed mainly to the dissociation of the protons on hydroxyl groups bridging silicon and aluminum cations [50]. Mortland and co-workers [51], have observed the transformation of NH_3 to NH_4^+, when NH_3 is chemisorbed on the surface of montmorillonite clays. The mechanism of the reaction was shown to involve an interaction between NH_3 and the residual water in the interlayer cavity. From this work, it appears that the residual water is dissociated to a greater extent than the free water.

The measured Brønsted acidity of natural montmorillonites ranges between +1.5 to -3 on Hammet's H_0 scale [41]. Exchanging metallic cations (Na^+, K^+, etc.) for H^+ brings these values into the range of -5 to -8, i.e., between concentrated nitric acid (H_0 = -5) and concentrated sulfuric acid (H_0 = -12). This high acidity stems from the group of exchangeable cations near the charged silicates. These cations polarize coordinated water molecules, thereby enhancing their dissociation [41]. Reactions, such as Diels-Alder reactions, are facilitated by the presence of acidic clays, since Brønsted acid catalysis is initiated [42]. Several other carbocationic reactions are catalyzed by acidic clays. One of these reactions is the transformation of acetals to enol ethers, to form precursors of a,b-unsaturated aldehydes [52].

III. Characterization Of Metal Oxides And Metal Oxide Supported Reagents.

The structure of metal oxides and supported metal oxides can be determined using a number of techniques,which, in combination, are capable of full structural elucidation. Methods such as x-ray, infrared,

and nuclear magnetic resonance spectroscopy are considered to be the prime tools for empirically characterizing clay structures [53]. These methods are often complementary rather than alternative.

a. Infrared Spectroscopy.

Transmission Fourier Transform Infrared (FT-IR) spectroscopy remains one of the most powerful tools for examining supported metal oxides suspended in KBr pellets. There has been a considerable amount of work aimed at characterizing materials such as alumina, silica,and aluminosilicates using FT-IR spectroscopy in the past few years. The acidity of dealuminated mordenites has been studied using i.r. spectroscopy [26]. Using pyridine as an adsorbate, mordenites has been studied and it was found that on dealumination the number of strong acid sites increases simultaneously with a decrease in the total number of acid sites.

Infrared spectroscopy has proven to be useful in monitoring species on the surface of fluorinated alumina [54]. This study showed that upon impregnation of alumina by large amounts of NH_4F, a $(NH_4)_3AlF_6$ phase is formed, which is transformed successively into NH_4AlF_4, α-AlF_3, and γ-AlF_3 upon heat treatment at progressively higher temperatures. Infrared spectroscopy provided complementary evidence for the diffusion of cations in the lattice of ion-exchanged clays [55], and the disappearance of octahedrally coordinated aluminum due to structural dehdroxylation at 700°C. Miller and co-workers [4,5,6] have used FT-IR as the primary tool in the analysis of the adsorption of alkali metal fluorides onto alumina, silica, and montmorillonite clay, and have found it to be quite a useful technique for observing new species on the surface of these inorganic solids.

b. NMR Spectroscopy.

One promising method in the study and elucidation of the nature and properties of surface active centers in solid catalysts, and the chemical processes occuring at these centers is NMR spectroscopy. In its modern form, NMR spectroscopy allows spectra to be recorded in high magnetic fields, while employing special methods to narrow the NMR lines of solid samples [58]. In a recent review [59], Mastikhi and Zamaraev studied heterogeneous catalysis and chemisorption with high resolution ^{1}H, ^{13}C, ^{15}N, ^{27}Al, ^{29}Si, ^{31}P, and ^{51}V solid state NMR. ^{51}V NMR studies of V_2O_5/MgO catalysts revealed the existence of different vanadium species on the MgO surface. Plausible structures were suggested for the observed vanadium species, using the principal values of the chemical shift tensor [60]. ^{31}P and ^{29}Si magic-angle spinning (MAS) NMR studies of H_3PO_4/SiO_2 catalysts, has also revealed the formation of surface silicon pyrophosphates, as well as polyphosphate surface clusters [59]. ^{1}H MAS NMR spectroscopy also played an important role in characterizing the nature and reactivity of surface OH groups. This method permits one to measure the concentration of the various OH groups and to determine their chemical shift, which can then be used to characterize the acid strength of the OH groups [59].

The newly developed solid-state NMR spectroscopy is considered to be a powerful tool for studying solids such as aluminosilicates [1], Thus ^{29}Si and ^{27}Al MAS NMR have been used to elucidate the nature of ^{29}Si and ^{27}Al environments respectively in the sheets of aluminosilicates and to monitor structural changes upon cation-exchange [56]. ^{27}Al MAS NMR spectra clearly distinguish between the tetrahedral and octahedral

coordination sites of aluminum; the chemical shift of these ^{27}Al signals are 60-70 ppm and 0-10 ppm respectively. The chemical shift associated with ^{29}Si and ^{27}Al nuclei depends on the nature of the second neighbour cations located in the tetrahedral and octahedral sheets and in the interlayer space [57]. Generally ^{29}Si MAS NMR is very useful for obtaining information about the ^{29}Si environment. For example, the possibility exists of observing up to five resonance lines, corresponding to the following units; $Si(OAl)_4$, $Si(OAl)_3(OSi)$, $Si(OAl)_2(OSi)_2$, $Si(OAl)(OSi)_3$, and $Si(OSi)_4$ [70].

Solid-state ^{19}F NMR is a useful tool for studying solid inorganic fluorides and the fluorinated surfaces of aluminosilicates, hydroxyapatites, etc. Miller and co-workers [61] used high resolution solid-state ^{19}F NMR to investigate the bonding in ionic fluorides for the first time. They concluded that a much wider range of chemical shifts can be observed for these ionic solids than for solutions, which is due to the effect of ion-pairing and the co-ordinative unsaturation of F^-. A recent study of a wide range of inorganic fluorides using fast-^{19}F MAS NMR has been reported [62]. This study demonstrated that the fast -MAS technique alone represents a viable option to multiple pulse techniques for reducing the F-F dipolar broadening in the ^{19}F NMR of simple inorganic fluorides. ^{19}F m.a.s NMR has some advantages to offer when exploring the surface chemistry of the reaction of fluoride ions with an inorganic solid support. Importantly it can detect all fluorides present, whether crystalline, or adsorbed on a surface, as it selectively probes only the fluoride environment [58].

^{19}F MAS NMR is of special importance in the study of fluorinated catalytic surfaces in silica, alumina, aluminosilicates, and hydroxyapatites. It has been applied to the determination of the concentration, chemical structure, and local distribution of fluorine in a silica network [63]. This study revealed that fluorine bonds only to silicon and that there is no evidence of oxyfluoride formation. Additionally, the study showed that the relative population of silicon monofluoride sites ($Si(O\text{-})_3F$) and silicon difluoride sites ($Si(O\text{-})_2F_2$) are nearly statistically random. ^{19}F NMR has also been used by Schlup and Vaughan to investigate the nature of fluorinated aluminosilicate [64], alumina [64], and silica [65] surfaces. The spectra of these samples have shown that Al-F and Si-F species appear on fluorine modified alumina and aluminosilicate surfaces, and that isolated Si-F groups show up on the surface of silica. Miller and co-workers [1,2,3] used ^{19}F MAS NMR for the analysis of alkali metal fluorides supported on montmorillonite clay, silica, and alumina. Yasinowski and Mobly [66] used the technique in the analysis of fluorinated hydroxyapatite surfaces and Maciel and co-workers [67] applied it to the study of fluorocarbon polymers.

IV. Magic-Angle Spinning (MAS) NMR.

Problems such as sample insolubility and the fact that a sample has different chemical properties while in solution as compared to its solid state were the main factors behind the development of the solid-state NMR technique known as MAS NMR. Earlier efforts by scientists like Andrew [68], Lowe [69], and Lippmaa [70], produced the high

resolution solid-state NMR technique, that is widely used by researchers in many different fields. The resolution problem which manifests itself in the NMR spectra of solid samples has been attributed to two main factors [71]. Firstly, there is the severe line-broadening effect which is characteristic of immobile solid-state systems. Secondly, there is the inherent sensitivity problem of NMR (associated with the low frequencies employed in non-proton NMR). Both of these difficulties have been addressed during the evolution of solid-state NMR technology. Line-narrowing techniques appear to be the solution to line-broadening problems, and I will be focusing on these in the following sections [71].

a. Theoretical Aspects of MAS NMR.

There are a number of major obstacles which prevent the experimenter from obtaining high resolution NMR spectra for solid systems. The first reason is the anisotropic dipole-dipole (DD) interactions which lead to line widths in the KHz or greater range, and can result from heteronuclear and homonuclear magnetic dipoles, elimination of the broadening caused by the latter has been a major challenge in NMR research. The second factor is the additional line broadening effect that is based on the nuclear electric quadrupole interactions for nuclides of spin quantum number > 1/2. The other obstacle arises from the phenomenon of chemical shift anistropy (CSA) which for powders leads to broad and complex line shapes even when the dipolar interaction is absent or eliminated. These interactions are also present in liquids but fortunately are averaged to zero by the rapid Brownian motion [72a,72b]. The pattern produced by chemical shift

anisotropy is quite broad, and from it the three principal elements of the shielding tensor (σ_{11},σ_{22},σ_{33}) can be obtained (see figure 1-2). These principal elements can be used to calculate the isotropic chemical shift(σ_{iso}).

$$\sigma_{iso} = 1/3(\sigma_{11}+\sigma_{22}+\sigma_{33})$$

The chemical shift anisotropy and the dipolar spin-spin interactions are scaled by the equation [72]:

$$(3\cos^2\theta - 1)$$

This expression led to the development of the line-narrowing technique best known as magic-angle spinning (MAS) NMR. It resulted in the marked narrowing of the broad band as shown in figure (1-2a). This is accomplished by physically spinning the solid rapidly about an axis tilted at an angle of 54°.44' ,the"magic-angle", with respect to the main magnetic field as shown, in figure(1-2b). The anistropic interactions are then averaged to zero [71], since

$$(3\cos^2\theta-1)=0 \text{ ,at } \theta=54^\circ.44'$$

Problems arise when the nucleus being studied is magnetically abundant,because broad band homonuclear decoupling is not possible; the decoupling would wipe out the spectrum. Complicated pulse sequences have been designed to simulate decoupled spectra, and have met with some success [73]. Magnetically dilute nuclei such as ^{13}C,^{29}Si,^{15}N,etc. are considered to be the nuclei of choice for solid

state NMR because of reduced dipole-dipole interactions; these interactions contribute greatly to the NMR line.

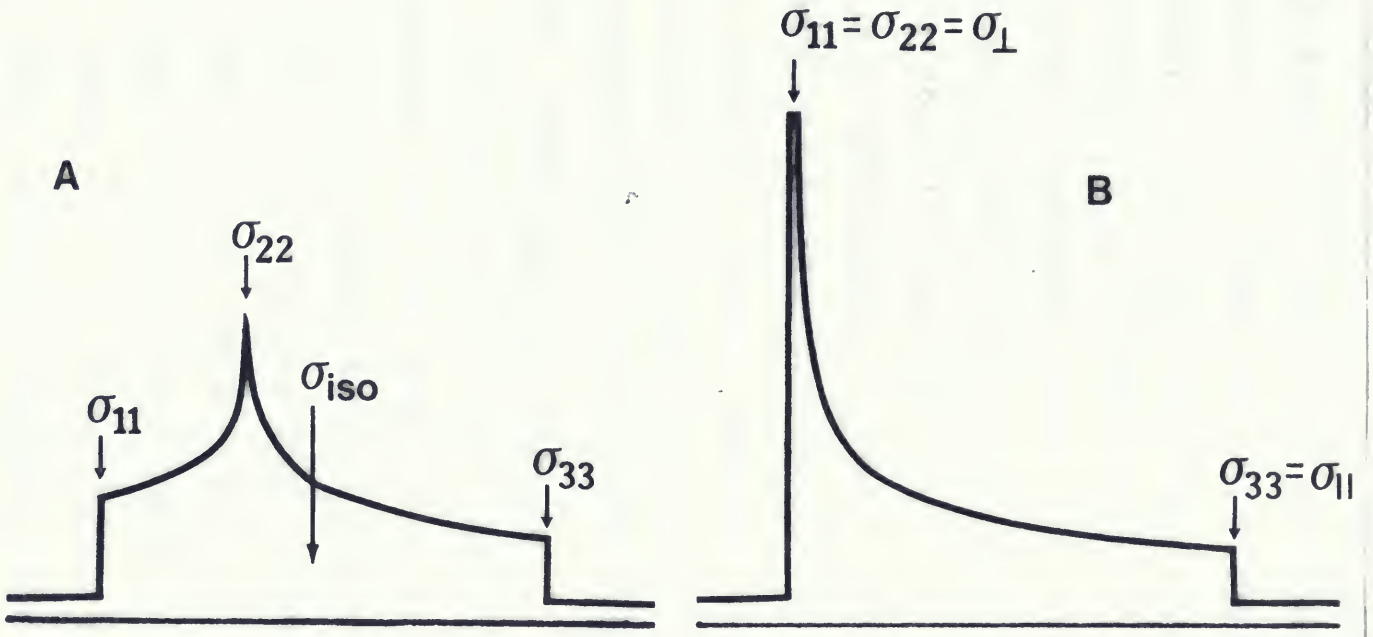

Figure(1.2) Schematic representation of theoretical powder line shapes fot the chemical shift tensor.
A. Asymmetric shift anisotropy
B. Axially symmetric shift anisotropy. (After Fyfe [72])

state NMR because of reduced dipole-dipole interactions; these interactions contribute greatly to the NMR line.

Sideband intensities in the NMR spectra of solid samples spinning at the magic-angle can be quite significant, depending on the spinning frequency [74]. These spinning sidebands result when the spinning frequency is lower than the chemical shift anistropy. In this situation the isotropic line in the NMR spectrum is flanked on both sides of the main peak by sidebands spaced at the spinning frequency [75]. This is illustrated by the ^{31}P m.a.s. NMR spectra of dipalmitoyl phosphatidyl choline [76], ^{19}F m.a.s. NMR spectra of synthetic fluoroapatite [58],and ^{31}P m.a.s. NMR spectra of barium diethyl phosphate [76]. Spinning sidebands can be either symmetric or asymmetric around the main peak. This symmetry of spinning sidebands depends on the local electronic environment of the nucleus being examined. This will be verified in the next section,in which I will be focusing mainly on ^{19}F m.a.s. NMR

b-^{19}F NMR Spectral features.

The shape of the ^{19}F m.a.s. NMR spectrum can be very helpful in interpretation, since this shape is dependent on the principal elements of the shielding tensor, which relates to the orientation of the local environment around fluorine [58]. There are two common situations, where the ^{19}F m.a.s. NMR spectra are expected to differ in terms of shape which can be seen from powder line shapes for the chemical shift tensor (figure 1.2). The first situation is that when signals result from each random crystallite orientation and a broad line results, the shape of the line will depend on the principal elements of the shielding tensor. This situation is usually refered to as the general case where the principal tensor elements have the values indicated (figure 1.2A). The

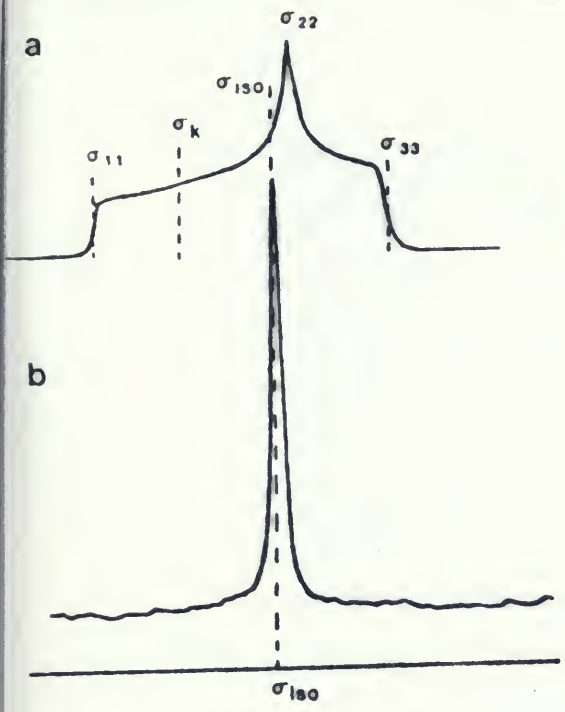

Fig. (1.2a) (a) CSA Powder Pattern Showing Principal Elements of the Chemical Shift Tensor (σ_{11}, σ_{22}, σ_{33})
(b) MAS, giving the Isotropic Chemical Shift σ_{iso}. (After Maciel [71])

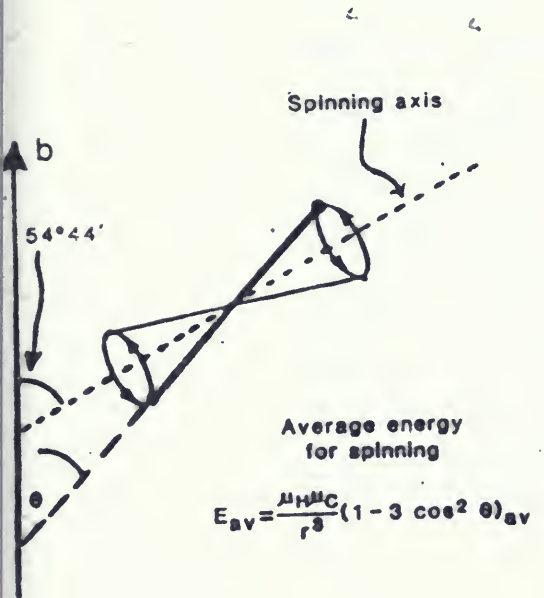

Fig. (1.2b) Effect of Magic-Angle Spinning (After Maciel [71])

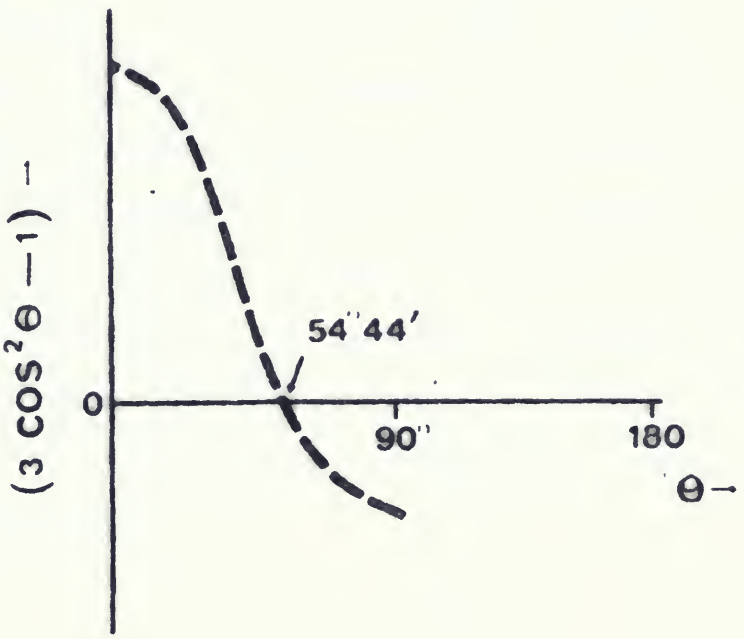

Fig. (1.2c) Variation of the Term $(3\cos^2\theta - 1)$ as a Function of θ. The curve crosses the axis at θ = 54°44'. (After Fyfe [72])

other situation [72a] is illustrated in Figure (1-2B) where two of the principal elements are identical (i.e. $\sigma_{11} = \sigma_{22}$) or an axially symmetric shielding pattern, and the third element (σ_{33}) is in a unique axis that is perpendicular to the plane of σ_{11} and σ_{22}. A typical example of this system would be the chemisorption of F^- on the surface of an oxide catalyst. An illustration of the second situation can be seen in figure 1.3, in which the chemisorbed F^- on silica surface is the reason for the spectrum taking this shape.

^{19}F MAS NMR offers some advantages when used to study or explore the surface chemistry of the reaction of fluoride ion with an inorganic solid support . The technique is highly advantageous for the detection of all fluoride present ,whether crystalline , amorphous, or adsorbed on a surface, as it selectively probes only the fluoride environment. Chemisorption, which involves an ion-exchange mechanism where one F^- replaces OH^- at the surface of an inorganic solid, can be easily observed using this technique. The introduction and development [79,80] of the combined Cross-Polarization/Magic-Angle Spinning (CP/MAS) has been a major step forward in the development of high resolution techniques for NMR spectra in the solid state. CP/MAS proved to be valuable for many chemical applications in solid systems [81,82], and further work is to be expected in this area.

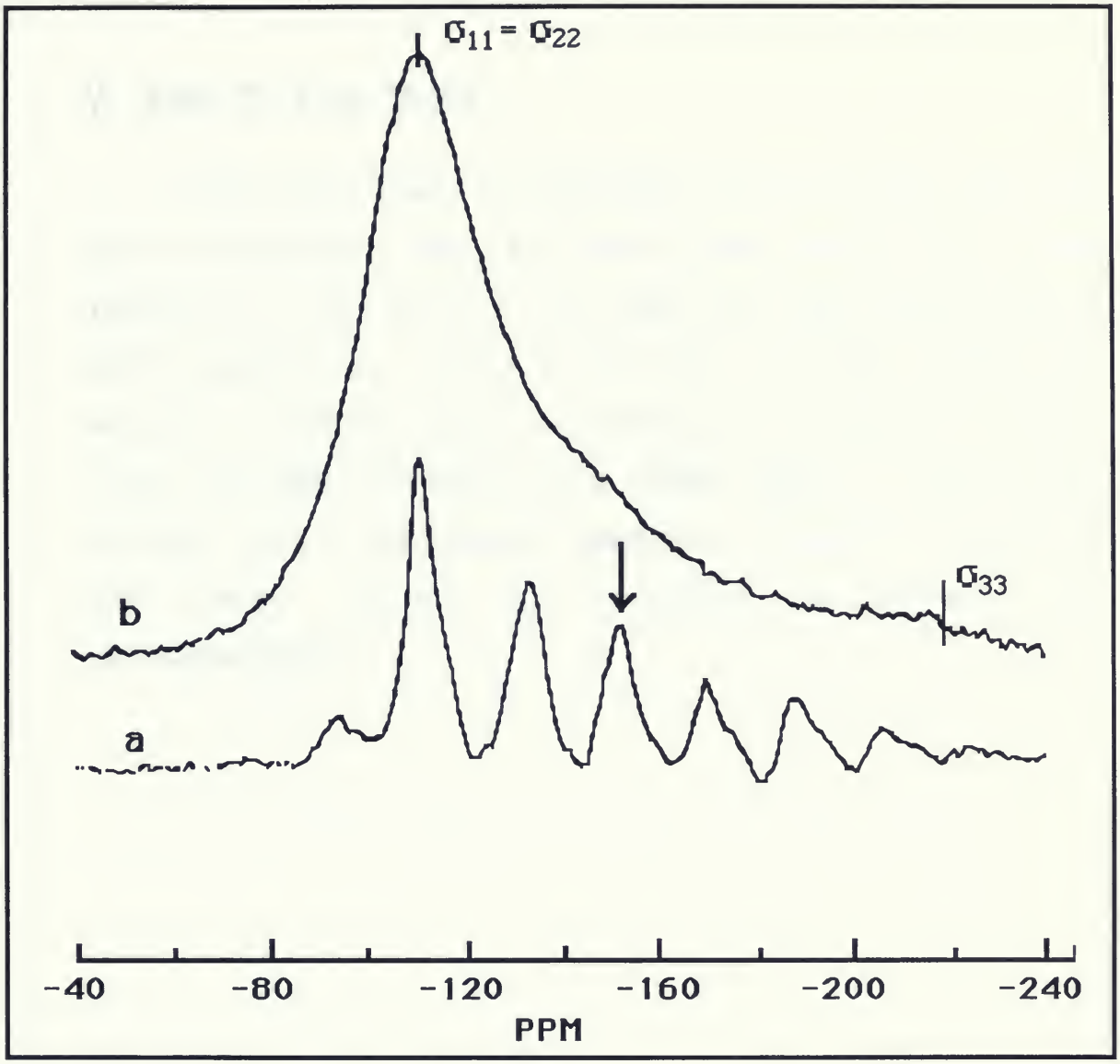

Figure(1.3). ^{19}F NMR spectra of CuF_2-silica

(a) MAS at 3.3 KHz (asymmetric spinning side bands)
(b) Non-spinning; Large Chemical Shift Anistropy

($\sigma_{11}=\sigma_{22}$; σ_{33} is $\perp$to σ_{11}, σ_{22})

(arrow points at σ_{iso})

V. Aim Of This Work

This work involves the adsorption of ZnF_2, CuF_2, and CdF_2 onto montmorillonite clay, and the resulting reagents have been analysed by FT-IR, and ^{19}F, ^{29}Si, and ^{27}Al magic-angle spinning NMR spectroscopy. In part of this study I will also examine the reactivity of these catalysts by applying the reaction of Friedel-Crafts benzylation of benzyl as a model reaction. I will try two different types of benzylation reactions, benzylation of benzene with benzyl chloride and alkylation of benzene with paraformaldehyde.

CHAPTER TWO
EXPERIMENTAL

II.1. Reagent preparation.

Chemicals Used.

ZnF_2 (Aldrich) 99%, CdF_2 (Aldrich) 98%, and CuF_2 (Aldrich) 98% were used without further purification. Montmorillonite K10 clay (surface area 220-270 m^2/g) was obtained from Fluka. Our samples have extractable iron content of between 0.3 and 1.3%. On removing iron by five successive extractions with 50 ml of 3M HNO_3, we extracted a total of 1.3% iron, after which no significant iron could be removed (this material contained about 3.0% iron according to Fluka spec. sheets, the difference is presumably tightly bonded iron). Sodium, potassium, and calcium are all below 0.1% extractable, with additonal amounts found in lattice sites. The silica gel was Merck Kieselgel 100, 70-230 mesh. The alumina was Merck 90 neutral, 70- 230 mesh activity 1, for chromotagrophy.

a.ZnF2-K10.

The samples of ZnF_2-K10 were prepared at loading range of 1.0, 3.5, and 5.0 mmol/g. They were prepared by dissolving the appropriate quantity of ZnF_2 in the required quantity of water (1 g/200 ml) and adding the solution of appropriate quantity of montmorillonite K10 to form a slurry. 1.0 mmol/g of ZnF_2-K10 was prepared by dissolving 1.03 g of ZnF_2 in 200 ml of water and adding the solution of 10 g of montmorillonite K10 to form a slurry. Water was then removed on a rotary evaporator at 70°C to leave a free-

flowing powder. Then the reagent was dried at the temperatures of 573K and 873K.

b. CuF2-K10.

A series of CuF_2-K10 reagents (1.0, 3.5, and 5.0 mmol/g) were prepared. The procedures applied in preparing these samples involve dissolving the appropriate amount of CuF_2 in the necessary amount of water, which was achieved by mechanically stirring the solution, then adding the appropriate weight of montmorillonite K10. CuF_2-K10 (1.0 mmol/g) was prepared by dissolving 1.02 g of CuF_2 in 200 ml of water and adding the solution to 10 g of K10 to form a slurry. A rotary evaporator was used to remove the water, leaving a free-flowing powder. All the prepared reagents were calcined at 573K and 873K.

c.CdF2-K10.

The CdF2-montmorillonite K10 reagents were prepared at loadings of 1.0, 3.5, and 5.0 mmol/g. This reagent preparation involved dissolving the appropriate quantity of CdF2 in the necessary amount of water. To insure dissolution of CdF2 in water, the solution is stirred mechanically for a period of time. The preparation of 1.0 mmol/g of CdF2-K110 took 1.50 g of CdF2 dissolved in 200 ml of water, and this solution was added to 10 g of K10 to form a slurry. the water was then removed by a rotary evaporator until the regent had caked to the wall of the surface of the flask. All of the samples were dried at 573K and 873K.

II.2. INSTRUMENTATION.

a.MAS-NMR SPECTROSCOPY.

^{29}Si and ^{19}F MAS NMR spectra were obtained on a Bruker AC-200 spectrometer at 39.74 MHz for ^{29}Si and at 188.3 MHz for ^{19}F using a home-built MAS probe. Figure 2.1 illustrates the probe and the Magic-Angle head of the ^{29}Si and ^{19}F MAS NMR probes. The samples were spun at approximately 3300 Hz at an angle of 54°44' to the applied magnetic field. Neither cross-polarization nor high power decoupling was used to achieve line narrowing. The ^{29}Si MAS NMR spectra were recorded using a spectral width of 50000 Hz, line broadening of 100 Hz, and a relaxation delay of 5.0 s. ^{29}Si chemical shifts were referenced to external tetramethylsilane (TMS).

The ^{19}F MAS NMR spectra were recorded using a spectral width of 70000 Hz, line broadening of 125 Hz, and a relaxation delay of 1.0 s. The chemical shifts were reported in ppm to external $CFCl_3$, and were determined with a reference of a secondary standard of hexafluorobenzene (C_6F_6) (-163.0 ppm [93]). ^{27}Al MAS NMR spectra were obtained on a Bruker AM-500 NMR spectrometer at a field strength of 11.8 T. The ^{27}Al MAS NMR spectra were recorded on a Bruker AM-500 at the NMR facility at McMaster University, at 130.32 MHz, line broadening of 100 Hz, and a relaxation of 1.0 s. The samples were spun at 8.0 KHz. ^{27}Al chemical shifts are reported in ppm of the resonance frequency with respect to standard aluminum nitrate $Al(NO_3)_3.xH_2O$ in aqueous medium. Table 2.1 lists the acquisition parameters employed for each nucleus.

Table (2.1) Aquisition parameters used for MAS NMR spectroscopy.

Nucleus	^{29}Si	^{19}F	^{27}Al
Instrument (Bruker)	AC-200	AC-200	AM-500
Frequncy (MHz)	39.74	188.15	130.32
Spectral Width(Hz)	50000	70000	100000
Aquisition Memory	8K	8K	16K
Working Memory	16K	16K	16K
Pulse Width	4.4	10	4.0

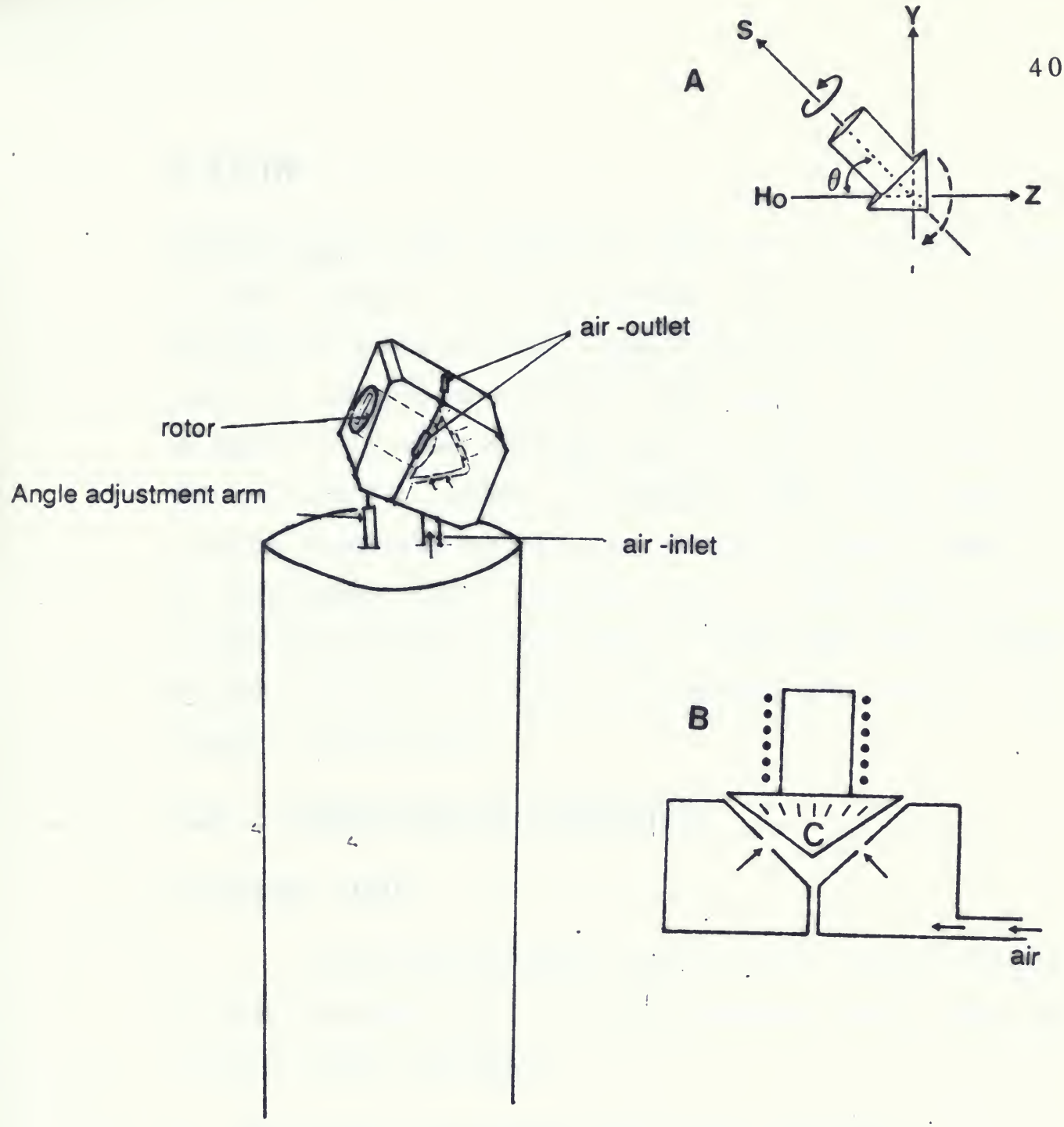

Figure (2-1) Schematic representation of the ^{19}F m.a.s NMR probehead;
(A).geometric arrangement for the Magic-Angle (After Fyfe [72])
(B).representation of the rotor cone,and position of spinner. (After Fyfe [72])

b.FT-IR.

Infrared spectra were recorded for solids using an Analect FX-6260 Fourier Transform spectrophotometer instrument at 4 cm^{-1} resolution, and a wavenumber range of 400-4000 cm^{-1}. The FT-IR system is attached to a MAP-66 data system. All spectra were obtained using pressed KBr discs, made up with a ratio of about 20:1 KBr to reagent by weight. A triglycine sulfate (TGS) detector is used for all spectra, being the most commonly employed detector in the mid-infrared region (400-4000 cm^{-1}). Both background and sample were acquired in 256 scans to ensure good noise averaging. Spectra of all samples were run immediately after drying to avoid moisture contamination.

II.3. Friedel-Crafts Alkylation.

Chemicals Used.

Benzyl chloride (BDH), benzene (BDH), paraformaldehyde (Lancaster Synthesis Ltd.), and diphenylmethane (Aldrich) were used without further purification.

a. benzylation of benzene with benzyl chloride.

The experimental procedure involved in the reaction of benzyl chloride with benzene took 0.05 mol of benzyl chloride and 0.8 mol of benzene warmed up at 70°C, then 4.0 g of the MF_2-K10 catalyst to be tested was added. After refluxing and stirring for 30 minutes the reaction was stopped, then the catalyst was filtered off and the

unreacted benzene was removed by a rotary evaporator. The isolated product yield was corrected by GC analysis and confirmed with ^1H NMR spectroscopy and GC-MS.

b. benzylation with paraformaldehyde.

This reaction took .025 g of paraformaldehyde and 0.5 mol of benzene. The mixture was warmed up at 80°C, then 10 g of 1.0 mmol/g of MF_2-K10 was added. After refluxing and stirring for 4 hours the catalyst was filtered off and the unreacted benzene was removed by a rotary evaporator resulting in the isolated product diphenylmethane. The product yield was corrected by GC analysis and confirmed with ^1H NMR spectroscopy and GC-MS.

CHAPTER THREE
RESULTS
AND
DISCUSSION

III. Results and Discussion.

III-1. ZnF_2 supported montmorillonite K10.(ZnF_2-K10).

(Tables, figures for section III.1 are found between p.p 53-62)

(Figures AI-1 to AI-6 are found in appendix I)

a.Infrared Spectroscopy.

The infrared spectra of montmorillonite K10 and ZnF_2-K10 reagents (0.5, 1.0, 3.5,and 5.0 mmol/g) dried at the temperatures of 573K,and 873K were carefully analyzed. Figure(3.1) shows the i.r. spectra for the various concentrations of ZnF_2 adsorbed on the surface of montmorillonite at a drying temperature of 573K. One can clearly observe that the band at 802 cm^{-1} gradually diminishes as the concentration of the ZnF_2 increases to a maximum (5.0 mmol/g); at the same time a new band is starting to develop at 663 cm^{-1}. The band at 802 cm^{-1} corresponds to the vibration of $[SiO_4]^{4-}$ (lit. value 795 cm^{-1}[55]), and the band at 663cm^{-1} corresponds to the newly formed species AlF_3 (lit. value 665 cm^{-1} [83]). The band at 527 is assigned to coupled Al-O and Si-O vibrations (lit. value 525 cm^{-1}[83]).

The spectra of ZnF_2-K10 samples dried at 873K (figure AI-1) show similar changes to those exposed to lower drying temperatures except for the band at 527 cm^{-1}, which diminishes as the concentration of ZnF_2 increases at higher calcining temperatures. To insure that these significant changes were really taking place, an additional sample with 6.5 mmol/g dried at 373K and 973K was

prepared and analyzed (figure 3.2). The spectrum corresponding to the low drying temperature clearly shows the two important bands at 755 cm^{-1} and 665 cm^{-1} corresponding to AlF_4^- (lit. value 760cm^{-1} [84]), or possibly SiF_6^{2-} (lit. value 745 cm^{-1} [84] and AlF_3 respectively, whereas the spectrum for the higher drying temperature shows a new band at 570 cm^{-1} which is presumably due to skeletal ZnO_4 (lit. value 570 cm^{-1} [84]). If SiF_6^{2-} is formed, it would decompose at even low calcining temperature to gaseous SiF_4 and F^-, which probably acts as a fluorinating agent. The spectrum also shows the well resolved band at 910 cm^{-1}, which is also due to α-AlF_3 species (lit. value 909 cm^{-1} [84]).

b.^{19}F MAS NMR spectroscopy.

^{19}F NMR spectra of ZnF_2-K10 samples (1.0, 3.5, and 5.0 mmol/g) dried at 573K and 873K were obtained. Spectra of montmorillonite supported ZnF_2 with a concentration of 1.0 mmol/g, dried at 573K and 873K (figure 3.3), show asymmetrical spinning side bands around the central peak, which has an isotropic chemical shift of -151 ppm. However, the spectra for the higher ZnF_2 loading (3.5 and 5.0 mmol/g) dried at 573K (figure 3.4) tend to show symmetrical spinning side bands around the central peak which is located at a chemical shift of -153 ppm. The ^{19}F chemical shifts and the shapes of the peaks in those spectra closely approximate the spectrum of an AlF_4^- and AlF_6^{3-} mixture (figure AI-2). Calcining the the higher loading reagent 5.0 mmol/g at 873K also resulted in a central band surrounded by symmetrical spinning side bands (figure AI-2), but the overall shape of the spectrum tends to be broader

compared to that of the corresponding reagent when dried at a lower temperature (figure AI-3). Table (3.1) lists the chemical shifts of all samples and $AlF_n^{(3-n)+}$ complexes. All of the $AlF_n^{(3-n)+}$ have a similar peak position which is indicative of tetrahedral geometry.

The shape of the spectra resulting in asymmetrical spinning side bands makes it difficult to identify the centre band, which need not be the most intense resonance. The centre band, i.e. the position of the isotropic chemical shift (σ_{iso}) can be found from the principal elements σ_{11}, σ_{22}, and σ_{33} of the chemical shift tensor:

$$\sigma_{iso} = 1/3(\sigma_{11}+\sigma_{22}+\sigma_{33})$$

The principal elements can be found from the spectrum of a non-spinning sample of ZnF_2-K10. Thus the centre band of the spectrum of ZnF_2-K10 (1.0 mmol/g) dried at 573K, is the resonance at -151 ppm.

c. ^{29}Si MAS NMR Spectroscopy.

The ^{29}Si NMR spectra of ZnF_2-K10 (1.0, 3.5, and 5.0 mmol/g)reagents calcined at 573K and 873K are shown in figure 3.5, and AI-4 respectively. The ^{29}Si MAS NMR spectrum of the low loading ZnF_2 (1.0 mmol/g) dried at 573K (figure 3.5.a) shows an intense resonance at -107ppm corresponding presumably to $Si(OSi)_3(OAl)$ [89,91], which is present in the clay prior to the fluorination and heat treatment (figure AI-5). In addition to this intense signal at -107ppm, there is a shoulder at -97ppm, which is

resolved as the concentration of ZnF_2 increased to the intermediate range (3.5 mmol/g) (figure 3.5.b).

As the loading of ZnF_2 is increased to 5.0 mmol/g, the signal at -97 ppm becomes quite sharp and intense, presumably indicating formation of $Si(OSi)_2(OAl)_2$ [89]. The original signal at -107 ppm has almost completely disappeared. Increasing the drying temperature seemed to have no apparent effect on the NMR signals; however a slight shift of about 2ppm took place, which is consistent with the signals of thermally treated montmorillonite clay (figure Al-5). This slight shift is probably due to interlayer water removal, which is accompanied by a contraction of the basal spacing [36].

d. ^{27}Al MAS NMR Spectroscopy.

^{27}Al NMR spectra of ZnF_2-K10 (1.0, and 5.0 mmol/g) dried at 573K and 873K were analyzed. These spectra indicated the presence of four- and six-coordinated aluminum, and to some extent, five-coordinated aluminum. Figure 3.6, shows spectra of 1.0 and 5.0 mmol/g loaded ZnF_2-K10 dried at 573K compared with spectra of pure montmorillonite K10. Two main resonances located at 3 ppm and 69 ppm, which correspond to six- and four-coordinated aluminum (lit value 5 ppm, 61 ppm and 69.3 ppm [90]) respectively. It is not clear if these signals correspond exclusively to Al-O coordinations or to other alternative possibilities such as six-coordinate layer $-AlO_4F_2-$, $-AlO_5F-$, or AlF_6^{3-} complex [85], or four-coordinate AlF_4^-.

The ^{27}Al MAS NMR spectrum of 1.0 mmol/g of ZnF_2-K10 dried at 873K, compared to its corresponding montmorillonite K10 spectrum (figure 3.7), shows an increase in the intensity of the tetrahedrally coordinated peak (at 61 ppm) compared to the unfluorinated clay. A hint of a peak at 30 ppm is presumably due to the five-coordinated aluminum containing species, AlO_5. The spectrum of the higher loading ZnF_2-K10, 5.0 mmol/g dried at 873K shows a more intense peak at 61 ppm than the corresponding reagent dried at 573K, which shows apeak at 69 ppm (figure Al-6). The striking feature of ^{27}Al NMR spectra is the clearly consistent change in the chemical shift for the tetrahedrally coordinated aluminium. All moderately dried reagents (at 573K) resulted in a chemical shift of 69 ppm for tetrahedral Al, whereas reagents dried at high calcining temperature resulted in a chemical shift of 61 ppm. The signal at 69 ppm corresponds to Al tetrahedra in the silicate layer, which is due to the isomorphous replacement of Si by Al [41].

e.Friedel-Crafts Alkylation.

The activity of montmorillonite K10 supported reagents is highly dependent upon the reagent loading and activation temperature. I have successfully employed ZnF2-K10 reagents (1.0, 3.5, and 5.0 mmol/g) dried at 573K, 673K, 773K,and 873K in the Friedel-Crafts benzylation of benzene with benzyl chloride to test the reactivity of this wide range of reagents.

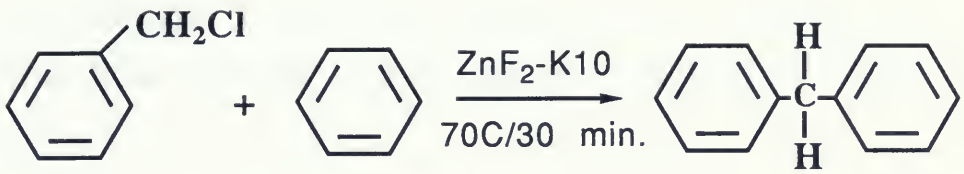

Table 3.2 shows the conversion of benzyl chloride and the calculated yield of diphenylmethane.

According to the results shown in table 3.3, the reactivity of ZnF_2-K10 reagents is highly dependent on the reagent loading and the drying temperature. The reactivity of the low loading reagent (1.0 mmol/g) seems to decrease as the calcining temperature of the reagent increases. This is deduced from the poor conversion of benzyl chloride, and the low yield of diphenylmethane. The highly loaded reagents 3.5 and 5.0 mmol/g acted differently than the lower loading (1.0 mmol/g) reagent. The calcining temperature had no significant effect on the higher loaded reagents. In fact, highly loaded and dried reagents seem to be more active than highly loaded and moderately dried reagents.

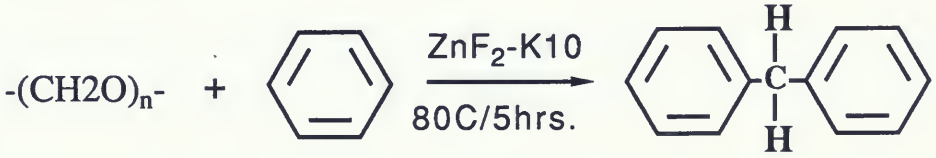

To further evaluate the catalyst, I selected another Friedel-Crafts reaction, which involves alkylation of benzene with paraformaldehyde. This reaction presumably involves the solid acid depolymerizing the polymer $(CH_2O)_n$ (to provide a source of CH_2O) as well as a Friedel-Crafts reaction. Product yield (75%) of this reaction is improved when compared to the yields which result when

the reaction is catalysed with $ZnCl_2$-K10 reagent(70% yield [88]) and those obtained when using aluminium chloride [88].

f.Discussion.

The results of infrared, and ^{19}F, ^{29}Si, ^{27}Al, MAS NMR spectroscopic studies indicate significant changes taking place on the surface and within the structure of montmorillonite K10 when treated with ZnF_2. Evidence from i.r. studies of the different reagent loadings (figure 3.1) clearly indicate structural rearrangement within the silica framework, since the i.r. band at 802 cm^{-1} corresponding to the free silica layer SiO_2, diminishes as loading increases. This rearrangement presumably involves the isomorphous replacement of Si by Al in the SiO_2 framework. Evidence for this is clearly seen in the ^{29}Si NMR spectra as well. ^{29}Si MAS NMR spectra (figure 3.5) show the change in the ^{29}Si environment from $^{29}Si(OSi)_3(OAl)$ to $^{29}Si(OSi)_2(OAl)_2$ (scheme 1.1). The increase in AlO_4 group concentration as loading increases has also been deduced from 27Al MAS NMR spectra (figureAl-6).

The formation of Al-F species is clear from both i.r. and ^{19}F MAS NMR results. The i.r. spectra show the formation of AlF_3 crystals (band at 665 cm^{-1}); this was further confirmed by obtaining the i.r. spectra of higher ZnF_2 loading (6.5 mmol/g) dried at 375K and 873K (figure 3.2). The spectrum of the low drying temperature showed two major bands at 755cm^{-1} and 665cm^{-1} corresponding to AlF_4^- and AlF_3 respectively. As drying

temperature increases unstable AlF_4^- is transformed into AlF_3 (i.r. bands at 665 cm^{-1} and 910 cm^{-1}), and formation of skeletal ZnO is evident (band at 570 cm^{-1}).

^{19}F MAS NMR results confirmed i.r. results on the formation of free Al-F species. Low loading samples showed asymmetrical spinning side bands which indicate formation of surface =Al-F groups (i.e chemisorption of F^- on the surface of Al-O layer), or possibly physisorption or chemisorption of F^- or Si-F species on the surface of SiO_2 tetrahedral layer. ^{19}F NMR studies [64,65] reported that surface Al-F and Si-F groups nearly have the same chemical shift. No clear i.r. evidence appeared to support the existence of the complex SiF_6^{2-}, but we think that F^- attacks the silica layer and pulls off the Si atoms as SiF_6^{2-}, which can easily decompose to SiF_4 and F^- at slightly raised temperatures. As Si atoms are removed from the silica layer, they are replaced by Al atoms. This replacement can be partial at low ZnF_2 loading, or can be maximum at high loadings. The maximum Si tetrahedra to be replaced by Al could reach only 50% according to Loewenstein's rule [92]. This rule is based on Pauling's electrostatic valence rule, which states that two aluminum tetrahedrons cannot be neighbours. For 50% substitution, rigorous alternation between silicon and aluminium tetrahedra becomes necessary. As the ZnF_2 loading increases symmetrical spinning side bands on the sides of ^{19}F NMR signals are observed, which indicate that the surface =Al-F structures are presumably the precursors to the Al-F free species,

and that as the concentration of ZnF_2 increases some of the Al is progressively removed.

What appears to be happening in this fluorination process is that at the low loading of 1.0 mmol/g of ZnF_2-K10, which is a rather less than a monolayer coverage, fluoride ion is replacing the surface hydroxyl groups (Al-OH); this is strongly indicated by our ^{19}F MAS NMR results. At this stage isomorphous replacement of Al by Zn is starting to take place. As the concentration of ZnF_2 increases Al atoms are removed from their layer as Al-F species, and more Zn occupies Al sites. Some Al isomorphously replaces Si in the SiO_2 layer resulting in new AlO_4 tetrahedra; this is strongly indicated by ^{29}Si and ^{27}Al MAS NMR results.

The strong Lewis acidity observed for the ZnF_2-K10 reagents probably stems from the newly generated Lewis acid sites. The first one is generated by the isomorphous replacement of Al by Zn [48,34], which becomes more pronounced at higher loadings of ZnF_2, and consequently leads to the substitution of Si^{4+} by Al^{3+}. This strong Lewis acidity is presumably due to the generation of coordinatively unsaturated sites (strong Lewis acid sites), which accept electrons. Mechanistically, an Al atom has only three valence electrons as compared with four electrons in silicon, and on substituting the latter in the tetrahedron it must attract an additional electron, assuming a negative charge.

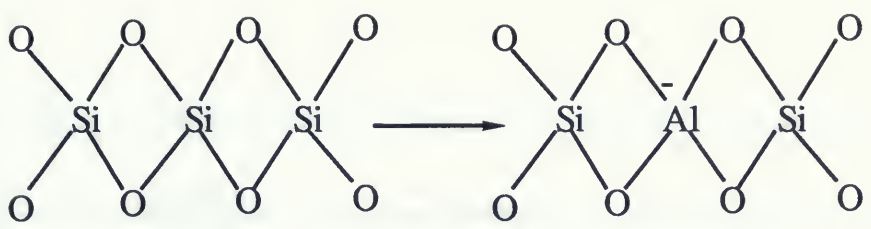

The isomorphous replacement of Zn by Al is also expected to contribute significantly to the strong Lewis acidity, except in this case the acidity results from the greater donation of electrons from the filled oxygen atoms s-orbital to the metal, which increases the partial positive charge on the bonded oxygen atoms that lead to a more stable p*-orbitals, and become better acceptor. Anion vacancies are the other possible source for Lewis acidity and can be easily created, since more Zn^{2+} is added, and most of the F^- is consumed in the formation of AlF free species. Anion vacancies [6] (high Lewis acidity) can capture electrons to form e^- centres. The other major source of Lewis acidity is the surface Al-F groups, which have been studied as strong Lewis acid sites in fluorinated alumina [54], and fluorinated aluminosilicates [30]. These Lewis acid sites (surface =Al-F groups) result in electron deficient centres, as one or probably two of the Al sites in these centres is occupied by highly electronegative F^- ions. To reiterate, one or more of these sites produced the strong Lewis acid that proved to be highly suitable for Friedel-Crafts alkylation.

TEXT CONTINUES ON P.63

Table(3.1) ^{19}F m.a.s. NMR chemical shifts for ZnF_2-K10 reagents, ZnF_2,and some Al-F species.

LOADING MMOL/G	DRYING TEMP./K	$\delta_{F/PPM}$(a)	REFERENCE
1.00	573	-151*	This work
	873	-151*	This work
3.5	573	-153*	This work
	873	-152*	This work
5.0	573	-153	This work
	873	-153	This work
$AlF_3.xH_2O$		-156	64
ZnF_2		-196	86
$[AlF4]^-$		-155	This work
$[AlF6]^{3-}$		-155	This work
$[AlF6]^{3-}$		-156	93
$[AlF]^{2+}$		-156.6	87

[a] measured from $CFCl_3$.

* Isotropic Chemical Shift (σ_{iso}) calculated from the principal components of the chemical shift tensor.

Table(3.2).Friedel-Crafts benzylation of benzyl chloride using ZnF2-K10 reagents[a].

Loading (mmol/g)	Activation Temp./K	benzyl chloride conversion(%)	diphenyl-methane %yield[b]
1.0	573	100	90
	673	90	70
	773	60	40
	873	40	23
3.5	573	80	70
	873	90	80
5.0	573	80	60
	873	90	82

(a) Reaction refluxed at 70C for 30 mintues.
(b) GC yield ,and product confirmed with 1H NMR 3.93(s,2H),7.2(m,10H).

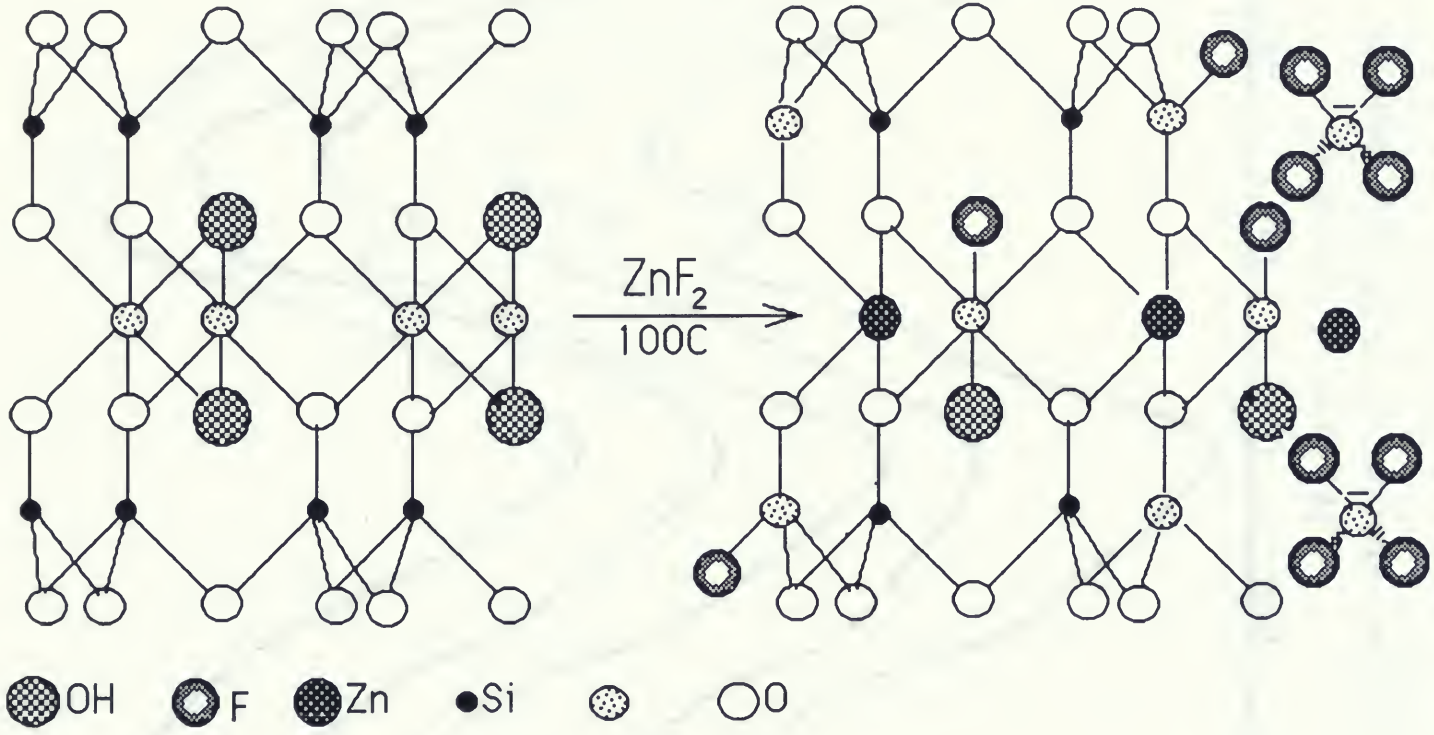

$$Zn(AlF_4)_2 \xrightarrow{300^\circ C} \gamma\text{-}AlF_3 \xrightarrow{700^\circ C} \alpha\text{-}AlF3$$

Scheme(3.1)

The layer structure of montmorillonite K10 showing the occurance of isomorphous replacement of Al^{3+} by Zn^{2+} and Si^{4+} by Al^{3+}, and the formation of Al-F species.

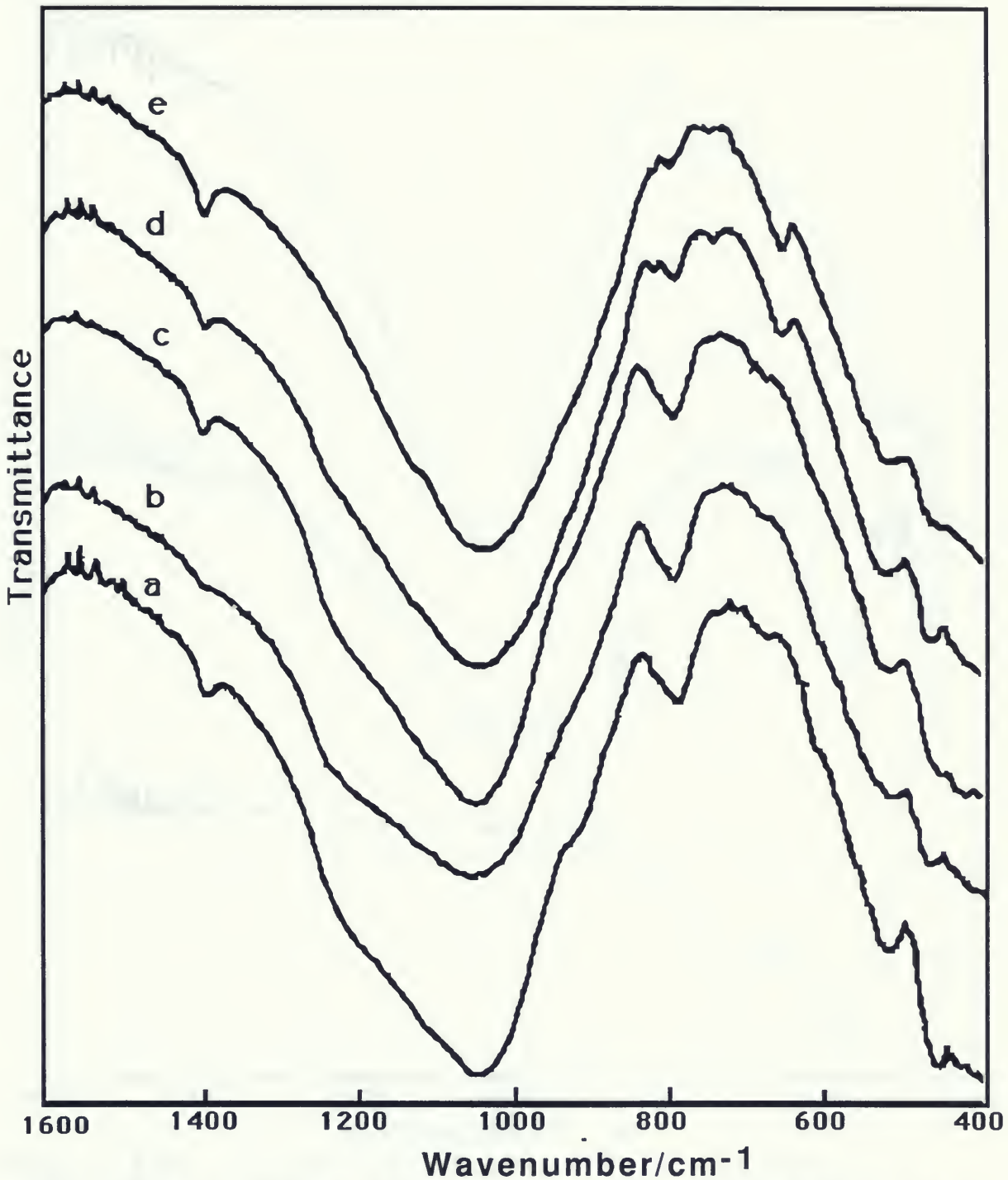

Figure(3.1). Infrared spectra of ZnF2-K10 reagents dried at 573K,
(a)montmorillonite K10 (b) 0.5 mm0l/g (c) 1.0mmol/g
(d) 3.5 mmol/g (e) 5.0 mmol/g.

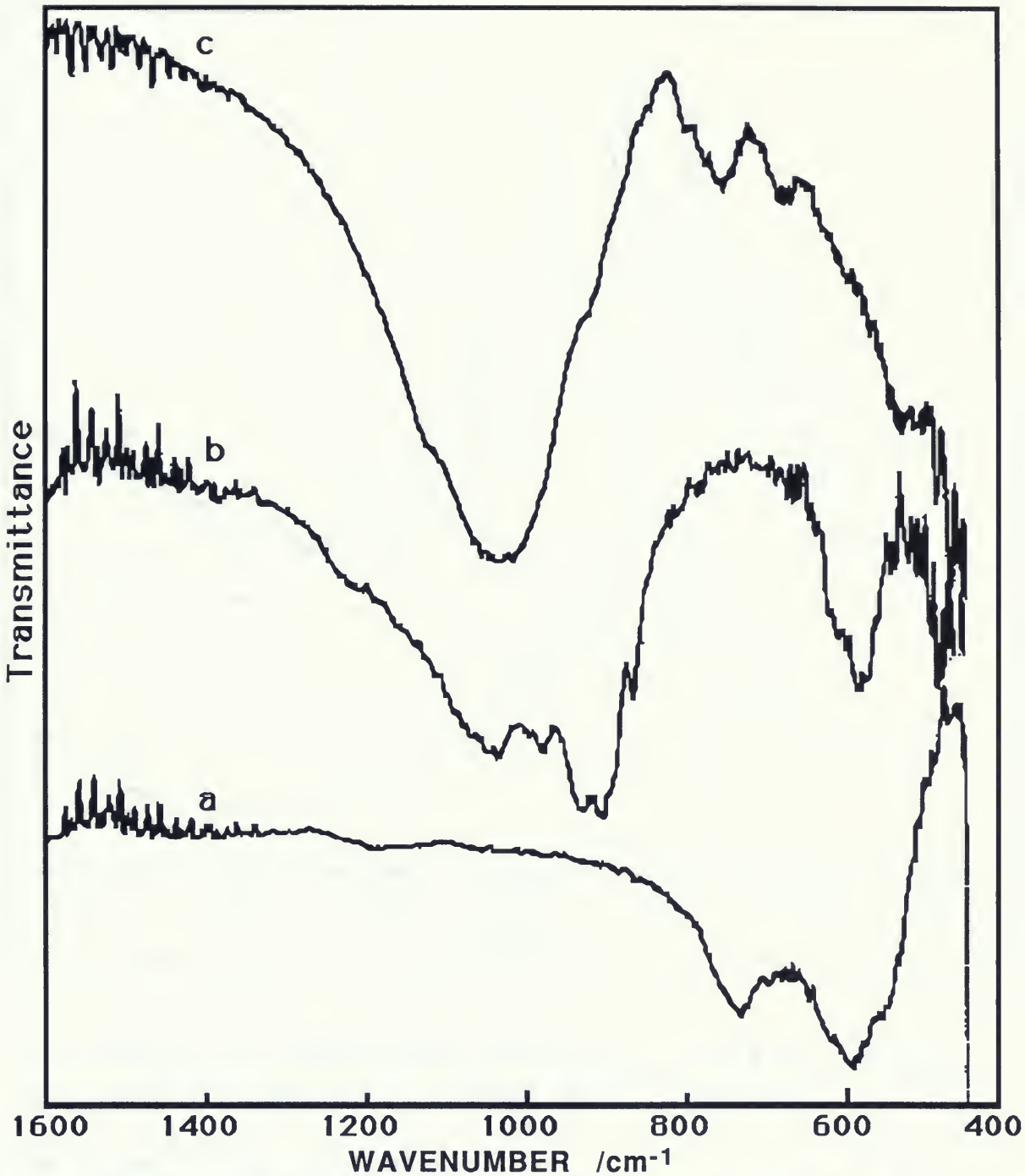

Figure(3.2). Infrared spectra of 6.5 mmol/g ZnF_2-K10 reagents compared to spectra of mixed AlF_6^{3-} and AlF_4^-. (a) Mixture of fluoroaluminosilicate (b)dried at873K (c)dried at373K

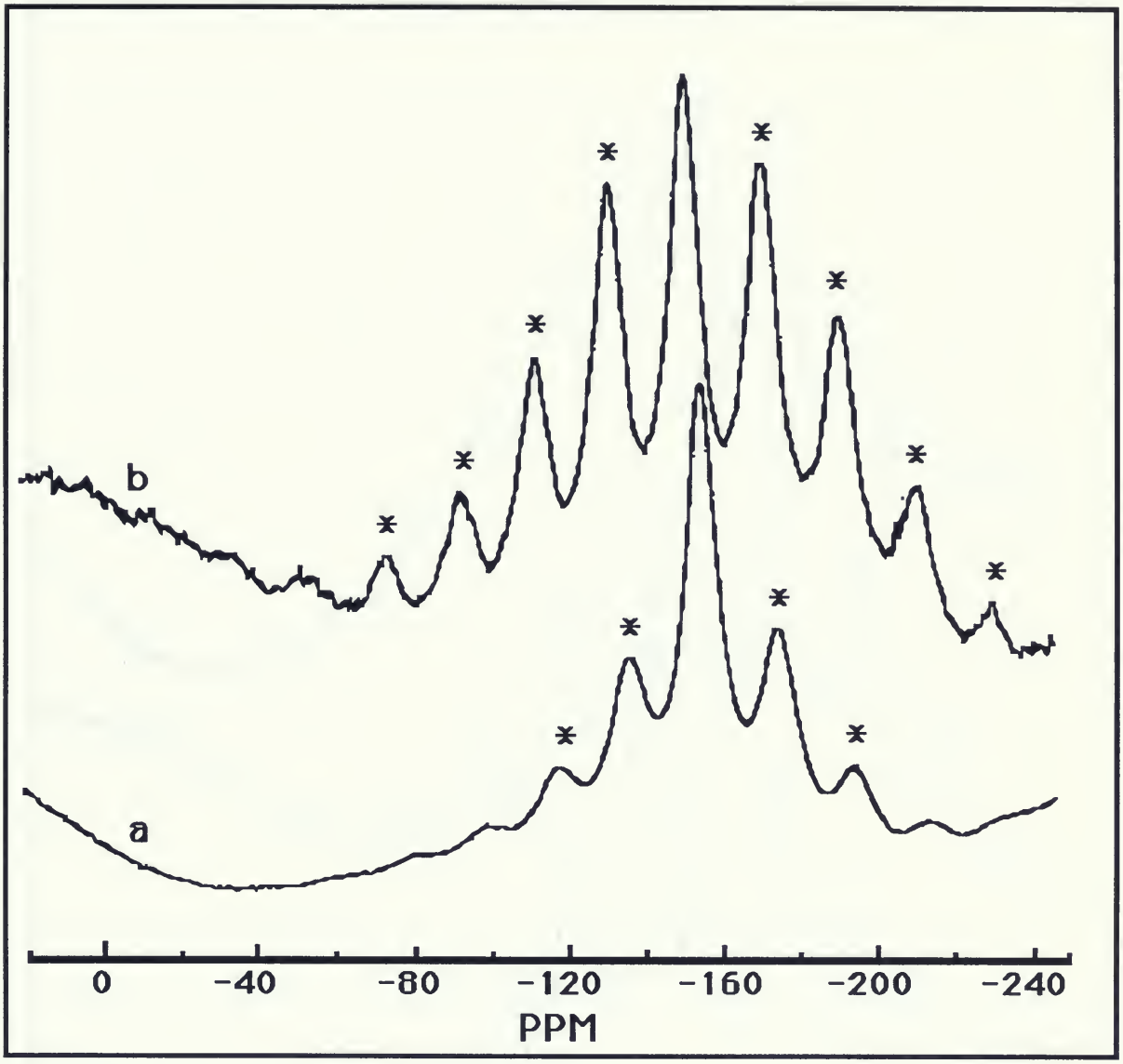

Figure(3.3) ^{19}F MAS NMR spectrum of ZnF_2-K10 reagent compared to spectrum of mixed AlF_6^{3-} and AlF_4^-,

(a) mixed AlF_6^{3-} and AlF_4^-.
(b) 3.5 mmol/g of ZnF_2-K10 dried at 573K.
*spinning side bands.

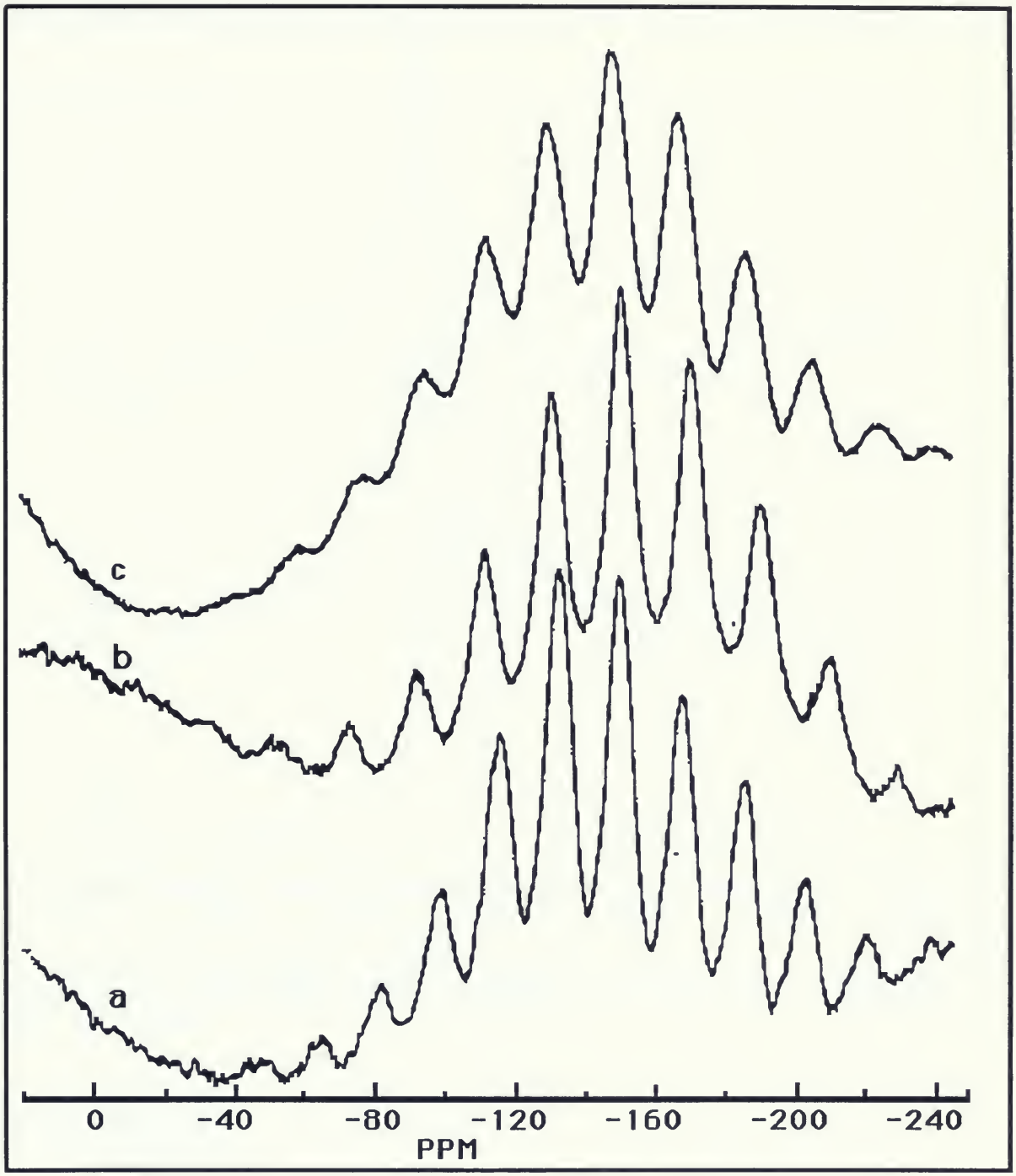

Figure(3.4) ^{19}F **MAS NMR spectra of** ZnF_2**-K10 reagents dried at 573,**

(a) 1.0 mmol/g.
(b) 3.5 mmol/g.
(c) 5.0 mmol/g.

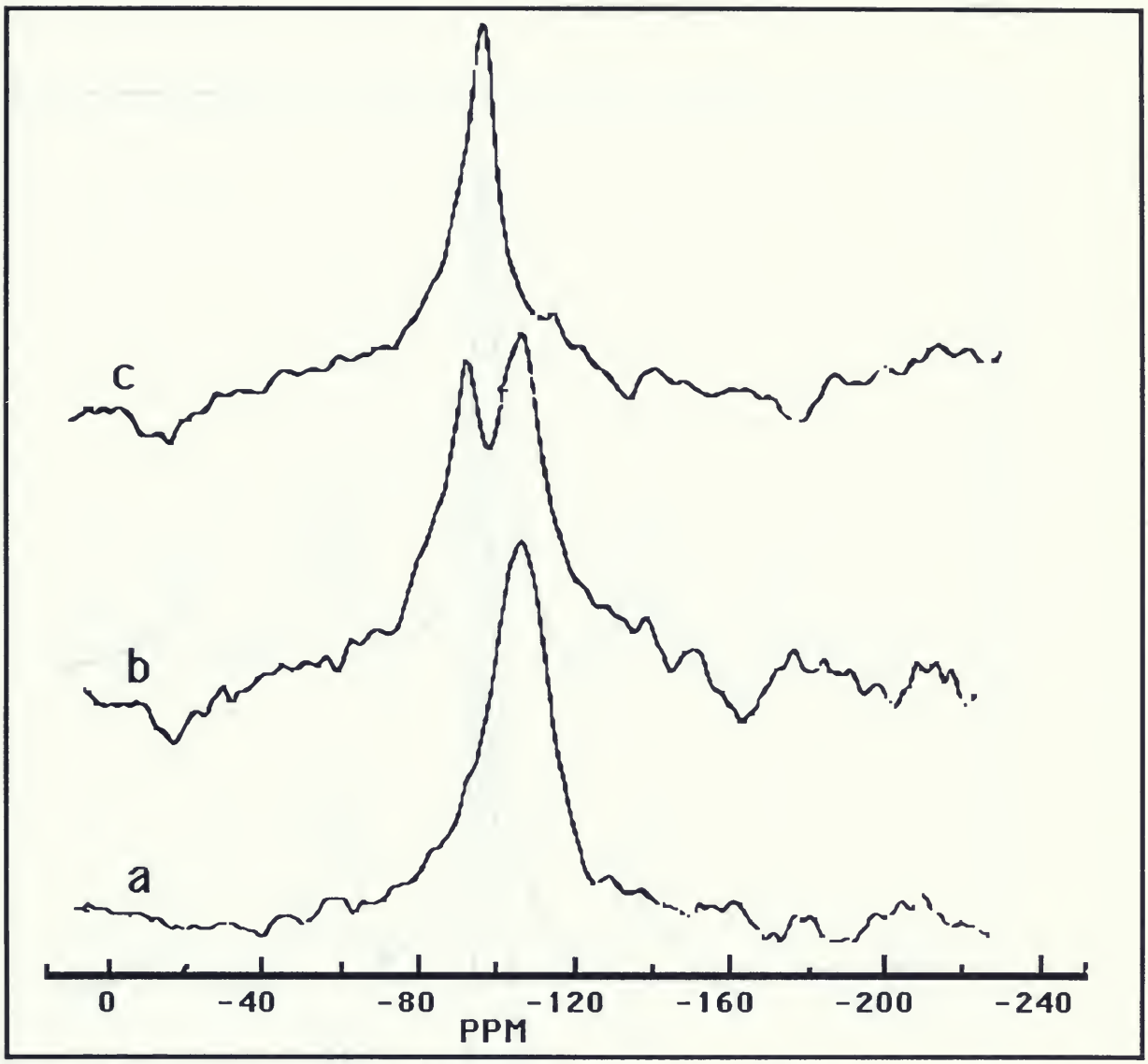

Figure(3.5). ^{29}Si MAS NMR spectra of ZnF_2-K10 reagents dried at 573K.

(a) 1.0 mmol/g.
(b) 3.5 mmol/g.
(c) 5.0 mmol/g.

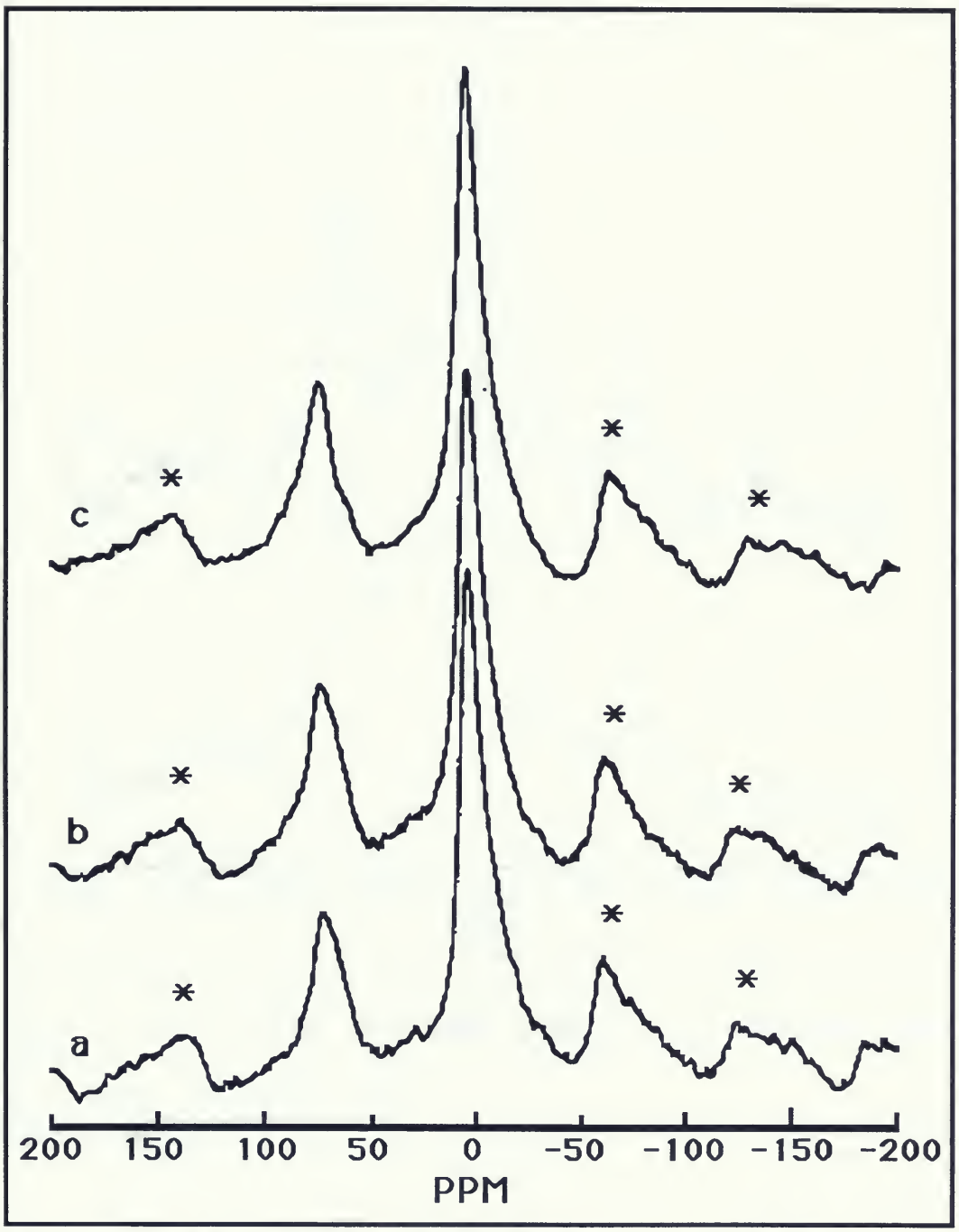

Figure (3.6) ^{27}Al **MAS NMR spectra of** ZnF_2**-K10 reagents dried at 573K,**
(a) montmorillonite K10
(b) 1.0 mmol/g.
(c) 5.0 mmol/g.
*** spinning side bands**

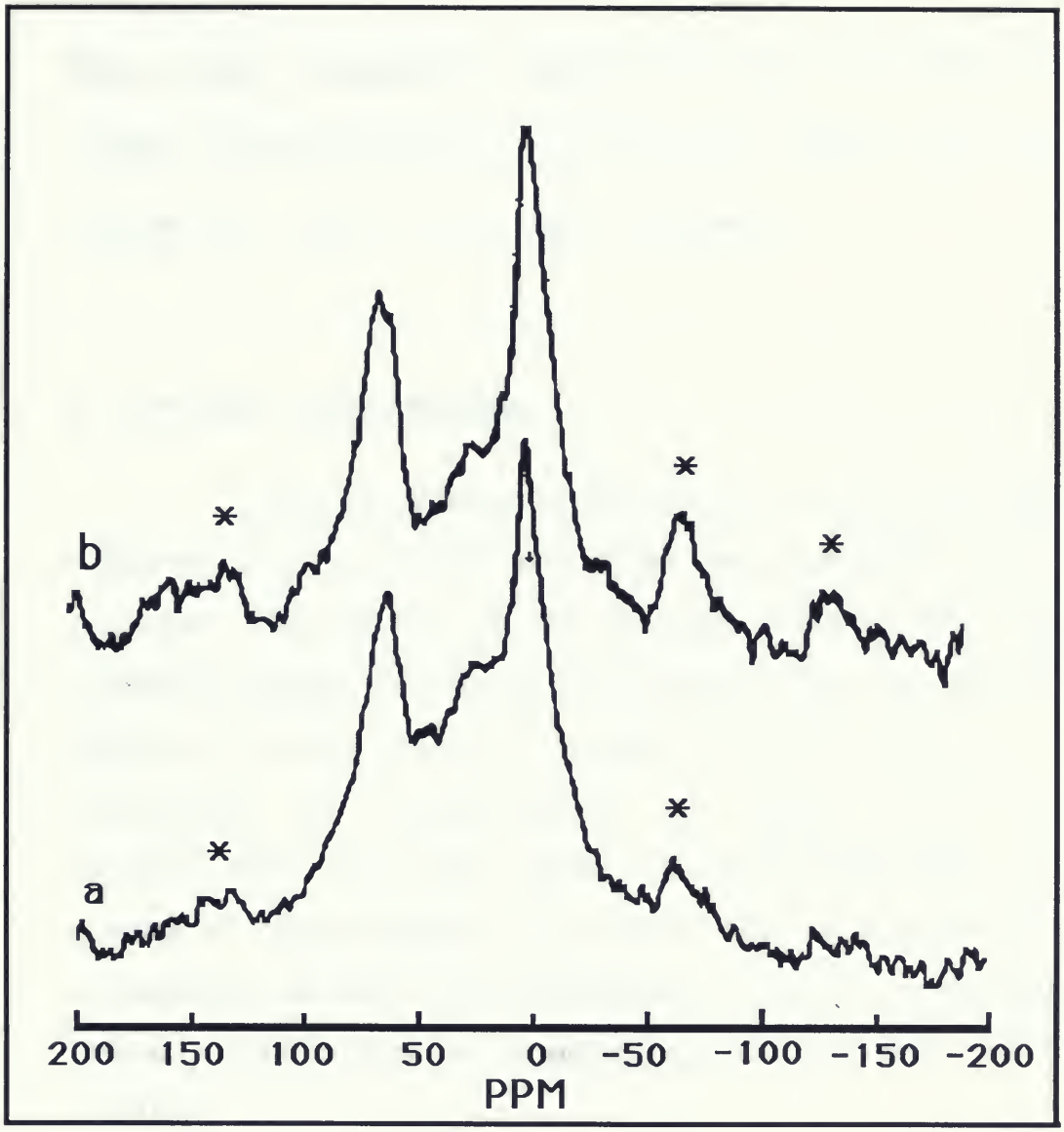

Figure (3.7). 27Al MAS NMR spectra of ZnF2-K10 dried at 873K,
(a) montmorillonite K10
(b) 1.0 mmol/g

III-2. CdF_2 supported montmorillonite K10.(CdF_2-K10).

(Tables, figures for section III.2 are found between p.p72-80)

(Figures AI-7 to AI-11 are found in appendix I)

a. Infrared Spectroscopy.

Infrared spectra of CdF_2-K10 (1.0, 3.5, and 5.0 mmol/g) reagents dried at 573K and 873K were obtained and carefully analyzed. The spectra of the reagents dried at 573K (figure 3.8) showed no major differences among each other, but were remarkably different from the previously studied ZnF_2-K10 reagents. Gradually increasing the concentration of CdF_2 on the surface of montmorillonite does not appear to have any effect on the i.r. spectra of these reagents (figure 3.8). The band at 802 cm^{-1}, which corresponds to layer SiO_4 tetrahedra remained unchanged in both intensity and shape, as loading approached the maximum (5.0 mmol/g).

Increasing the calcining temperature to 873K produced a small effect on the highly loaded sample 5.0 mmol/g (figure AI-7), which can be seen from the distortion of the band at 802cm^{-1}. Infrared spectra of the additional reagent of the loading of 6.5 mmol/g dried at 373K and 873K (figure AI-8) were examined to see the effect of high concentration of CdF_2 on montmorillonite. The

spectrum of the sample dried at low temperatue showed a band ranging from 802cm^{-1} to 760cm^{-1}, which presumably indicates formation of the Al-F free species AlF_4^-. The highly dried sample showed no evidence of the band at 802cm^{-1}.

b. ^{19}F MAS NMR Spectroscopy.

^{19}F NMR spectra of CdF_2-K10 (11.0, 3.5, and, 5.0 mmol/g) reagents dried at 573K and 873K were recorded and analyzed. Spectra of these reagents showed some remarkable changes when compared with ZnF_2-K10 reagents. The spectra of the low loading reagent 1.0 mmol/g dried at 573K and 873K (figure 3.9) produced similar results to those of the corresponding ZnF_2-K10 reagents. Asymmetric spinning side bands were the characteristic feature of these spectra, which corresponds to chemisorption of F^- on the surface of the Al-O layer. The central band has a chemical shift of -152 ppm. This chemical shift may also correspond to chemisorbed or physisorbed F^- or other Si-F species on the surface of the SiO_2 tetrahedral layer of montmorillonite K10 [64,65] .

^{19}F NMR spectra of the highly loaded CdF_2-K10 (3.5, and 5.0 mmol/g) dried at 573K (figure AI-9) also showed asymmetric spinning side bands surrounding the central band at -150 ppm. However, a very noticable change is the broadening of the spectrum which is presumably due to ^{19}F-^{19}F dipolar interactions in the layer AlO_4F_2 group (scheme 3.2). As the calcining temperature increased to 873K, the ^{19}F NMR spectrum of the intermediate loading 3.5 mmol/g (figure 3.20b) showed a clearly observable shift of a signal

at -152 ppm (corresponding to Al-F species) to a signal at -200 ppm, which presumably corresponds to CdF_2 (lit. value -196 ppm). The high loading CdF_2-K10 sample 5.0 mmol/g dried at 873K responded with an ^{19}F NMR signal at -199 ppm surrounded by symmetrical spinning side bands. These spinning side bands tend to be further away from the central peak, which indicates that this signal corresponds to a single crystal, presumably CdF_2. Figure Al-10 compares the spectrum of CdF_2 to that obtained from the highly loaded and dried CdF_2-K10 reagent.

c.^{29}Si MAS NMR Spectroscopy.

^{29}Si NMR spectra of CdF_2-K10 (1.0, 3.5, and 5.0 mmol/g) reagents dried at 573K and 873K were obtained. As with the infrared spectra, the ^{29}Si NMR spectra of these reagents showed no apparent changes in the ^{29}Si signal as the concentration of CdF_2 or drying temperature changed. Spectra of the CdF_2-K10 reagents dried at 573K (figure 3.11) show a signal at a chemical shift of -108 ppm, which corresponds to $^{29}Si(OSi)_3(OAl)$ [91]. Figure 3.22 also shows that, as the concentration of CdF_2 increases from 1.0 to 5.0 mmol/g, so the signal remains unchanged in shape and position.

As the drying temperature increased to 873K, the ^{29}Si NMR signals for the reagents 1.0, 3.5, 5.0 mmol/g of CdF_2-K10 (figure Al-11) showed no significant shift away from -109ppm. The shape of the signal, however tends to slightly broaden compared to that of the moderately dried reagents. This broadening is

presumably due to increased disorder introduced by heating, or perhaps by the closer approach of the paramagnetic Fe^{3+} site to the ^{29}Si environment, since this broadening is not influenced by the other changing variable, CdF_2 concentration.

d.^{27}Al MAS NMR Spectroscopy.

^{27}Al NMR spectra of CdF2-K10 (1.0, and 5.0 mmol/g) reagents dried at 573K and 873K, showed significant differences as loading and drying temperature varied. Spectra of the low loading sample (1.0 mmol/g) dried at 573K and 873K (figure 3.12) clearly show the effect of calcining temperature on this reagent. One of these effects is the significant change in chemical shift observed for the tetrahedral site at both drying temperatures. The low temperature dried reagent resulted in a tetrahedral site (AlO_4) signal at 69ppm, whereas the highly dried reagent showed a signal at 61ppm. The other change is the marked increase in the intensity of the tetrahedral signal, which indicates that this tetrahedral environment exists in higher concentration. A slight decrease in the intensity of the octahedral aluminium signal positioned at 3ppm, can also be observed for the highly dried reagent.

^{27}Al NMR spectra of the sample with higher loading (5.0 mmol/g) dried at 573K and 873K are shown in figure 3.13. Again, the sample dried at the lower temperature showed a signal at 69ppm which corresponds to one of the tetrahedral sites, but the highly dried sample showed signals at both 61ppm and 69ppm, which clearly indicates that there are two different tetrahedral sites

available. No significant shift is observed for the octahedrally coordinated aluminum at 3ppm. There is however a noticeable decrease in the intensity of this signal as the drying temperature is increased to 873K.

e.Friedel-Crafts Alkylation.

The Friedel-Crafts benzylation of benzene was used as a model system for the study of the catalytic activity of montmorillonite K10 supported CdF_2. Samples of CdF_2-K10, prepared at a range of loadings (1.0, 3.5, and 5.9 mmol/g), and dried at 573K and 873K, were used. The observed yields of diphenylmethane are given in table 3.3. The reactivity of these reagents also showed dependence on the loading used and activation temperature. The low loading 1.0 mmol/g reagent appeared to be quite active at the low activation temperature 573K. It resulted in a nearly complete conversion of benzyl chloride, whereas the highly activated reagent showed markedly less conversion of benzyl chloride, and consequently a lower yield of diphenylmethane.

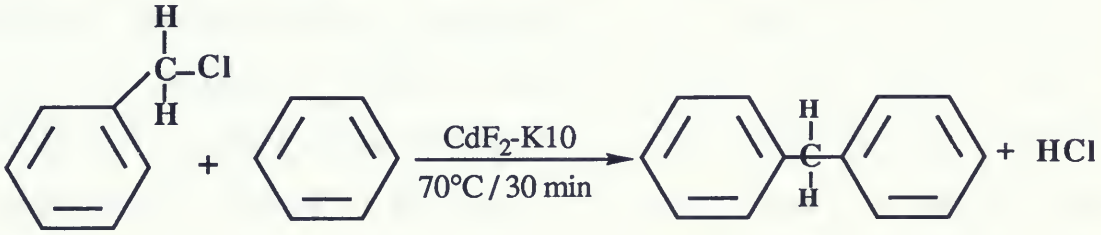

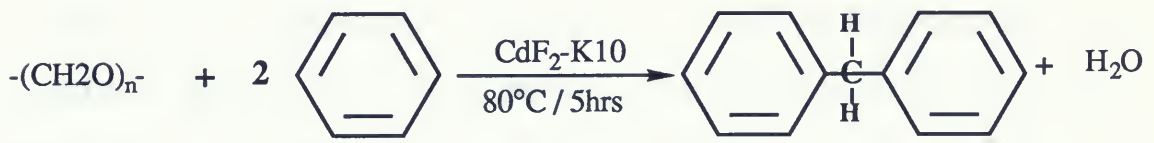

Highly loaded reagents (3.5 and 5.0 mmol/g) were not as active as those of the corresponding ZnF_2-K10 reagents. The high activation temperature of the intermediate loading reagent 3.5 mmol/g did not have an apparent effect on the reactivity of this reagent, but this high activation temperature improved the conversion of benzyl chloride for the high loading reagent (5.0 mmol/g). To further evaluate the reagent of 1.0 mmol/g of CdF_2-K10, Friedel-Crafts benzylation of benzene with paraformaldehyde was tested; the yield was slightly lower than that of the corresponding of ZnF_2-K10 reagent.

f.discussion.

The results I have presented above indicate various changes taking place on the surface and within the layers of the structure of montmorillonite K10 as it is coated with CdF_2. Infrared spectroscopy results did not show any noticeable evidence of the structural changes that are expected to take place, as observed for ZnF_2-K10 reagents. The i.r. band observed at 802cm-1, which corresponds to layer SiO_4 tetrahedra remained unchanged at all CdF_2 concentrations (figure 3.8), which indicates that the silica layer remained almost undisturbed. ^{19}F NMR spectra, however, indicated major changes as shown in scheme 3.2. These changes are dependent on the concentration of CdF_2 and the drying temperature. Low loading reagent (1.0 mmol/g which corresponds to rather less than a monolayer coverage) dried at 573K behaved similarly to that of the

corresponding ZnF_2-K10 reagent. The CdF_2-K10 reagent also showed asymmetrical spinning side bands which indicate the formation of surface Al-F groups or possibly Si-F groups, since F^- can easily replace surface OH groups.

As the CdF_2 concentration increased to 3.5 and 5.0 mmol/g (still dried at 573K), further replacement of surface OH groups by F^- is observed, presumably forming surface AlO_4F_2 groups (scheme 3.2). These groups are evident from the large broadening of the ^{19}F NMR spectrum of these samples, which is presumably due to ^{19}F-^{19}F dipolar interactions (figure AI-9). Then as the calcining temperature increased to 873K, Cd^{2+} tends to pull off F^- ions from the Al-O layer to form CdF_2, as is evident from the ^{19}F NMR signal at -199ppm (figure 3.10). The most important feature in the ^{27}Al NMR spectra is the observation of signals corresponding to two different tetrahedral Al sites. One is observed for the reagents dried at 573K, and located at 69ppm, and an additional signal is observed for reagents dried at 873K, positioned at 61ppm. The notable observation of the highly loaded CdF_2-K10 reagents is that both tetrahedra seem to exist at high calcining temperature, since ^{27}Al NMR shows both signals for this reagent (figure 3.13).

A number of chemical reactions appear to take place as we fluorinate montmorillonite K10 with CdF_2. Some of these changes are clearly represented in scheme 3.2, as depicted by the various spectroscopic techniques applied. Chemically, it is expected that the divalent Cd^{2+} ion will isomorphously replace trivalent Al^{3+}, however we expect only partial replacement, and not as

extensive replacement as we saw for the Zn^{2+} ion. This partial replacement is evident from infrared spectra, since it showed no significant changes in the SiO_2 tetrahedral layer. This conclusion was made on the basis that if a large number of Al atoms was replaced by Cd atoms the Al atoms would subsequently replace Si atoms. At low CdF_2 concentration (1.0mmol/g) F^- partially replaced surface hydroxyl groups in the octahedral layer. As the concentration of CdF_2 increased more surface hydroxyl groups are replaced, to resulting in the surface formation of AlO_4F_2 groups, as evident from the ^{19}F NMR spectra. Chemically, fluoride ions are expected to pull off some Si atoms from the SiO_2 tetrahedral layer, and form the thermally unstable SiF_6^{2-} complex, but there is no clear evidence to confirm this suspiscion.

High calcining temperatures resulted in new chemical changes. First, the regeneration of CdF_2 compound was confirmed by comparing the ^{19}F NMR spectra of these reagents to the spectrum of CdF_2. This may be due to the availability of a large number of unconsumed Cd^{2+} ions. The other change has to do with the new Al tetrahedral site, that is evident from ^{27}Al NMR spectra. This new site is presumably due to the isomorphous replacement of Si by Al in the SiO_2 tetrahedral layer [90].

The observed Lewis acidity of the CdF2-K10 reagents seem to be stemming from various numbers of possible Lewis acid sites. The primary suspected Lewis acid site due to partial isomorphous replacement of Al by Cd, which cosequently results in the substitution of Si^{+4} by Al^{3+} that is kown to be responsible for

the catalytic properties of aluminosilicates, because it generates Lewis acid centres characterized by a high deficiency of electrons.

The other potential Lewis acid site that is expected to contribute to the overall activity of these catalysts is the aluminum fluoride surface groups . These sites also are expected to result in electron deficient centres [54,30], since one or more of the aluminum sites is occupied by the highly electronegative F^- ions. This is based on the fact that, the ability of a Lewis acid to accept an electron pair would be greater the greater the electronegativity of the central atom and the greater the number and electronegativity of the attached atoms or groups [94].

TEXT CONTINUES ON P.81

Table(3.3) ^{19}F m.a.s. NMR chemical shifts for CdF_2-K10 reagents, and CdF_2.

LOADING MMOL/G	DRYING TEMP./K	$\delta_{F/PPM}$[a]	REFERENCE
1.00	573	-150*	This work
	873	-153*	This work
3.5	573	-150*	This work
	873	-152, -198	This work
5.0	573	-150	This work
	873	-197	This work
CdF_2		-197	This wrok
CdF_2		-196	86

[a] measured from $CFCl_3$.

* Isotropic Chemical Shift (σ_{iso}) calculated from the principal components of the chemical shift tensor.

Table(3.4).Friedel-Crafts benzylation of benzyl chloride using CdF2-K10 reagents[a].

Loading (mmol/g)	Activation Temp./K	benzyl chloride conversion(%)	diphenyl-methane %yield[b]
1.0	573	90	90
	873	60	40
3.5	573	50	60
	873	40	40
5.0	573	50	60
	873	60	80

(a) Reaction refluxed at 70C for 30 mintues.
(b) GC yield ,and product confirmed with 1H NMR 3.93(s,2H),7.2(m,10H).

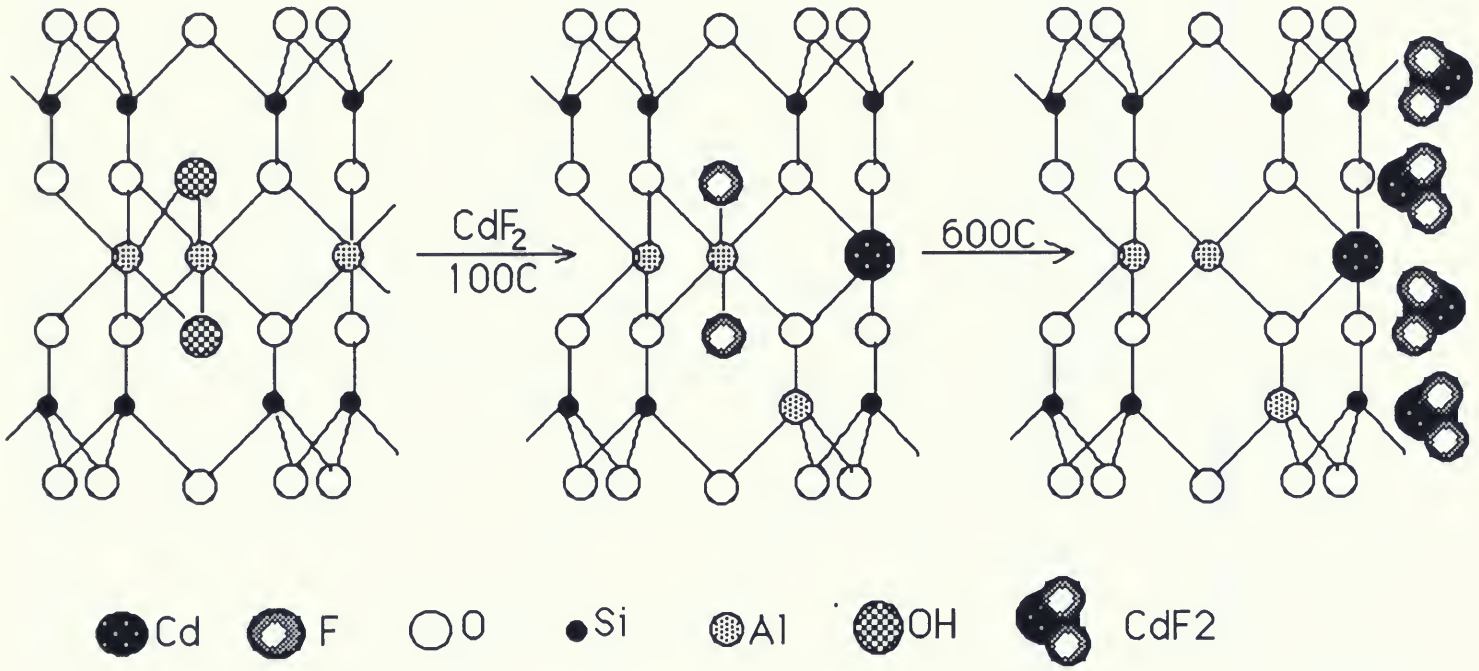

Scheme(3.2)

The layer structure of montmorillonite K10 showing the occurance of isomorphous replacement of Al^{3+} by Cd^{2+} and Si^{4+} by Al^{3+}, and the formation of CdF_2.

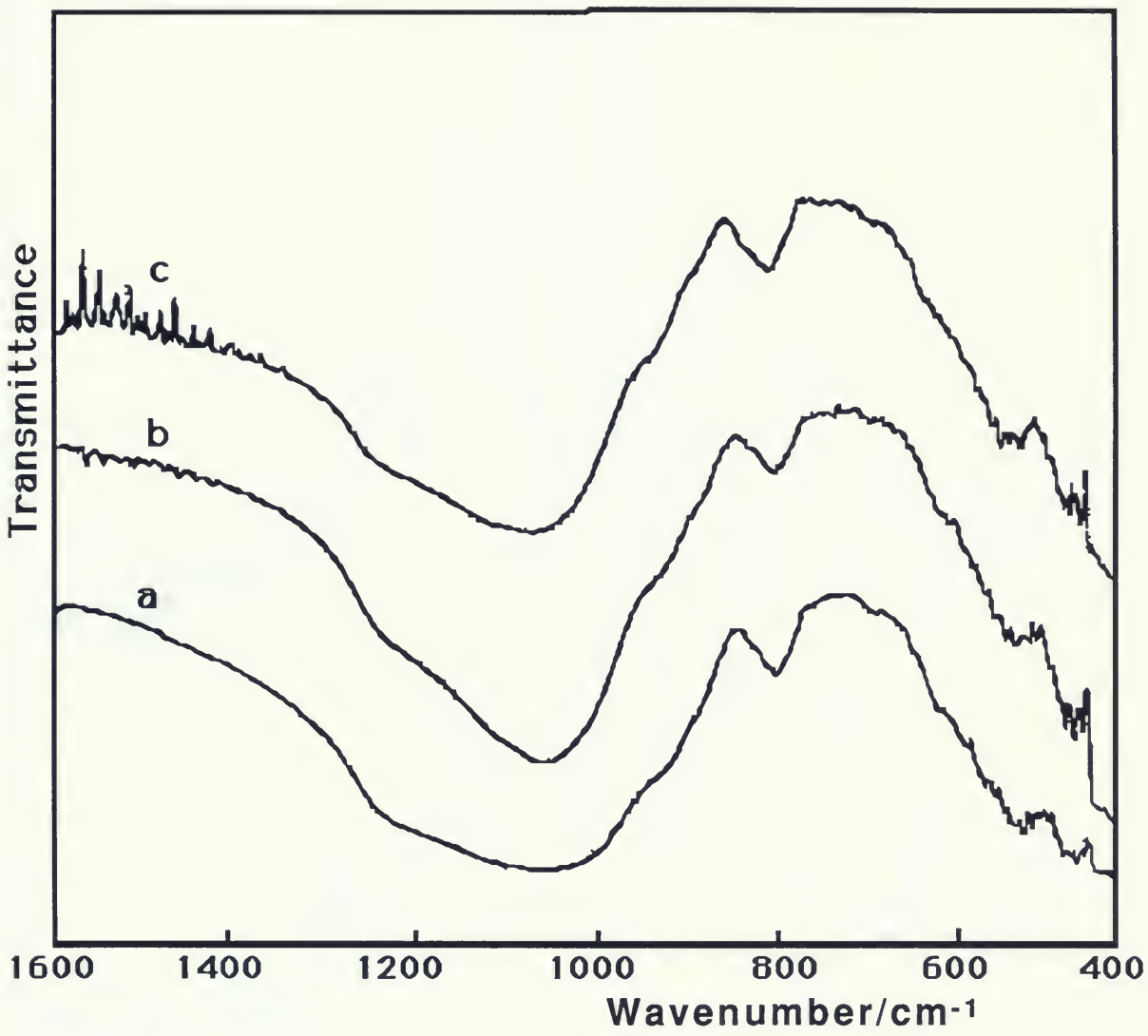

Figure(3.8) Infrared spectra of CdF_2-K10 reagents dried at 573K,
(a) 1.0 mmol/g
(b) 3.5 mmol/g
(c) 5.0 mmol/g

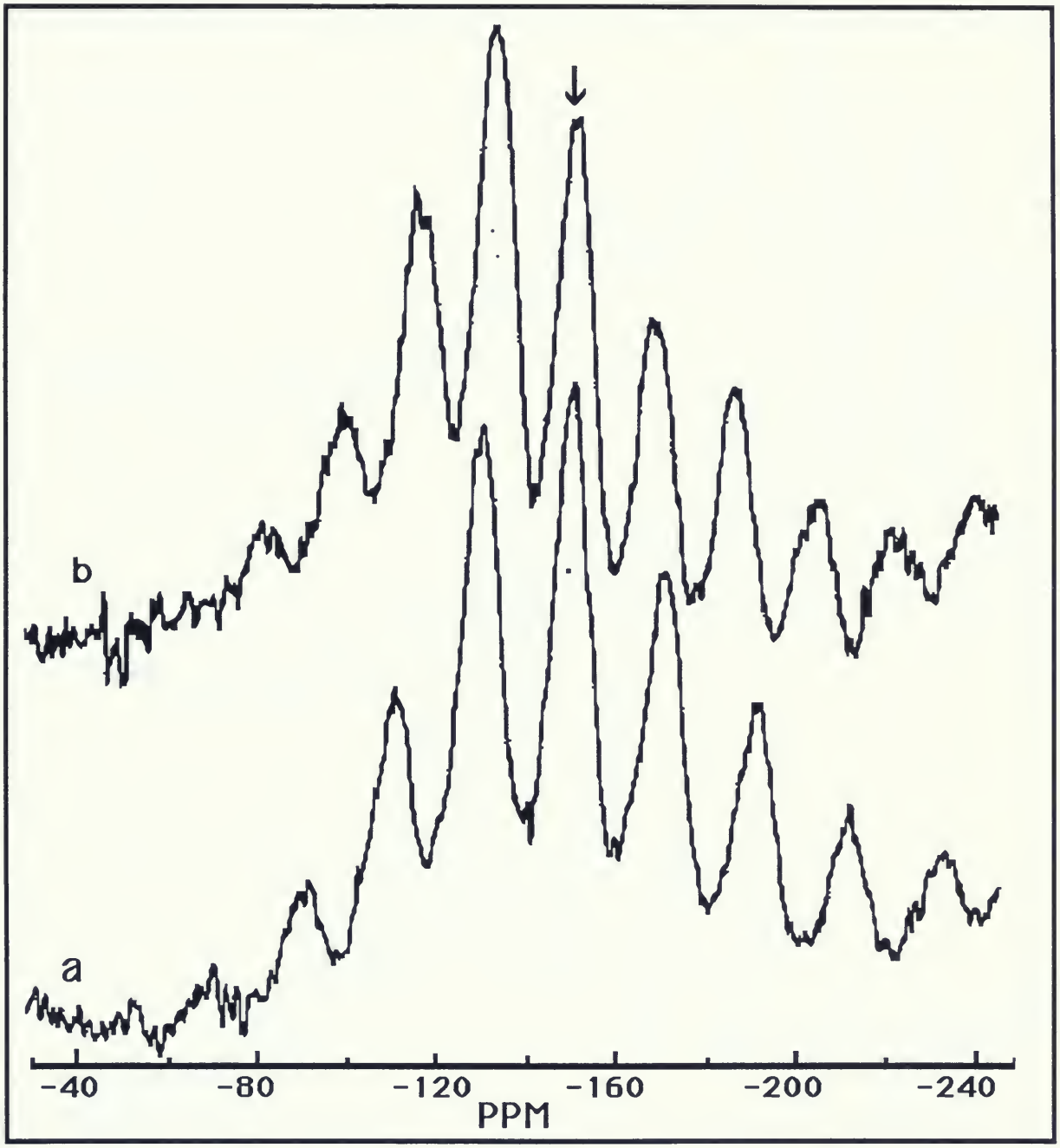

Figure(3.9) ^{19}F **MAS NMR spectra of 1.0 mmol/g of** CdF_2**-K10 reagents dried at,**

(a) 573K.
(b) 873K.
[arrow points towards central peak]

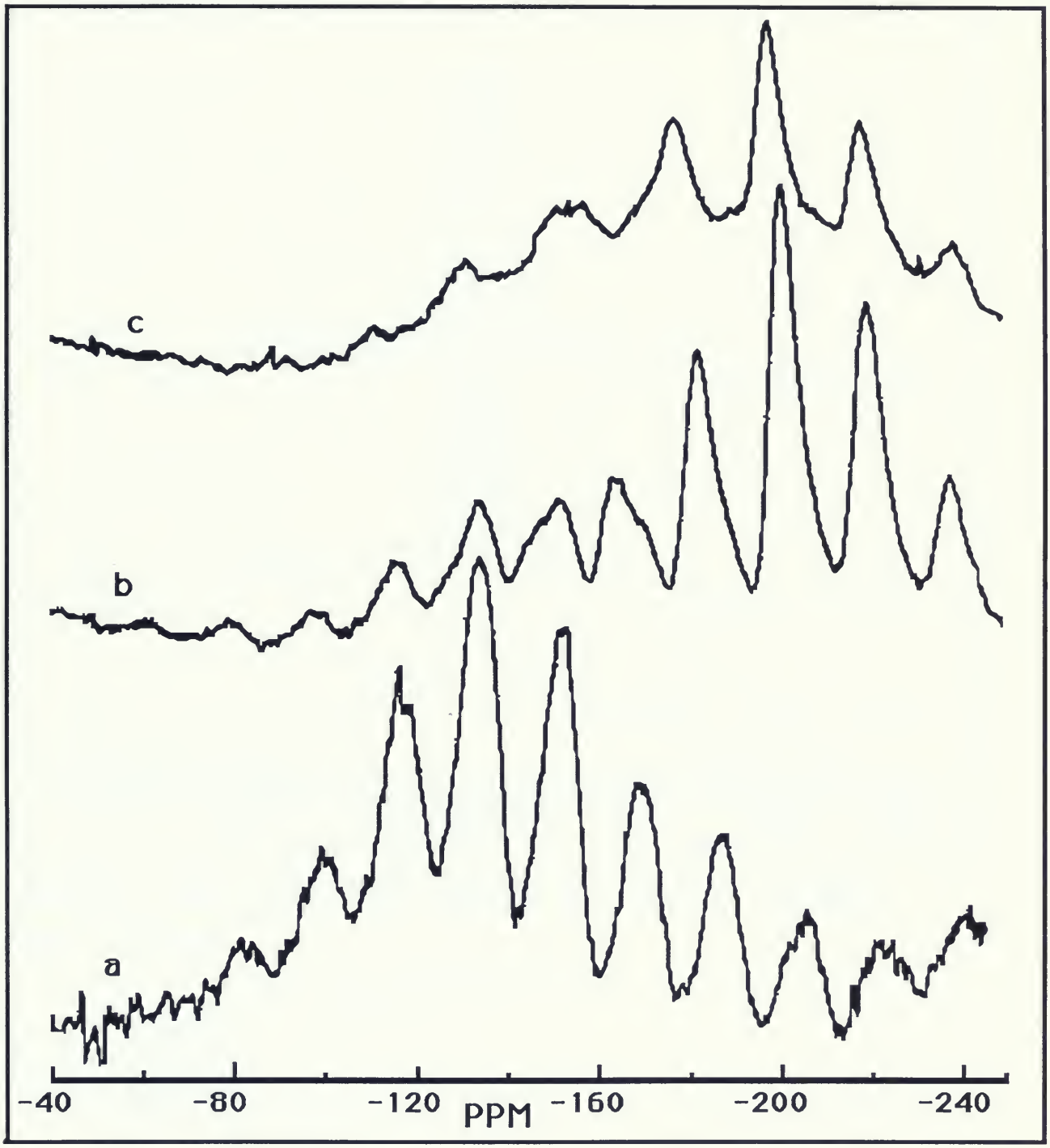

Figure(3.10) ^{19}F **MAS NMR spectra of** CdF_2**-K10 reagents dried at 873K,**
(a) 1.0 mmol/g.
(b) 3.5 mmol/g.
(c) 5.0 mmol/g.

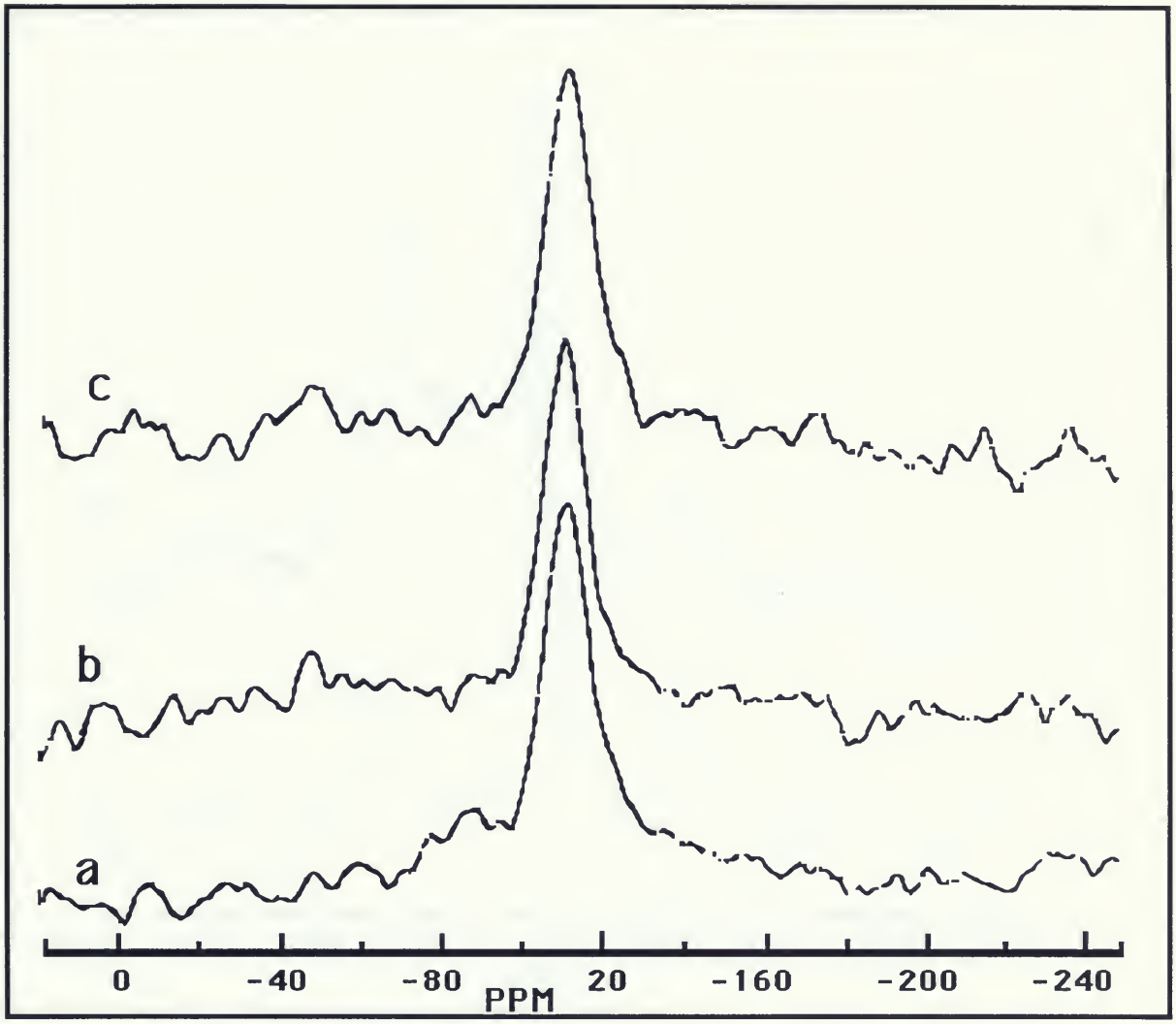

Figur(3.11). 29Si MAS NMR spectra of CdF2-K10 reagents dried at 573K.

(a) 1.0 mmol/g.
(b) 3.5 mmol/g.
(c) 5.0 mmol/g.

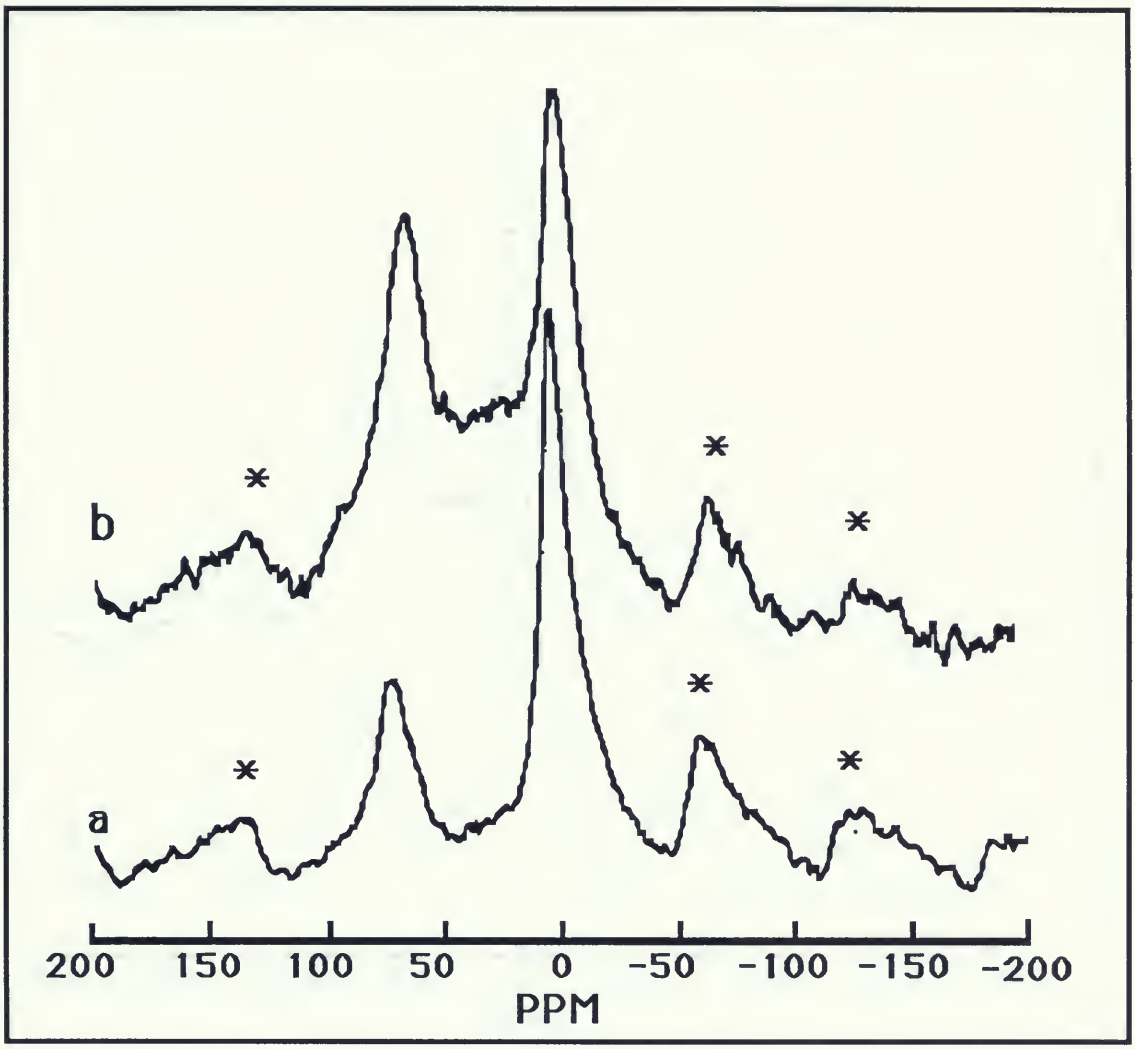

Figure(3.12) ^{27}Al MAS NMR spectra of 1.0 mmol/g of CdF_2-K10 reagent dried at,
(a) 573K.
(b) 873K.
*spinning side bands

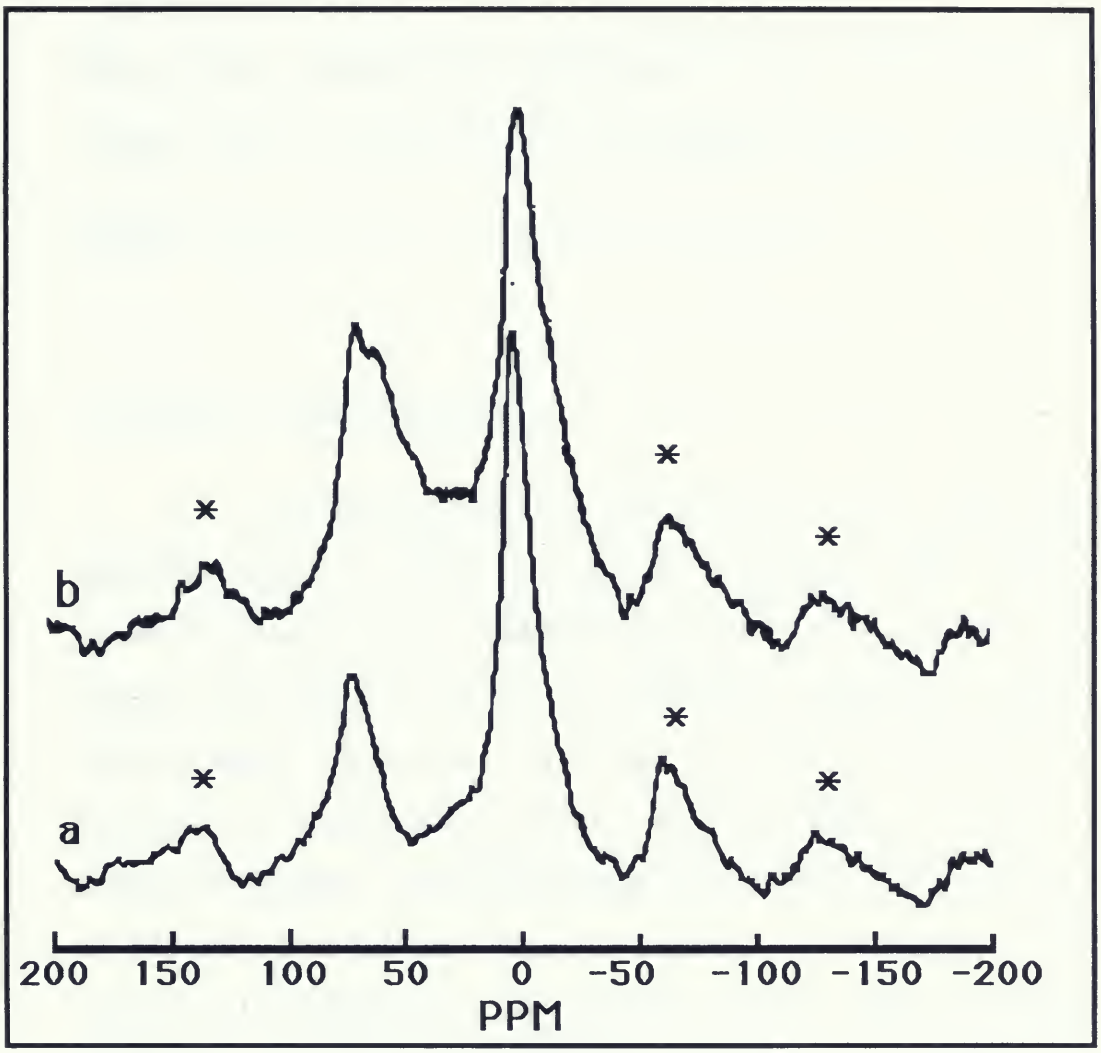

Figure(3.13) ^{27}Al MAS NMR spectra of 5.0 mmol/g of CdF_2-K10 reagents dried at

(a) 573K.
(b) 873K.
* spinning side bands.

III-3. CuF_2 supported montmorillonite K10.(CuF_2-K10).

(Tables, figures for section III.3 are found between p.p 89-97)

(Figures AI-12 to AI-14 are found in appendix I)

a.Infrared Spectroscopy.

Infrared spectra of CuF_2-K10 (1.0, 3.5, and 5.0 mmol/g) reagents dried at 573K and 873K appeared rather different from those of the previous studied reagents ZnF_2-K10 and CdF_2-K10. Figure 3.14 shows spectra of CuF_2-K10 reagents dried at 573K, which clearly illustrates the effect of CuF_2 concentration on the structure of montmorillonite K10. As the loading of CuF_2 increases a band at 802cm^{-1} gradually disappears, and consequently new bands at 743cm^{-1} and 668cm^{-1} start to appear. As the CuF_2 concentration reached a maximium (5.0 mmol/g) these bands become clearly resolved. The bands at 802cm^{-1} and 668cm^{-1} correspond to SiO_4 tetrahedra and AlF_3 respectively, and the band at 743cm^{-1} corresponds to either AlF_4^- (lit value 760cm^{-1}[84]) or SiF_6^{2-} (lit. value 740cm^{-1}[84])

High calcining temperature (873K) resulted in a significant effect on these samples. As shown on figure AI-12, the band at 802cm^{-1} gradually disappears, but this effect is as a result of CuF_2 concentration increase. The band at 743cm^{-1} is not observed at this high drying temperature, which indicates that this band clearly corresponds to thermally unstable species such as SiF_6^{2-}. A

shoulder at 668cm^{-1} still can be seen for these reagents, and it becomes more prnounced as the concentration of CuF_2 is increased to maximium. To confirm these observations i.r. spectra of another loading (6.5 mmol/g) dried at 373K aand 873K were obtained (figure AI-13). The band at 743cm^{-1} is shown to be quite intense for the reagent dried at 373K. The highly dried reagent showed only a small band at 688cm^{-1}, and total removal of the band at 743cm^{-1}.

b.^{19}F MAS NMR Spectroscopy.

^{19}F NMR spectral results for CuF_2-K10 (1.0, 3.5, and 5.0 mmol/g) reagents dried at 573K and 873K were obtained and analyzed. Spectra of the low loading reagent 1.0 mmol/g dried at 573K and 873K shown on figure 3.15, appeared to be similar to those of the corresponding CdF_2-K10 and ZnF_2-K10 reagents. Perhaps the most characteristic feature of these spectra is the high irregularities of the spinning side bands surrounding the central peak at -149 ppm. These asymmetrical spinning side bands, as discussed previously seem to be due to chemisorbed fluoride ions or physisorbed Al-F or Si-F species on the surface of montmorillonite K10. Surface Si-F was reported to have a chemical shift at -152ppm and Al-F groups at -154ppm [64,65]. Data reported by Schlup et.al. suggest that the Al-F bond in the lightly fluorinated alumina are chemically similar to those of $AlF_3.xH_2O$. Chemisorption of fluoride ions is highly expected to take place, since these ions have the tendency to replace surface hydroxyl groups. It is not clear whether

this chemisorption takes place on the surface of the silicate sheet or the aluminum octahedral layer.

Spectra of the high loading reagent 3.5 mmol/g dried at 573K and 873K shown on figure 3.16, surprisingly showed no significant difference from those of the low loading reagent (1.0 mmol/g). The absence of the symmetrical spinning side bands for this high loading reagent clearly indicates the absence of free aluminum fluoride or silicon fluoride species. The central peak for the highly loaded reagent also appeared at -149 ppm, which is presumably due to physisorbed Si-F or Al-F species on the surface of montmorillonite K10. Table 3.5 summarises the chemical shift values obtained for these reagents.

c. ^{29}Si MAS NMR Spectroscopy.

^{29}Si NMR spectra of CuF_2-K10 (1.0, 3.5, and 5.0 mmol/g) reagents dried at 573K and 873K also appeared to be slightly different from the corresponding CdF_2-K10 and ZnF_2-K10 reagents. Spectra of the samples dried at 573K showed marked differences among each other (figure 3.17). As the concentration of CuF_2 increased the signal gradually broadened and a shoulder at -96 ppm became more pronounced as the concentration of CuF_2 reached a maximum. This shoulder clearly indicates the presence of a new ^{29}Si environment. Similar to that of the parent clay, CdF_2-K10, and the ZnF_2-K10 reagents CuF_2-K10 also showed the main signal to be

positioned at -107ppm, which corresponds to the group $^{29}Si(OSi)3(OAl)$ [91].

Spectra of the reagents dried at the high calcining temperature 873K, showed no apparent change from those of the samples dried at low calcining temperature. The high loaded sample, however, resulted in a spectrum showing the shoulder at -96 ppm beginning to resolve (figure AI-14). This shoulder presumably corresponds to the group $^{29}Si(OSi)_2(OAl)_2$.

d.^{27}Al MAS NMR Spectroscopy.

^{27}Al NMR spectra of CuF_2-K10 (1.0, 3.5, and 5.0 mmol/g) reagents dried at 573K and 873K showed some similarities to those of CdF_2-K10 reagents. Spectra of the low loading reagent 1.0 mmol/g dried at 573K and 873K are shown on figure 3.18 illustrate some structural changes taking place in the layers of montmorillonite. These changes appear to occur mainly around the tetrahedrally and octahedrally coordinated aluminium. This can be seen from the strong intensity of the tetrahedral signal at 62 ppm of the sample dried at 873K. A hint of apeak at 30 ppm, which presumably corresponds to pentahedrally coordinated aluminium also becomes more noticeable for the highly dried sample. The other significant observation is the reduction of the intensity of the octahedral aluminium located at 2ppm as calcining temperature increased to 873K.

The high loading sample 5.0 mmol/g dried at 573K and 873K also resulted in marked changes (figure 3.119). Like CdF_2-K10 reagents, CuF_2-K10 highly dried sample also resulted in two signals at 69ppm and 62ppm indicating the presence of two different types of tetrahedrally coordinated aluminium. A shoulder at 30 ppm can be clearly seen for the highly dried sample. This shoulder again indicates the presence of 5-coordinated aluminium.

e Friedel-Crafts Alkylation.

The reactivity of CuF_2-K10 reagents towards Friedel-Crafts alkylation is also observed to be dependent on the CuF_2 loading and activation temperature. CuF_2-K10 reagents activated at 573K and 873K were found to promote the model reaction of benzene with benzyl chloride. The reactivity of these reagents varied from one loading to another (table 3.6). The low loading reagent of 1.0 mmol/g activated at 573K is observed to be the most active. This can be seen from the high yield of diphenylmethane. As the activation temperature increased to 873K, the reactivity of the reagent was reduced markedly..

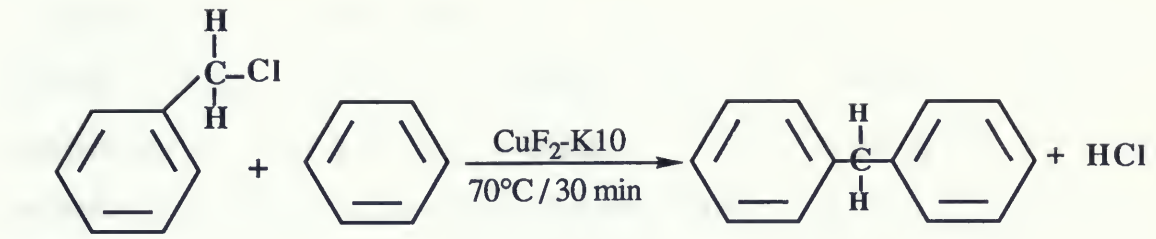

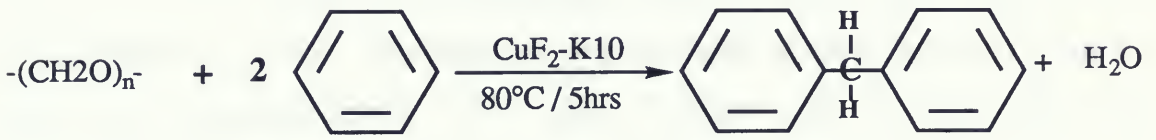

High CuF_2-K10 loadings (3.5,and 5.0 mmol/g) were also found to catalyse the reaction of benzene with benzyl chloride to form diphenylmethane. Calcining temperature does not seem to have any significant effect on the overall reactivity of the high loading reagents. CuF_2-K10 (1.0 mmol/g dried at 573K) reagent was also used to catalyse the reaction of paraformaldehyde with benzene to form diphenylmethane. The measured yield of diphenylmethane obtained was 60% . Generally, CuF_2-K10 resulted in poor reactivity towards Friedel-Crafts alkylation reactions compared to the reagents of CdF_2-K10 and ZnF_2-K10.

f. Discussion.

FT-IR spectroscopic results for CuF_2-K10 reagents differed considerably from those of CdF_2-K10 and ZnF_2-K10. The i.r. spectra of CuF_2-K10 reagents clearly indicates the formation of SiF_6^{2-} complex at low drying temperature. Formation of the SiF_6^{2-} indicates that surface Si-F groups are formed prior to the SiF_6^{2-} complex specially at low CuF_2 loadings (i.e. at monolayer coverage).

To confirm this observation, the infrared spectrum of CuF_2-silica (figure 3.20) showed a strong band at $743cm^{-1}$ which is characteristic of the SiF_6^{2-} complex. Formation of SiF_6^{2-} was not evident from either of the previously studied reagents ZnF_2-K10 or CdF_2-K10.

^{19}F NMR spectroscopic results were also indicative of the presence of Si-F species on the surface of the SiO_2 tetrahedral layer of montmorillonite K10 when coated with CuF_2. This was confirmed by the ^{19}F NMR spectroscopic results of CuF_2-silica, which clearly indicate the presence of physisorbed Si-F species on the surface of silica gel. The absence of the large broadening in the spectra of CuF_2-K10 suggests that surface Al-F groups may be present, but in low concentration. When the highly loaded CuF_2-K10 reagents were dried at 873K, the results from the infrared spectroscopy indicate that the complex SiF_6^{2-} decomposed presumably to gaseous SiF_4 and F^-, which could act as a fluorinating agent.

^{29}Si NMR spectra indicated the presence of two different ^{29}Si environments for CuF_2-K10 reagents. We suspect that since Si atoms are lost from the SiO_2 layer as SiF_4, Al atoms isomorphously replace Si atoms. This isomorphous replacement seems to be partial, since the signal at -97ppm (corresponding to $Si(OSi)_2(OAl)_2$) is not completely resolved from the peak at -107ppm which corresponds to $Si(OSi)_2(OAl)_2$. As was the case for CdF_2-K10,the ^{27}Al NMR spectra of CuF_2-K10 reagents also indicated the presence of two types of tetrahedrally coordinated alumnium. One of these

tetrahedral Al sites presumably is located in the SiO_2 tetrahedral layer and the other, which is resulted from dehydroxylation is located in the aluminium layer.

The reactivity of CuF_2-K10 reagents towards Friedel-Crafts benzylation of benzene with benzyl chloride is observed to be low compared to that of CdF_2-K10 and ZnF_2-K10 reagents. This is probably due to the absence of some Lewis acid sites, or the blocking of Lewis acid sites by SiF_6^{2-}. The prime source for Lewis acidity in CuF_2-K10 may very well be due to the isomprphous replacement of Al^{3+} by Cu^{2+} and of Si^{4+} by Al^{3+}. This type of substitution chemically results in electron deficient centres capable of behaving as Lewis acid sites.

TEXT CONTINUES ON P.98

Table(3.5) ^{19}F m.a.s. NMR chemical shifts for CuF_2-K10 reagents,

LOADING MMOL/G	DRYING TEMP./K	$\delta_{F/PPM}$(a)	REFERENCE
1.00	573	-150*	This work
	873	-151*	This work
3.5	573	-149*	This work
	873	-152*	This work
5.0	573	-142*	This work
	873	-152*	This work

[a] measured from $CFCl_3$.

* Isotropic Chemical Shift (σ_{iso}) calculated from the principal components of the chemical shift tensor.

Table(3.6).Friedel-Crafts benzylation of benzyl chloride using CuF2-K10 reagents[a].

Loading (mmol/g)	Activation Temp./K	benzyl chloride conversion(%)	diphenyl-methane %yield[b]
1.0	573	82	70
	873	40	25
3.5	573	70	60
	873	65	55
5.0	573	70	60
	873	70	65

(a) Reaction refluxed at 70C for 30 mintues.
(b) GC yield ,and product confirmed with 1H NMR 3.93(s,2H),7.2(m,10H).

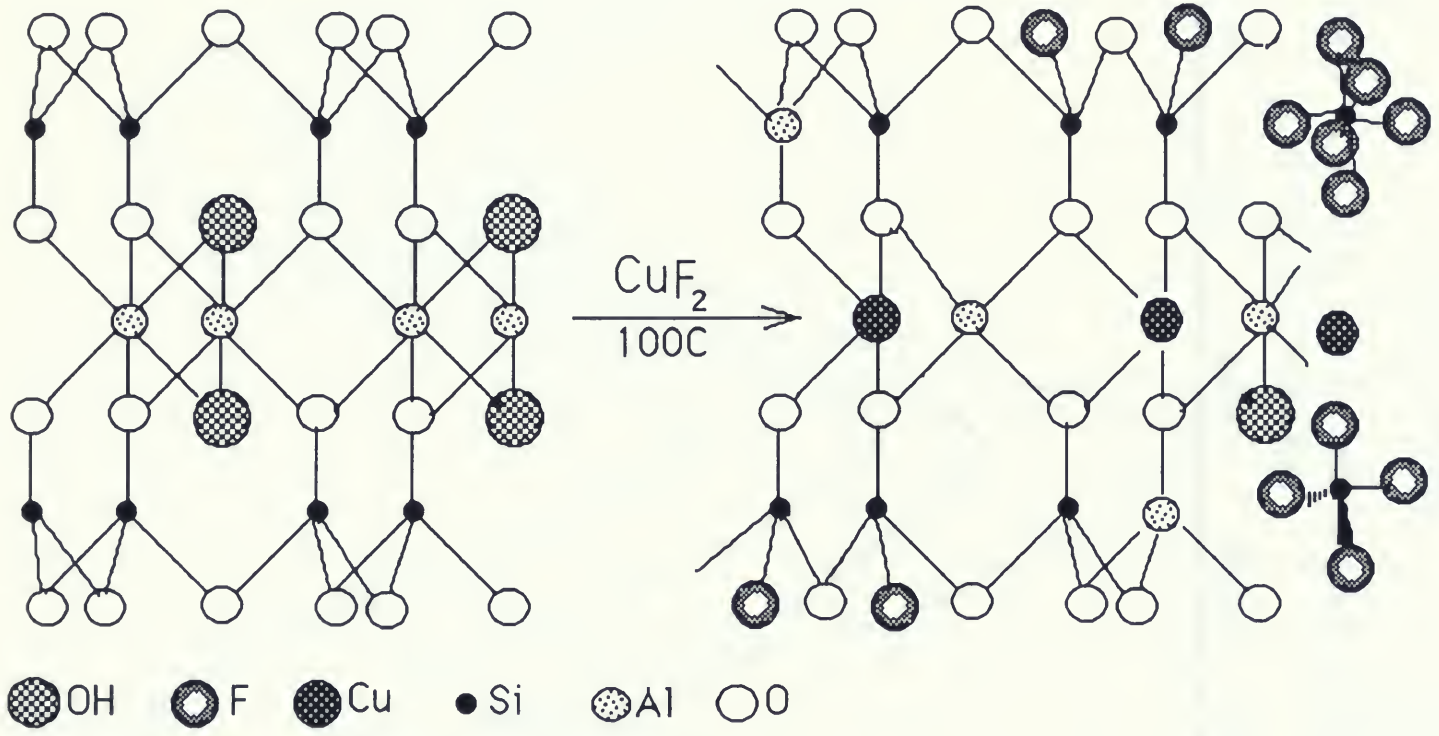

Scheme(3.3)

The layer structure of montmorillonite K10 showing the occurance of isomorphous replacement of Al^{3+} by Cu^{2+} and Si^{4+} by Al^{3+}, and the formation of SiF_6^{2-} and SiF_4.

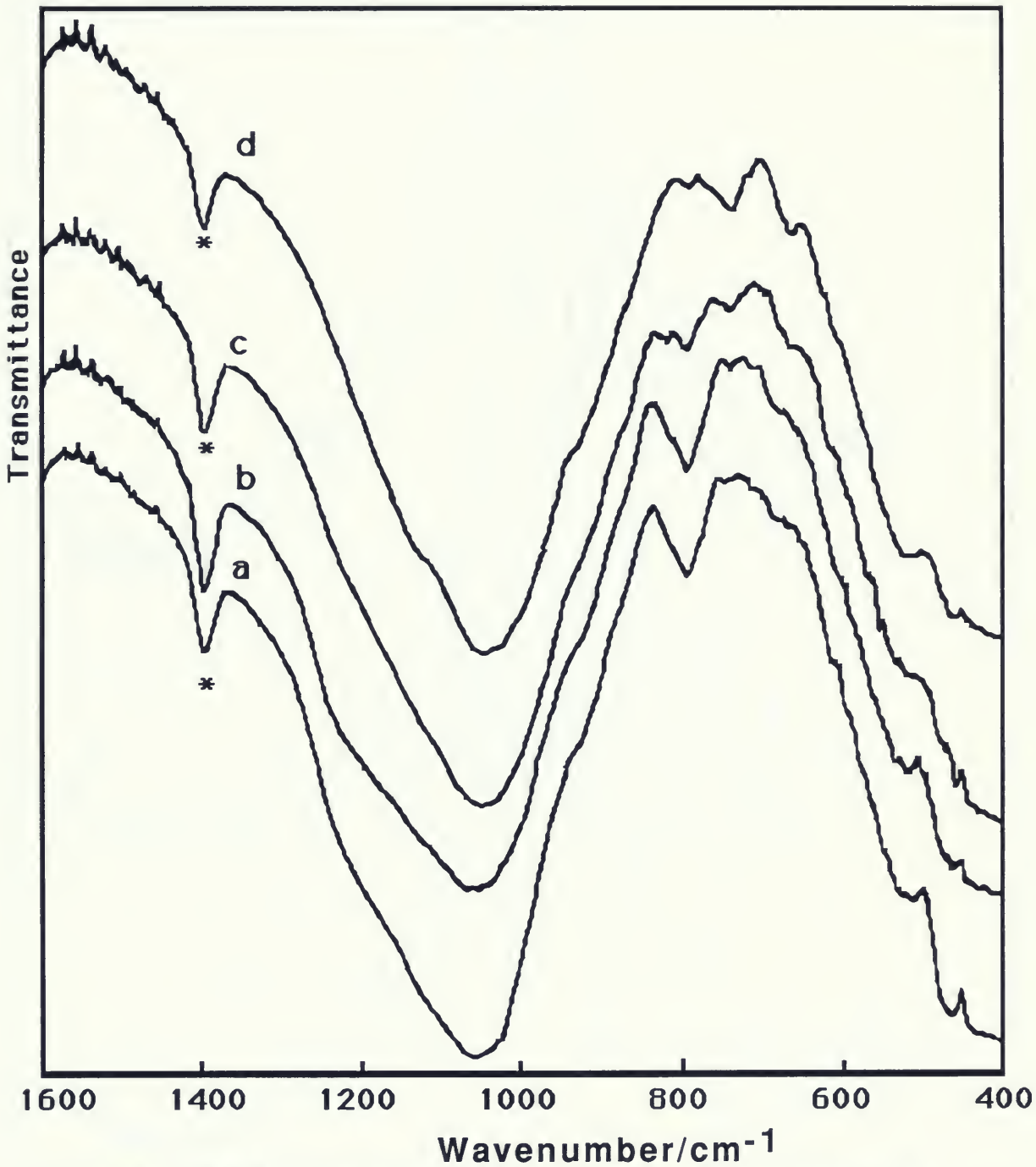

Figure (3.14). Infrared spectra of CuF_2-K10 reagents dried at 573K,

(a) 0.5 mmol/g (b) 1.0 mmol/g

(c) 3.5 mmol/g (d) 5.0 mmol/g

[* indicates impurities]

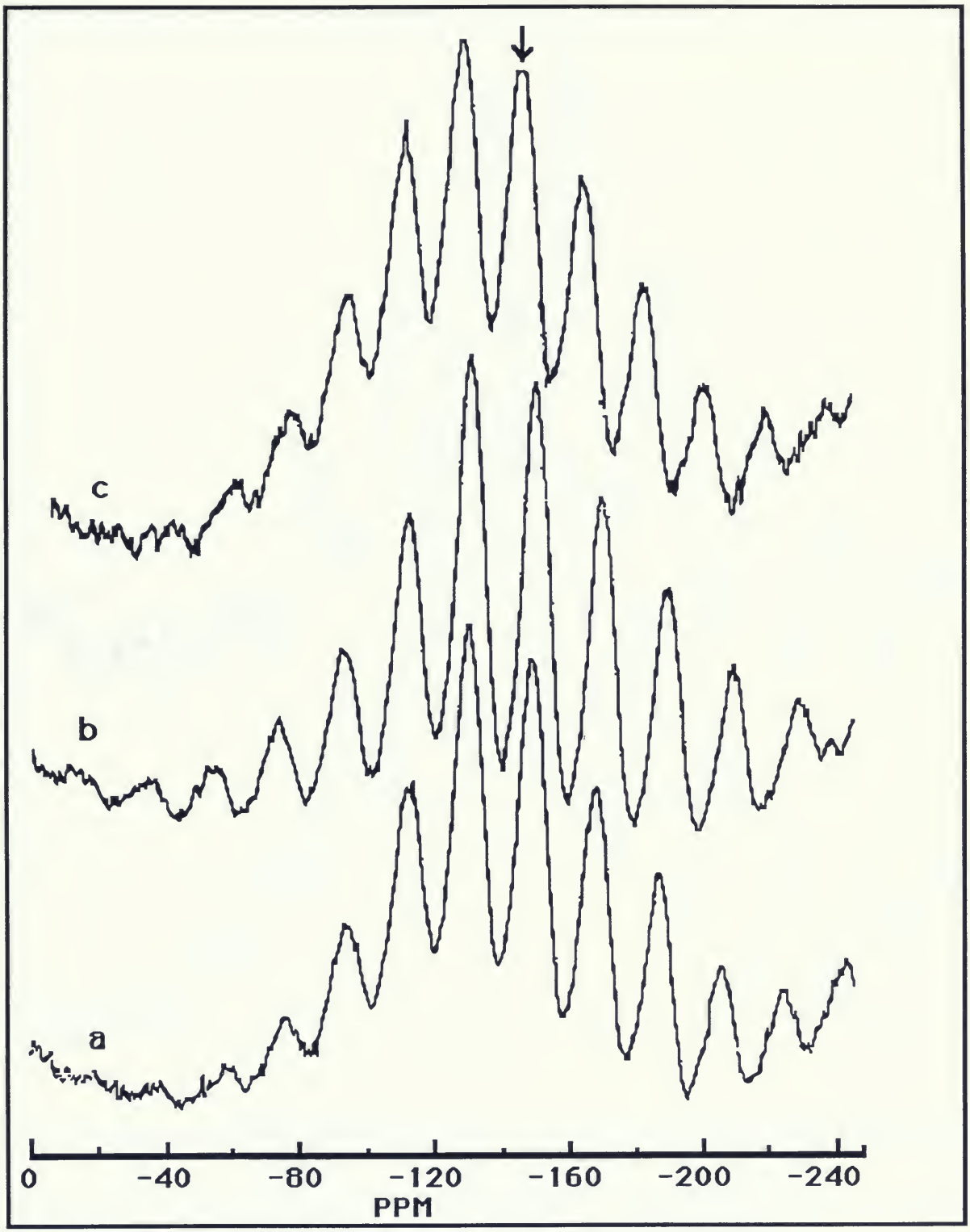

Figure(3.15) ^{19}F MAS NMR spectra of CuF_2-K10 reagents,
(a) 1.0 mmol/g dried at 573K.
(b) 1.0 mmol/g dried at 873K.
(c) 3.5 mmol/g dried at 573K.

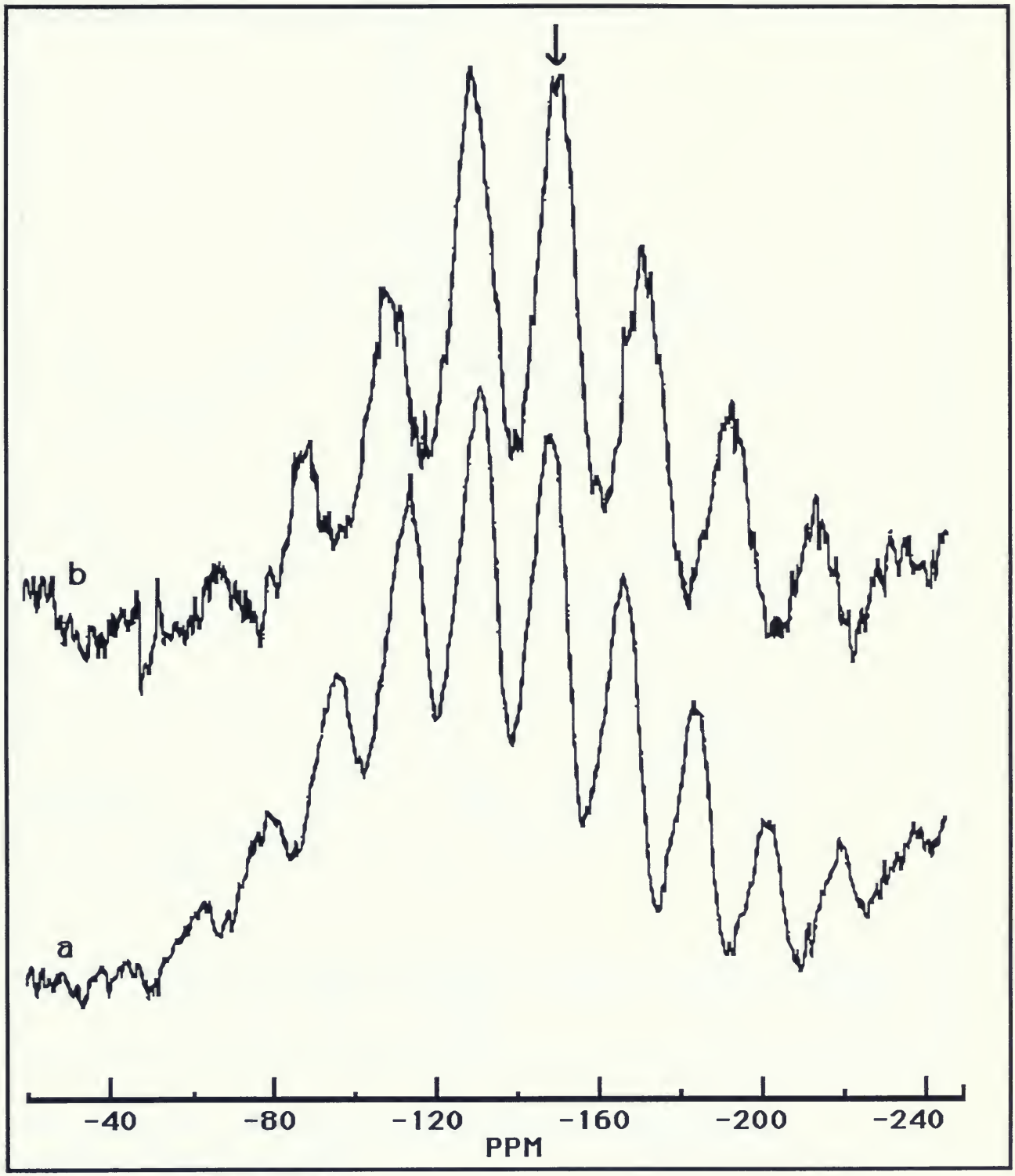

Figure(3.16) ^{19}F MAS NMR spectra of 3.5 mmol/g CuF_2-K10 reagents dried at,
(a) 573K.
(b) 873K.

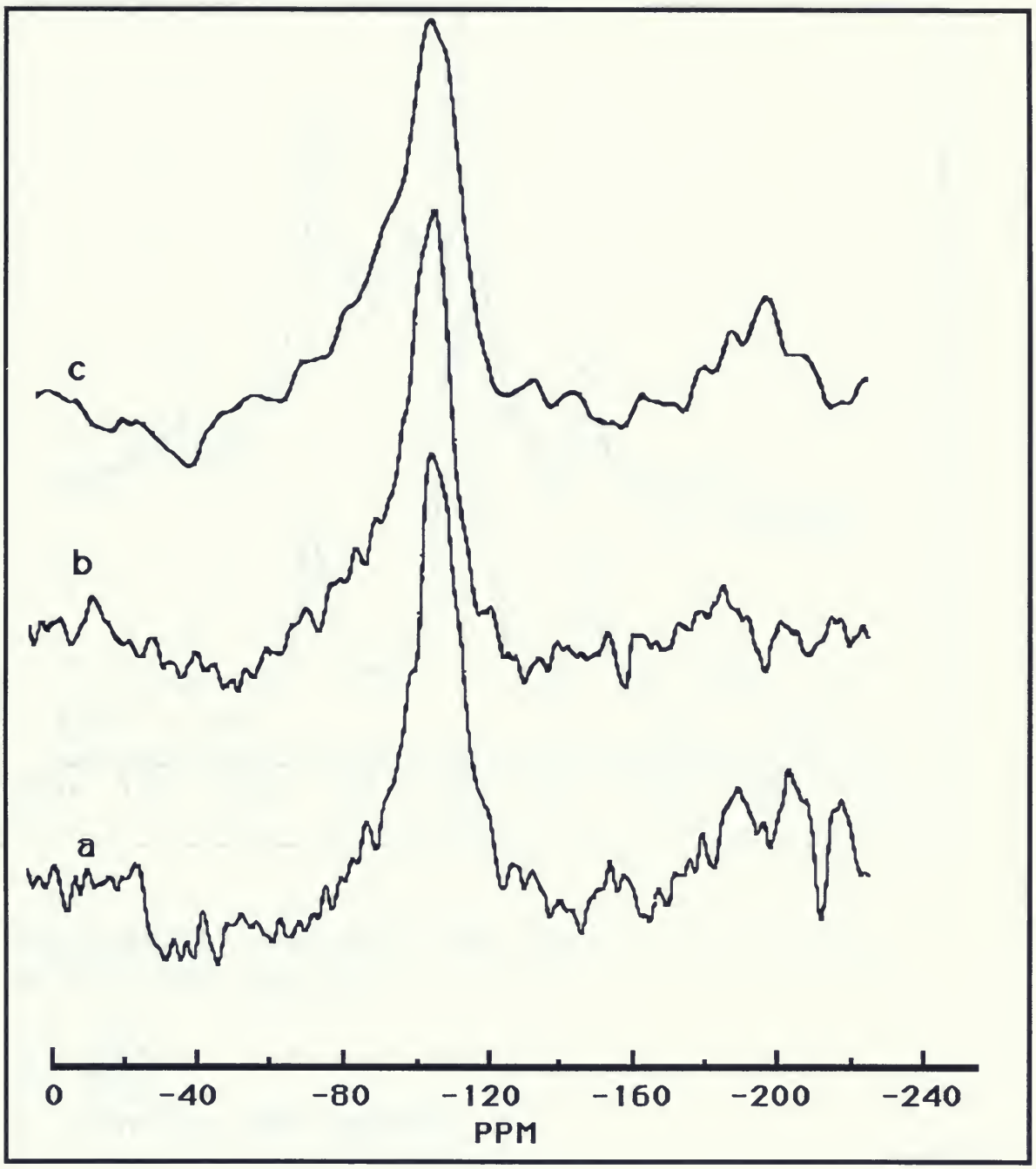

Figure(3.17) ^{29}Si MAS NMR spectra of CuF_2-K10 reagents dried at 573K,

(a) Montmorillonite K10.
(b) 1.0 mmol/g.
(c) 3.5 mmol/g.

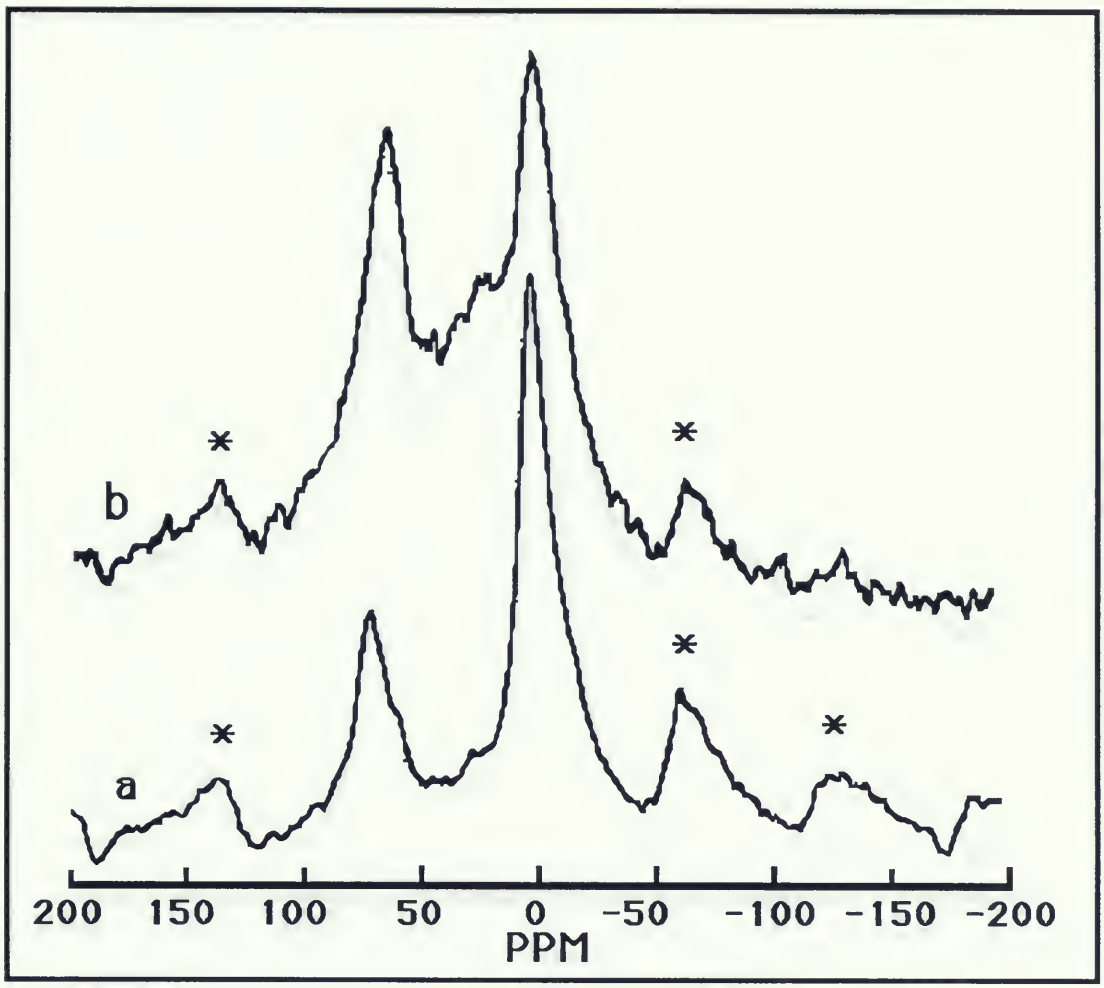

Figure(3.18) ^{27}Al MAS NMR spectra of 1.0 mmol/g of CuF_2-K10 dried at,

(a) 573K.
(b) 873K.
[* spinning side bands]

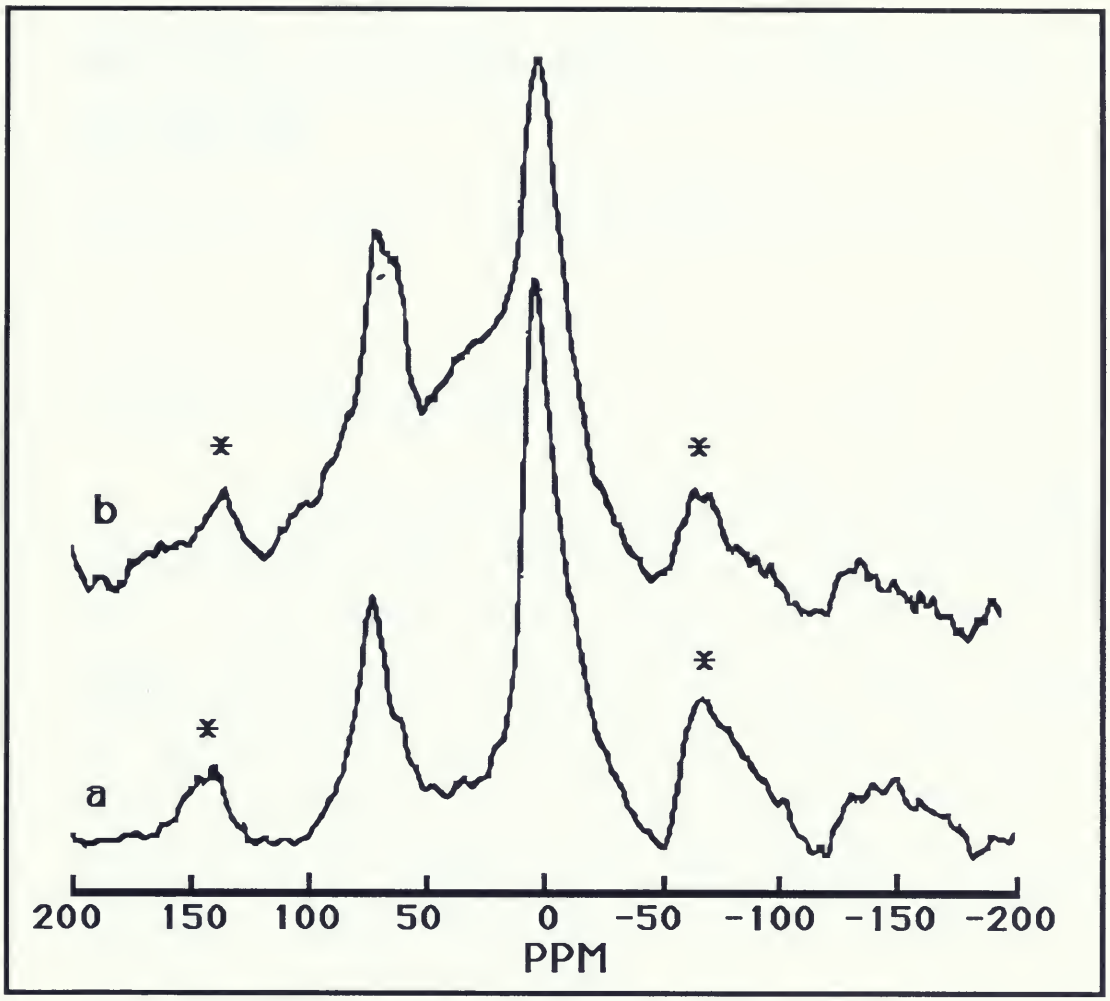

Figure(3.19) ^{27}Al **MAS NMR spectra of 5.0 mmol/g of** CuF_2**-K10 dried at,**

(a) 573.
(B) 873.
[* spinning side bands]

III-4. MF_2 supported silica gel (MF_2-silica) (M=Cu, Zn, and Cd)

(Figures for section III.4 are found between p.p100-102)

a.Infrared Spectroscopy.

Infrared spectra of 5.0 mmol/g of ZnF_2-silica, CdF_2-silica, and CuF_2-silica reagents dried at 373K are shown in figure 3.20. These spectra clearly indicate that CuF2-silica is the only reagent that resulted in a band at 743 cm^{-1}, which corresponds to the complex SiF_6^{2-} (lit. value 740 cm^{-1} [84]). ZnF_2-silica reagent resulted in a shoulder on the side of the band at 802 cm^{-1}, which is probably due to distortion of the SiO_2 tetrahedral structure or the presence of surface Si-F species. The infrared spectrum of CdF_2-silica showed no clear absorption that may indicate presence of surface Si-F species.

b.^{19}F MAS NMR spectroscopy.

^{19}F MAS NMR spectra of the MF_2-silica reagent (figure 3.21) gave similar results to those obtained from i.r. results. CuF_2-silica resulted in a peak at -149 ppm surrounded by asymmetrical spinning side bands, which presumably indicates physisorption of SiF_6^{2-} on the silica surface. ZnF_2-silica resulted in a sharp and intense peak at -124 ppm, which correspond to free F^- ion or probably $F^-H_3O^+$ species (lit. value -125 ppm [93]); in addition it resulted in a weak peak at -149 ppm, which also indicates the presence of the

physisorbed SiF_6^{2-} complex on the silica surface. CdF_2 proved to be unreactive towards silica layer, since the ^{19}F NMR spectra of CdF_2-silica resulted in no evidence of any Si-F species. The only ^{19}F NMR signal was observed is located at -124 ppm, which corresponds to free F^-, or probably $F^-H_3O^+$.

c.Discussion.

The above results are presented to illustrate the reactivity of CdF_2, ZnF_2, and CuF_2 towards the SiO_2 teterahedral layer, since these i.r. results followed a similar pattern observed for those of MF_2-K10 reagents (figure 3.22). These results led to the conclusion that some of these MF_2 such as CuF_2 attack the SiO_2 tetrahedral layer forming Si-F species, and some showed no clear evidence that may indicate formation of any Si-F species. ^{19}F MAS. NMR of the MF_2-silica reagents also indicate that CuF_2 behave differently from the other reagents. All F^- ions of the CuF_2 reagent are consumed in the formation of Si-F species, whereas in the case of the ZnF_2 reagent only some of the F- ions are consumed in the formation of Si-F species, but CdF2 showed the presence of only free F^- ions on the surface of silica gel.

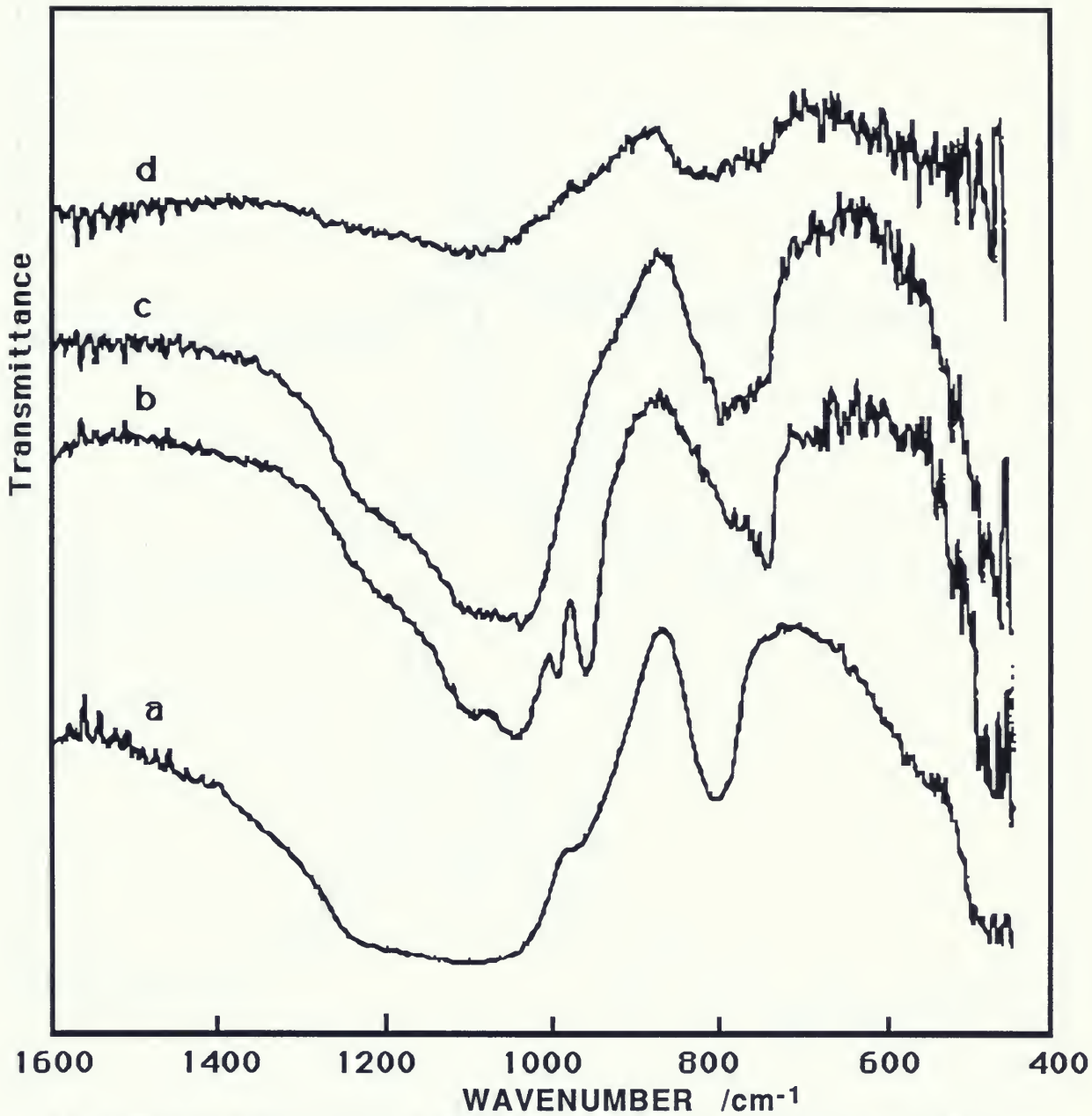

Figure(3.20). Infrared spectra of MF_2-silica reagents dried at 373K,
(a) silica gel
(b) CuF_2-silica
(c) ZnF_2-silica
(d) CdF_2-silica

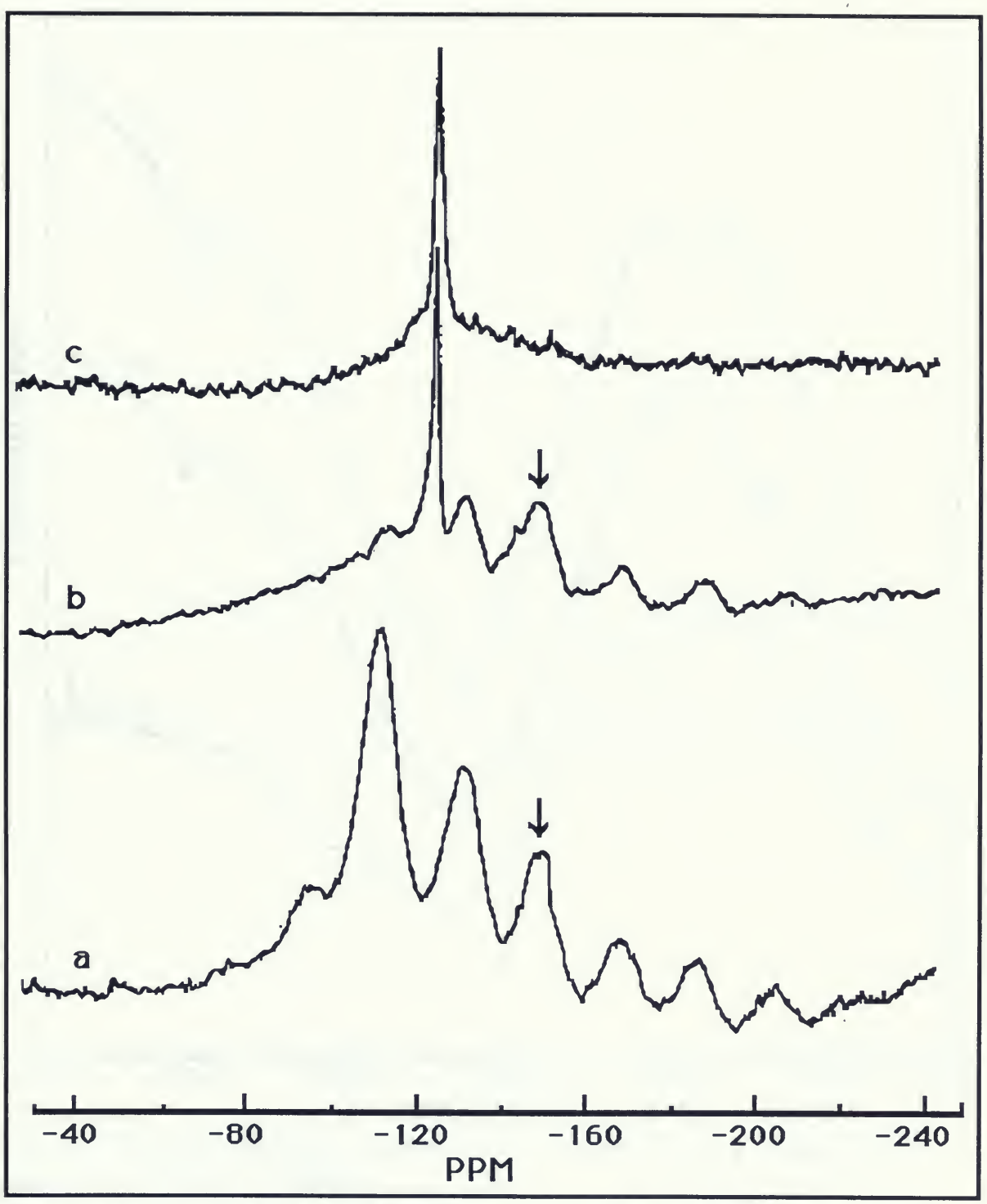

Figure(3.21). ^{19}F **MAS NMR spectra of** MF_2**-silica reagents dried at 373K,**

(a) CuF_2-silica
(b) ZnF_2-silica
(c) CdF_2-silica

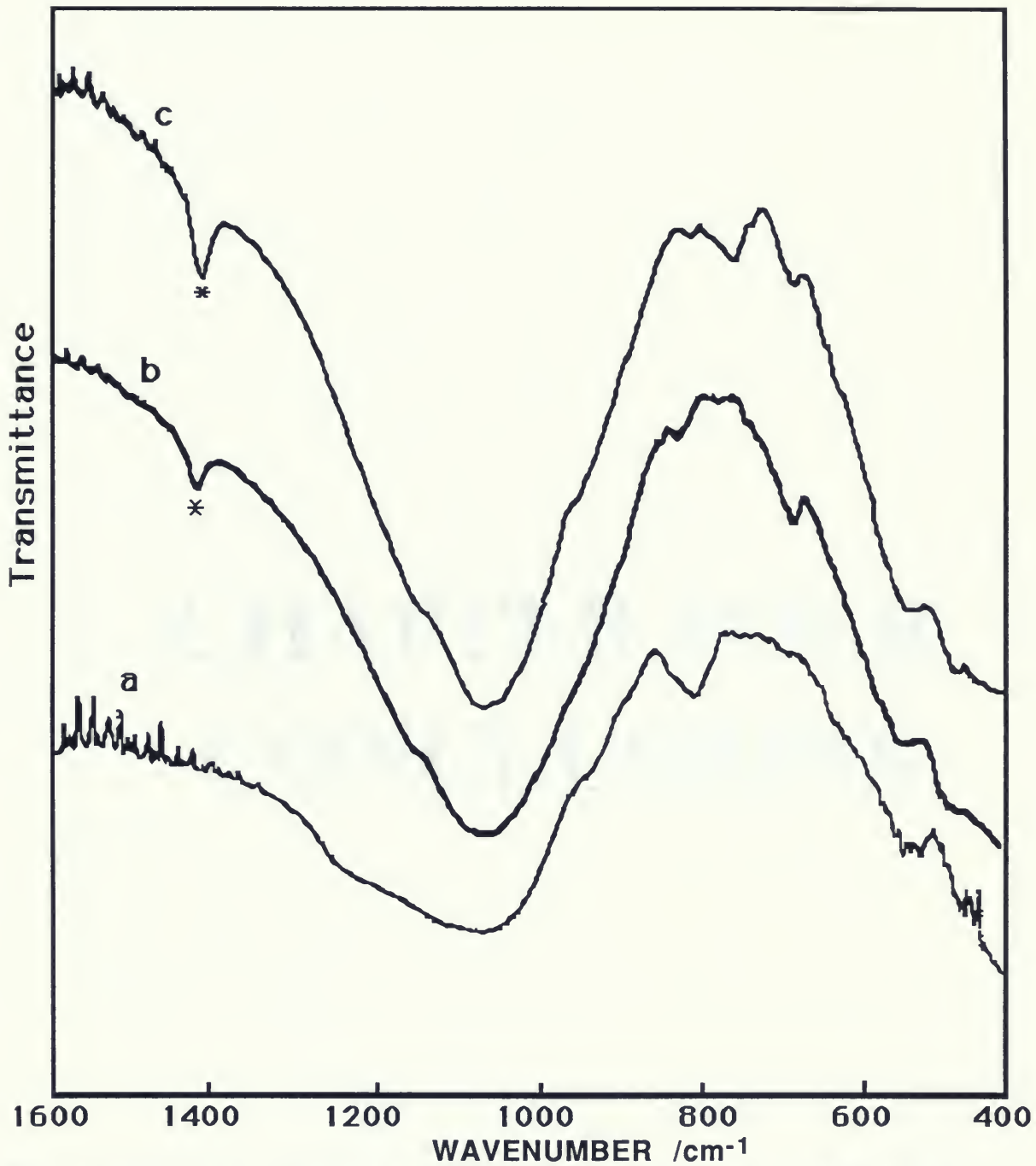

Figure(3.22). Infrared spectra of 5.0 mmol/g of MF_2-K10 reagents dried at 573K,

(a) CdF_2-K10
(b) ZnF_2-K10
(c) CuF_2-K10

CHAPTER FOUR
CONCLUSIONS

IV. Conclusions.

To summarize what has been observed thus far, MF2-K10 reagents were prepared at several loadings and dried over a range of temperatures. As the reagents were analyzed, some differences became apparent. The i.r. spectra of ZnF_2-K10 reagents showed bands at 755 cm-1 and 663 cm-1 which suggest the formation of AlF_4^- and AlF_3 respectively, and the spectra of CdF_2-K10 remained nearly unchanged from the original spectrum of montmorillonite K10. I.r. spectra of CuF_2-K10 showed a band at 743 cm-1 which suggest the formation of the SiF_6^{2-} complex.

^{19}F NMR spectra of low loading ZnF_2-K10 reagent resulted in line shape of asymmetrical spinning side bands with the central peak at -151 ppm which corresponds to either surface Si-F or Al-F groups. The high loading samples showed symmetrical spinning side bands with the centre peak at -153 ppm, and the highly dried samples resulted in very broad lines suggesting the formation of AlF_3. ^{19}F NMR results were similar to those of ZnF_2-K10, except for the high loaded reagents dried at high temperature, which resulted in a signal at -197 ppm suggesting the reformation of CdF_2. Spectra of CuF_2-K10 reagents also showed a signal at -151 ppm corresponding to either surface Si-F or Al-F groups.

^{29}Si m.a.s. NMR spectra of ZnF_2-K10 reagents suggest that as the loading of ZnF_2 increases, further replacement of Si by Al takes place. ^{29}Si NMR spectra of CuF_2-K10 indicated only partial replacement of Si by Al, whereas the spectra of CdF_2-K10 gave no indication of any changes regarding the ^{29}Si environment. ^{27}Al NMR spectra of the high loading highly dried samples of MF_2-K10

reagents show some differences, which appear mainly around the tetrahedral Al signal at 61-69 ppm. ZnF_2-K10 reagent showed a signal intense peak at 61 ppm, whereas CdF_2-K10 and CuF_2-K10 showed an additional signal at 69 ppm. The signal observed at 61 ppm presumably corresponds to the dehydroxylated tetrahedral aluminum in the SiO_2 tetrahedral layer, and the signal at 69 ppm corresponds to hydroxylated tetrahedral aluminum.

The reactivity of MF_2-K10 reagents in the catalysis of Friedel-Crafts benzylation of benzene with benzyl chloride is considerably greater than that of cation exchanged M(II)-K10 [48] and MCl_2-K10 reagents [49] (table 4.2). ZnF_2-K10 was observed to be the most reactive of the series, and CuF_2-K10 showed significantly low reactivity compared to the other MF_2-K10 reagents. It is not fully understood as to what might be the cause for the difference in the strength of the observed Lewis acidity. The only valid possibility we could think of is the newly formed surface Al-F groups, which have been reported to contribute to Lewis acidity [30,54}. The other possibility which cannot be ruled out is the formation of the strongly acidic species HF_2^-, but there is no definite spectroscopic evidence that could rule on the presence of such species,. Recent ^{19}F NMR studies [95,96] reported different values of HF_2^- chemical shifts (range from -167 ppm to -146 ppm), which fall in the range obtained for some of the MF_2-K10 reagents. Table 4.1 compares the values of electronegativities and atomic radii of Al to those of Zn, Cd, and Cu. The Zn atom, whose size and electronegativity appear to be very close to those of the Al atom, replace Al quite extensively. The size of theCu atom also is

comparable to that of Al, but its electronegativity is high, as a result Cu did not replace Al as extensively. The large size of Cd atom is probably the only factor responsible for the lack of replacement of Al by Cd.

Table 4.1. Electronegativities and Atomic Radii of Zn, Al, Cu,and Cd

ELEMENT	ELECTRONEGATIVITY[a]	ATOMIC RADDII[b] [A]
Al	1.61	1.25
Zn	1.65	1.35
Cd	1.69	1.55
Cu	1.90	1.35

[a]Electronegativity values from Pauling (1967)
[b]Atomic Radii from Slater (1964, 1972)

Table 4.2. Friedel-Crafts benzylation of benzene using the following montmorillonite K10 suuported reagents.

Reagent	Alkylator	%Yield	Reference
ZnF_2-K10	A	90	This work
ZnF_2-K10	B	75	This work
CuF_2-K10	A	70	This work
CuF_2-K10	B	65	This work
CdF_2-K10	A	80	This work
CdF_2-K10	B	60	This work
ZnCl2-K10	A	80	49
ZnCl2-K10	B	70	88
CuCl2-K10	A	41	49
CdCl2-K10	A	32	49
Zn(II)-K10	A	60	48
Cu(II)-K10	A	60	48
K10	A	48	48

A benzyl chloride
B paraformaldehyde

References

[1]Laszlo, P. Preparative Chemistry Using Supporting Reagents, Academic Press, Inc. 1987. 288-312, 151-162.

[2]Somorjai, G.A., *Chem.Soc.Rev.*, **13**, 321-349, (1984).

[3]Kemball, C., *Chem.Soc.Rev.*, **13**, 375-392, (1984).

[4]Asseid, F.A., Duke, C.V.A., and Miller, J.M.,*Can.J.Chem.*, **68**,1420-1424 (1990)

[5]Miller, J.M. ,Duke, C.V.A., Clark, J.H.,and Kybett, A.P, *Spectrochim. Acta*, **64A**, 1381-1389, (1990).

[6]Miller, J.M. ,Duke, C.V.A., Clark, J.H.,and Kybett, A.P., *J.Molec.Catal.*, **62**,233-242,(1990).

[7]Evans,J., and Gracey, B.P., *J.Chem.Soc.,Chem.Commun.*,852-853,(1980).

[8]Riseman, S.M., Massoth, F.E.,Dhar, G.M., and Eyring,E.M., *J.Phys.Chem.*, **86**, 1760-1763, (1982).

[9]Ripmeester, J.A., *J.Am.Chem.Soc.*, **105**, 2925-2927, (1983).

[10]Miller, J.C.,and Majda, M., *J.Am.Chem.Soc.*, **107**, 1419-1420, (1985).

[11]Ando, T., Yamawaki, J., Kawate, T., Sumi, S., and Hanafusa,T.,*J.Chem.Soc., Chem.commun.*, 439-440, (1984).

[12]Duke, C.V.A., and Clark, J.H., *J.Org.Chem.*, **50**, 1330-1332, (1985).

[13]Akmertova, N.E.,and Yakobson, G.G., *Synthesis*, 169-184, (1983).

[14]Miller, J.M.,and Clark, J.H.,*J.Am.Chem.Soc.*, **99**, 498-504, (1977).

[15]Miller, J.M.,and Clark, J.H.,*J.Chem.Soc.,Chem.Commun.*, 1318-1319, (1982).

[16]Villemin, D. and Richard, M., *Tet. Lett.*, **25**, 1059, (1984).

[17]Ando, T., Yamawaki, J., Kawate, T., Sumi, S., and Hanafusa, T., *Bull Chem. Soc. Jpn.*, **55**, 2504, (1982).

[18]Ando, T., Brown, S.J., Clark, J.H., Cork, D.G., Hanafusa, T., Ichihara, J., Miller, J.M., and Robertson, M.S., *J. Chem. Soc., Perkin Trans. II,* 1133-1139, (1986).

[19]Fischer, A. and Henderson, G.N., *Synthesis*, 641, (1985).

[20]Wolfe, S., and Ingold, C.F., *J.Am.Chem.Soc.*, **105**, 7755, (1983).

[21]Connel, G., and Dumesic, J.A., *J.Catal.*, 105, 285-298, (1987).

[22]Choudhavy, V.R, *Ind. Eng. Chem. Prod. Res. Dev.*, **16**, 12-22 (1977).

[23]Chapman, I.D. and Hair, M.L., *J. Catal.*, **2**, 145-148, (1963).

[24]Gates, B.C., Katzer, J.B., and Schirif, G.C.A., Chemistry of Catalytic Processes, McGraw-Hill, Inc. (1979).

[25]Aldridge, L.P., Mclaughlin, J.R., and Pope, C.G., *J.Catal.* **30**, 409-416, (1973).

[26]Ghosh, A.K., and Curthoys, G., *J.Chem.Soc., Faraday Trans. 1,* **79**, 805-813, (1983).

[27]Kojima, M., Rautenbach, M.W., and Connor, C.T., *J.Catal.*, **112**, 505-515, (1988).

[28]Kumar, R., and Ratnasamy, P., *J.Catal.*, **121**, 89-98, (1990).

[29]Ghosh, A.K., and Kydd, R.A., *J.Catal.*, **103**, 399-406, (1987).

[30]Becker, K.A, and Kowalak, S., *J.Chem.Soc.,Faraday Trans. 1*, **81**, 1161-1166, (1985).

[31]Goovaerts, F., Vansant, E.F., Philippaerts, J., De Hulsters, P., and Gelan, J., *J.Chem.Soc., Faraday Trans. 1*, **85**, 3675-3685, (1989).

[32]Swartezen-Allen, L., and Matijevic, E., *Chem.Rev.*, **74**, 385, (1974).

[33a]Nemecze, E., Clay Minerals, 1981, Akademiai, Budapest, pp 43-65.

[33b]Foger, K., Catalysis Science and Technology, **6**, 1984. pp. 232-233.

[34]Laszlo, P., *Science*, **235**, 1473, (1987).

[35]Farmer, V.C., and Russell, J.D., *Spectrochimica Acta*, **20**, 1149 (1964).

[36]Brown, I.W.M., Mackenzie, K.J.D., and Meinhold, R.H., *J. Material Sci.*, **22**, 3265-3275 (1987).

[37]McKillop, A. and Young, D.W., *Synthesis*, 401-422, 481-500, (1979).

[38]McKillop, A., and Taylor, .E.C., *endeavour*, **35**, 88-93, (1976).

[39]McKillop, A., Taylor, .E.C., Chaing, C., and White, J.F., *J.Am.Chem.Soc.*,**98**, 6750, (1976).

[40]Laszlo, P. Cornelius, A., and Pennetreau, P., *Syntesis.*, 909-918 (1985).

[41]Laszlo, P, and. Cornelius, A.,Aldrichimica Acta, 21, 97-103, (1988).

[42]Laszlo, P., and Lucchetti, J., *tet.Lett.*,**25**, 1567, 2147, 4387, (1984).

[43]Laszlo,P., Balogh, M., Hermecz, I., and Meszaros, Z., *Helv.Chim.Acta*, **67**, 2270, (1984).

[44]Balogh, M., Hermecz, I., Pennetreau, P., and Gerstmans, A., *J.Org.Chem.*,**55**, 6198, (1990).

[45]Yamawaki, J., and Ando, T., *Chem. Lett.*, 755-758, (1979).

[46]Schwab, G.M., Catalysis Science and Technology, **2**, 1981. pp. 75-76.

[47]Uytterhoeven, B.,Chistner, L.G., and Hall, W.K., *J.Phys.Chem.*, **69**, 2117, (1965).

[48]Laszlo, P., and Mathy, A., *Helv.Chim.Acta*, **70**, 577, (1987).

[49]Clark, J.H., Kybett, A.P., Macquarrir, D.J., Barlow, S.J., and Landon, P., *J.Chem.Soc.,Chem.Commun.*, 1353, (1989).

[50]Mckeever, W.S.S., and Coyne, L.M., *ACS SYMOSIUM SERIES* ***415***, 13, (1990).

[51]Uytterhoeven, I ,Mortland, M.M., Fripiat, J.J.,and Chaussidon, J., *J.Phys.Chem.*, **67**, 248, (1963).

[52]Fishman, D., Klug, J.T., and Shani, A., *Synthesis*, 137, (1981).

[53]Austermann, R.L., Denley, D.R., Hart, D.W., Himelfarb, P.B., Irwin, R.M., Narayaua, M., Szentirmay, R., Tang, S.C., and Yeates, R.C., *Anal. Chem.,* **59**, 68R-102R (1987).

[54]Scokart, P.O., Selim, S.A., Damon, J.P., and Rouxhet, P.C., *J. Coll. and Interface Sci.,* **70**, 209-222 (1979).

[55]Tennakoon, D.T.B., Thomas, J.M., Jones, W., Carpenter, T.A., and Ramdas, S., *J.Chem.Soc., Faraday Trans. 1*, **82**, 545, (1986).

[56]Tennakoon, D.T.B., Thomas, J.M., Jones, W., *J.Chem.Soc., Faraday Trans. 1*, **82**, 3081, (1986).

[57]Sanz, J., and Serratosa, J.M., *J.Am.Chem.Soc.*, **106**, 4790, (1984).

[58]Misra, D.N., Adsorption on and Surface Chemistry of Hydroxyapatite, Plenum Press. 1984. pp. 151-175.

[59]Zamaraev, K.I., Mastikhin, V.M., *Applied Magnetic Resonance* , **1**, 295, (1990).

[60]Mastikhin, V.M., Lapina, O.B., Simakov, A.V., Venlaminov, S.A., and Shubin, A.A., *J.Molec.Catal.*, **50**, 55, (1989).

[61]Clark, J.H., Goodman, E.M., Smith, D.K,. Brown, S.J., and Miller, J.M., *J. Chem Soc. Chem. Commun.,* 657 (1986).

[62]Kreinbrink, A.T., Sazavsky, C.D., Pyrz, J.W., Nelson, D.G.A., and Honkonen, R.S., *J.Mag.Res.*,**88**, 267, (1990).

[63]Duncan, T.M., Douglass, D.C., Csensits, R., and Walker, K.L., *J.Appl.Phys.*, **60**, 130, (1986).

[64]Schlup. J.R., and Vaughan, R.W., *J. Catal.*, **99**, 304-315 (1986).

[65]Schlup. J.R., and Vaughan, R.W., *J. Catal.*, **85**, 311-323 (1984).

[66]Yesinowski, J.P., and Mobley, M.J., *J. Am. Chem. Soc.,* **105**, 6191-6193 (1983).

[67]Dec., S.F., Wind, R.A., and Maciel, G.E., *Macromolecules*, **20**, 2754 (1987).

[68]Andrew, E.R., Bradbury, A., and Eades, R.G., *Nature*, **182**, 1659, (1958).

[69]Lowe,I.J., *Phys.Rev.Lett.*, **2**, 285, (1959).

[70]Lippmaa, E., Magi, M., Samoson, A., Engelhardt, G., and Grimmer, A.R., *J.Am.Chem.Soc.*, **102**, 4889, (1980).

[71]Maciel, G.E.., *Science*, **226**, 282 (1984).

[72a]Fyfe, C.A., Solid State NMR for Chemists, C.F.C. Press. 1983. pp. 139-173.

[72b]Engelhardt, G., and Michel, D. High Resolution Solid State NMR of Silicates and Zeolites, John Wiley and Sons, 1987.

[73]Waugh, J.S., Huber, L.M., and Haeberlent, V., *Phys.Rev.Lett.*, **20**, 180 (1968).

[74]Herzfeld, J. and Berger, A.E., *J. Chem. Phys.*, **73**, 6021-6030 (1980).

[75]Herzfeld, J., Griffin, R.G., and Harberkon, R.A., *J. Am. Chem. Soc.*, **100**, 1296-1298 (1978).

[76]Goovaerts, F., Vansant, E.F., Philippaerts, J., De Hulsters, P., and Gelan, J., *J.Chem.Soc., Faraday Trans. 1*, **85**, 3675, (1989).

[78]Pichat, P., Beaumont, R., and Barthomeuf, D., *J. Chem. Soc. Faraday Trans. I*, **70**, 1402-1407 (1974).

[79]Schaefer, J., and Stejskal, E.O., *J. Am. Chem. Soc.*, **98**, 1031 (1976).

[80]Schaefer, J., Stejskal, E.O., and Buchdahl, R., *Macromolecules*, **10**, 384 (1987).

[81]Miknis, F.P., Bartuska, V.J., and Maciel, G.E., *Am. Lab.*, 19 (1979).

[82]Alemany, L.B., Grant, D.M., Pugmire, R.J., Alger, T.D., and Zilm, K.W., *J.Am.Chem.Soc.*, **105**, 2133, (1983).

[83]Shin, D.B., Crocket, D.S., and Haendler, H.M., *Inorg.Chem.*, **5**, 1927, (1966).

[84]Nakamoto, K., Infrared and Raman Spectra of Inorganic and Coordination Compounds, Wiley-Interscience. 4th ed. 1986.

[85]Kohn, S.C., Dupree, R., Mortuza, M.G., and Henderson, C.B.M., *Amer.Miner.*, **76**, 309-312, (1991).

[86]Vaughan, R.W., Elleman, D.D., Rhim, W.K., and Satcey, L.M., *J.Phys.Chem.*, **57**, 5383, (1972).

[87]Connick, R.E., and Poulson, R.E., *J.Am.Chem.Soc.*, **79**, 5153, (1957).

[88]Clark, J.H., Kybett, A.P., Barlow, S.J., Darby, M.R., Landon, P., and Martin, K., J.Chem.Research (S)., 74-75, (1991).

[89]Manning, D.A.C., Hamilton, D.L., Henderson, C.B.M., and Dempsey, M.J., *Contrib.Mineral.petrol.*, **75**, 257-262, (1980).

[90]Plee, D., Borg, F., Gatineau,L.,and Fripiat, J.J., *J.Am.Chem.Soc.*, **107**, 2362-2369, (1985).

[91]Lippmaa, E., Samoson, A., Alma, N.C.M., and Hays, G.R., *Anal.Chem.*, **56**, 729-733, (1984).

[92]Loewenstein, W., *Amer.Miner.*, **39**, 92, (1954).

[93]Duncan, C.H., and VanWozer, J.R., Compilation of Reported ^{19}F NMR Chemical Shifts, Wiley-Interscience, 1970.

[94]Olah, G.A., Friedel-Crafts and Related Reactions, Interscience Publishers, New York, Vol. 1, 1963.

[95]Hudlicky, M., *J.Fluor.Chem.*, **28**, 461-472, (1985).

[96]Christe, K.O., and Wilson, W.W., *J.Fluor.Chem.*, **46**, 339-342, (1990).

[97]Freeman, E.S., and Hogan, V.D., *Anal. Chem.* **36**, 120, 1964

[98]Scholz, G.,Sauer, J., and Menz, D., *Chem. Phys. lett.*, **156**, 125,1989

[99]Purcell, K., and Kotz, J.C., Inorganic Chemistry, W.B. Saunders Company, London, 1977, p.202.

[100]Guertin, J.P.,and Onyszchuk, M., *Can. J .Chem.*, **41**, 1477, 1963.

Appendix.I

Figure(AI-1). Infrared spectra of ZnF_2-K10 reagents dried at 873K.

Figure(AI-2) ^{19}F MAS NMR spectrum of ZnF_2-K10 reagent compared to spectrum of mixed AlF_6^{3-} and AlF_4^-.

Figure(AI-3) ^{19}F MAS NMR spectrum of ZnF_2-K10 reagent compared to spectrum of mixed AlF_6^{3-} and AlF_4^-.

Figure(AI-4) ^{29}Si MAS NMR spectra of ZnF_2-K10 reagents dried at 873K.

Figure(AI-5) ^{29}Si MAS NMR spectra of montmorillonite K10.

Figure(AI-6) ^{27}Al MAS NMR spectra of 5.0 mmol/g reagents of ZnF_2-K10 dried at.

Figure(AI-7) Infrared spectra of CdF_2-K10 reagents dried at 873K.

Figure(AI-8) Infrared spectra of 6.5 mmol/g ofCdF2- K10 reagents.

Figure(AI-9) ^{19}F MAS NMR spectra of CdF_2-K10 reagents dried at 573K.

Figure(AI-10) ^{19}F MAS NMR spectrum of CdF_2-K10 reagent compared to spectrum of CdF_2.

Figure(AI-11) ^{29}Si MAS NMR spectra of CdF_2-K10 reagents.

Figure(AI-12). Infrared spectra of CuF_2-K10 reagents dried at 873K.

Figure(AI-13) Infrared spectra of 6.5 mmol/g of CuF_2-K10 reagents.

Figure(AI-14) ^{29}Si MAS NMR spectra of CuF_2-K10 reagents dried at 873K.

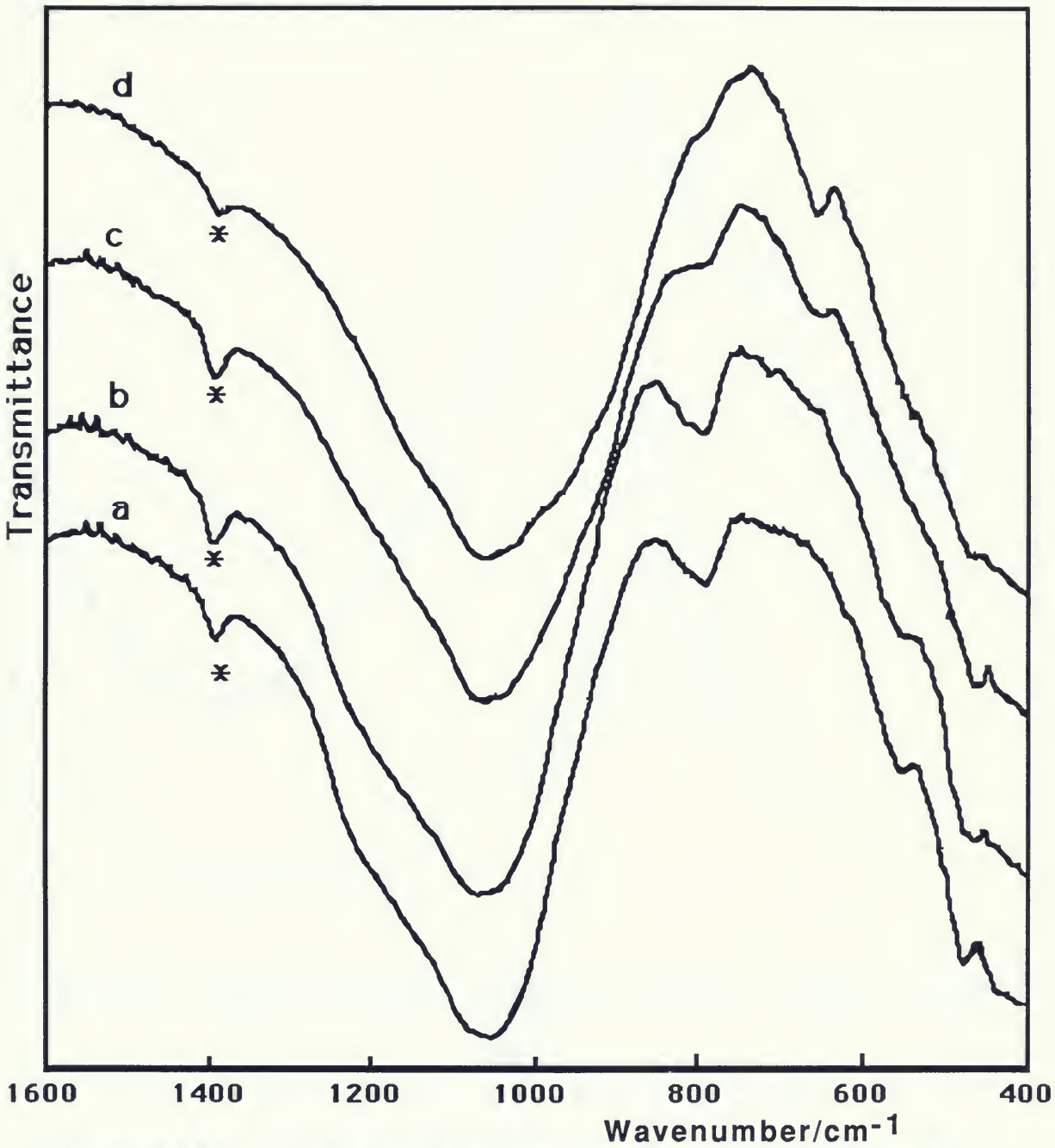

Figure(AI-1). Infrared spectra of ZnF_2-K10 reagents dried at 873K,

(a). Montmorillonite K10 (b). 1.0 mmol/g

(c). 3.5 mmol/g (d). 5.0 mmol/g

(* band due to impurities)

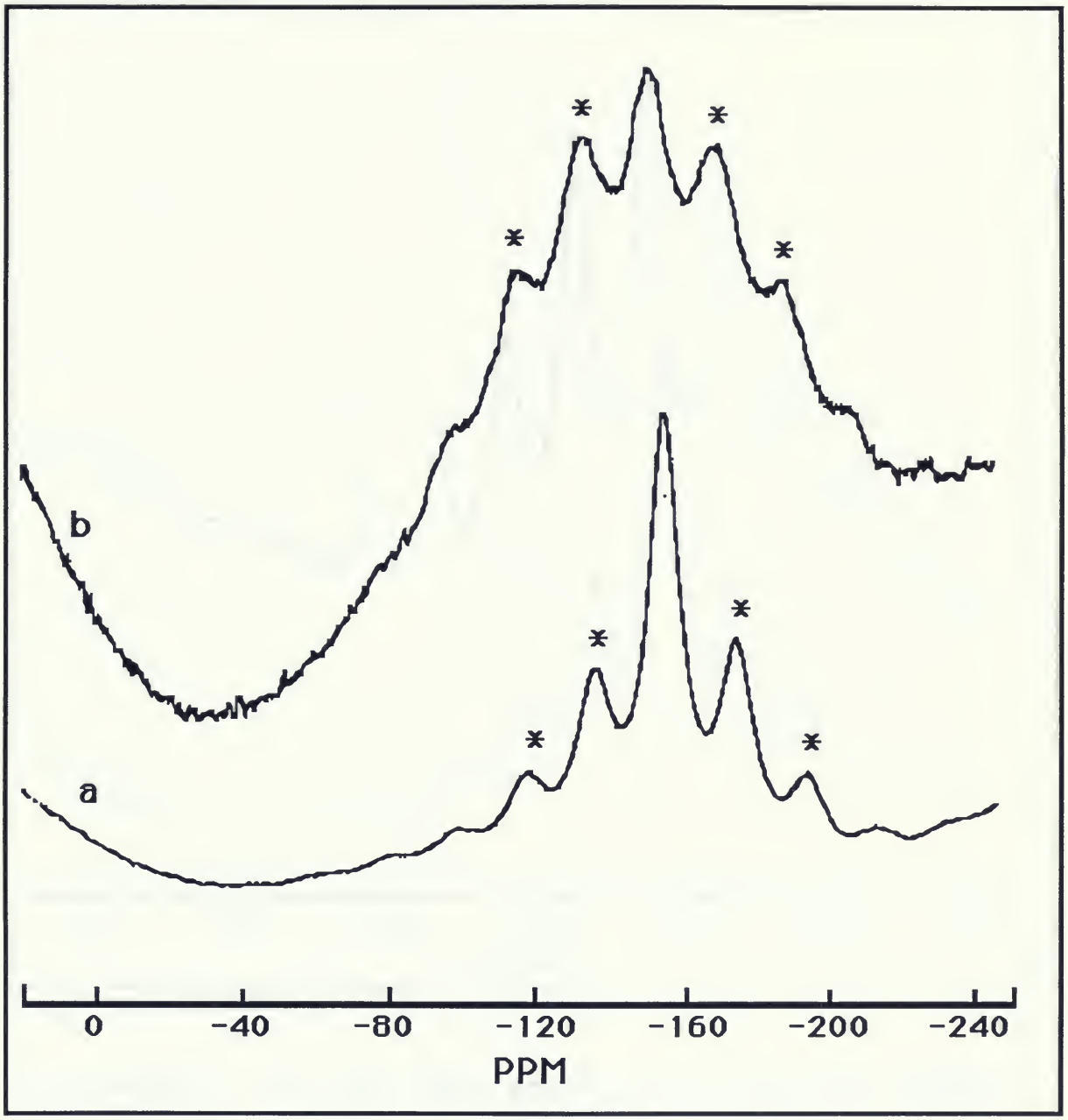

Figure(Al-2) ^{19}F MAS NMR spectrum of ZnF_2-K10 reagent compared to spectrum of mixed AlF_6^{3-} and AlF_4^-,

(a) Mixed AlF_6^{3-} and AlF_4^-.
(b) 5.0 mmol/g of ZnF_2-K10 dried at 873K.
* spinning side bands.

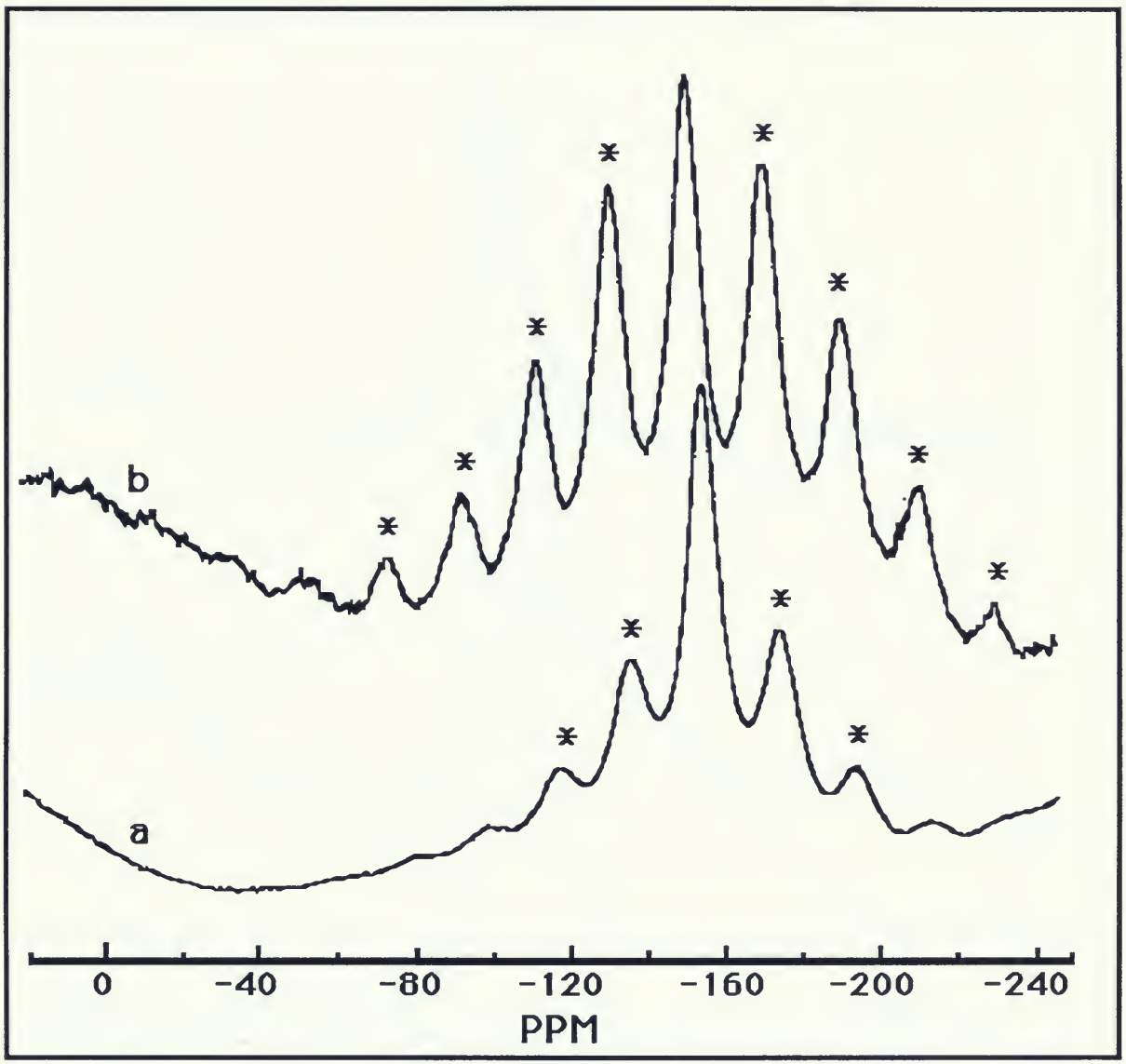

Figure(AI-3) ^{19}F MAS NMR spectrum of ZnF_2-K10 reagent compared to spectrum of mixed AlF_6^{3-} and AlF_4^-,

(a) mixed AlF_6^{3-} and AlF_4^-.
(b) 3.5 mmol/g of ZnF_2-K10 dried at 573K.
*spinning side bands.

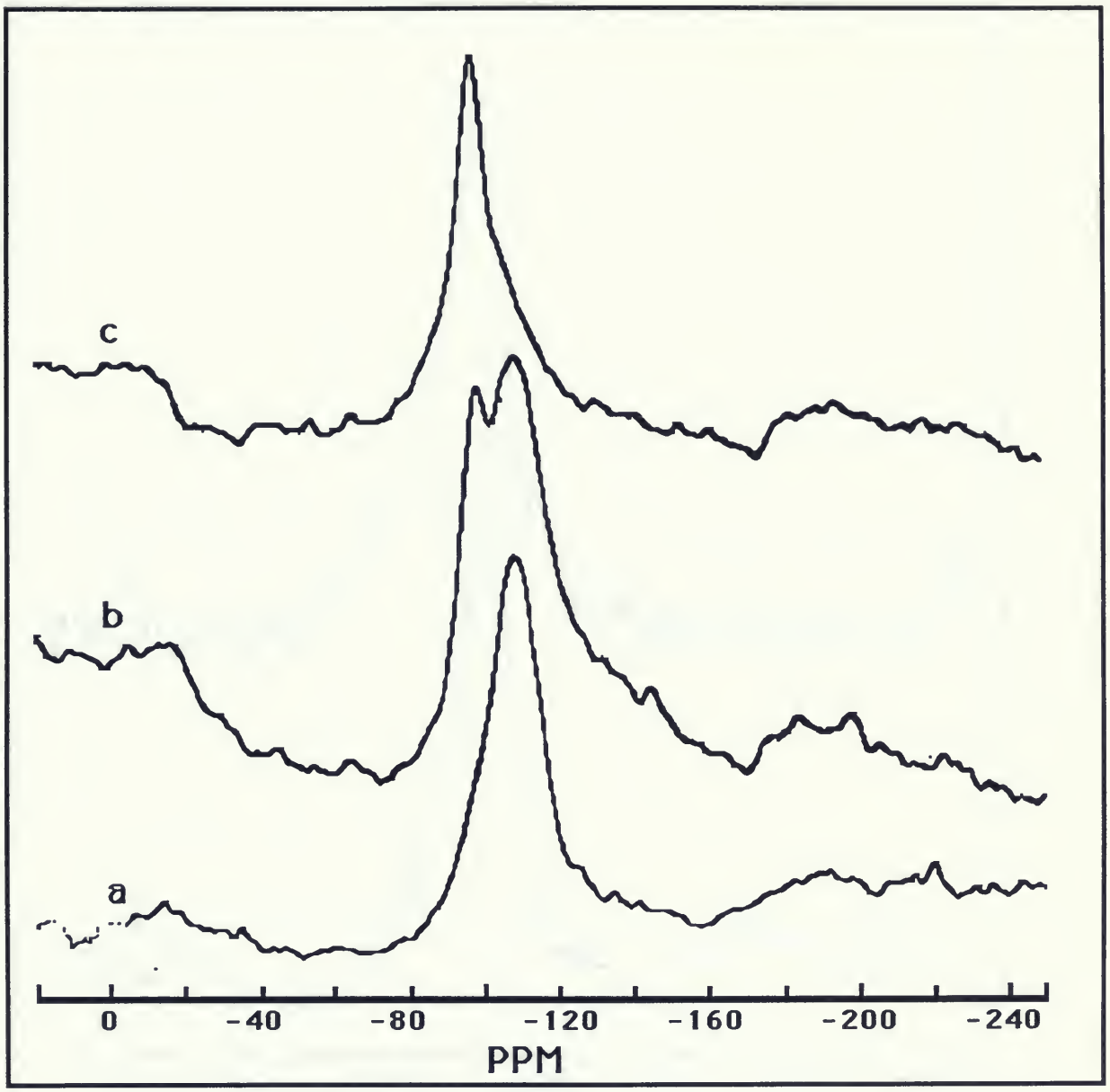

Figure (Al-4) ^{29}Si MAS NMR spectra of ZnF_2-K10 reagents dried at 873K,

(a) 1.0 mmol/g.
(b) 3.5 mmol/g.
(c) 5.0 mmol/g.

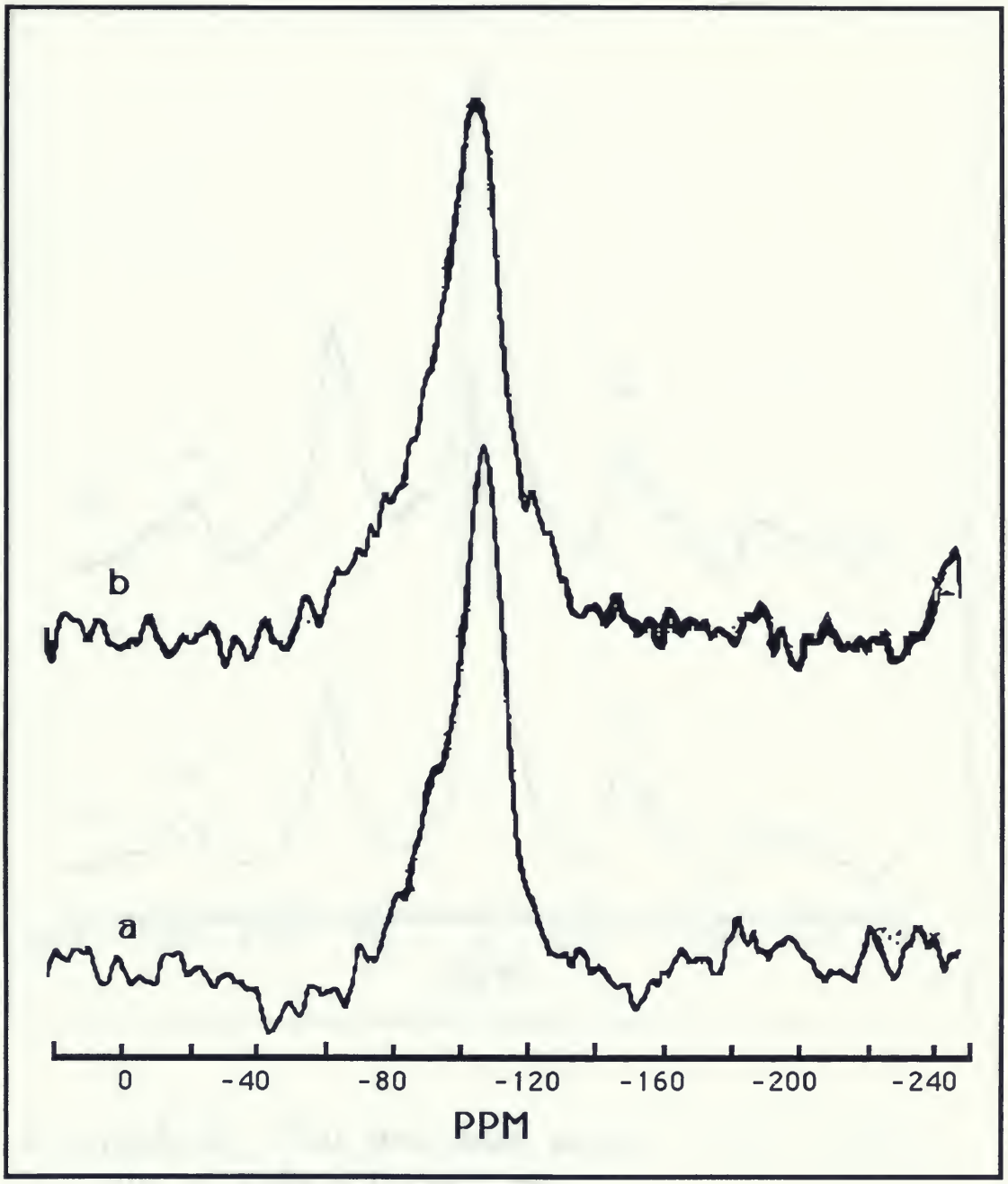

Figure(Al-5) ^{29}Si **MAS NMR spectra of montmorillonite K10,**

(a) Unheated
(b) dried at 573K

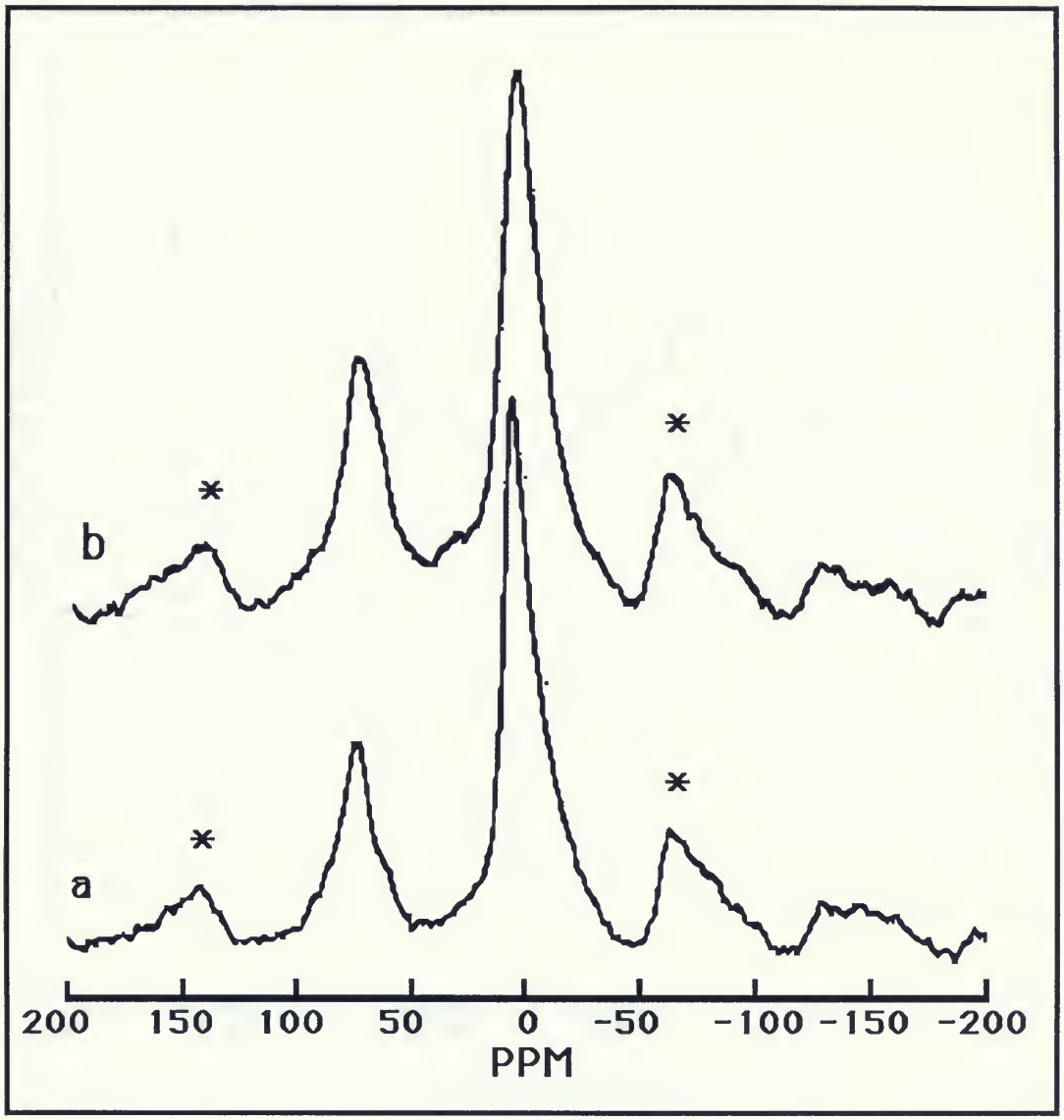

Figure(Al-6) ^{27}**Al MAS NMR spectra of 5.0 mmol/g reagents of ZnF_2-K10 dried at,**

(a) 573K
(b) 873K

***spinning side bands**

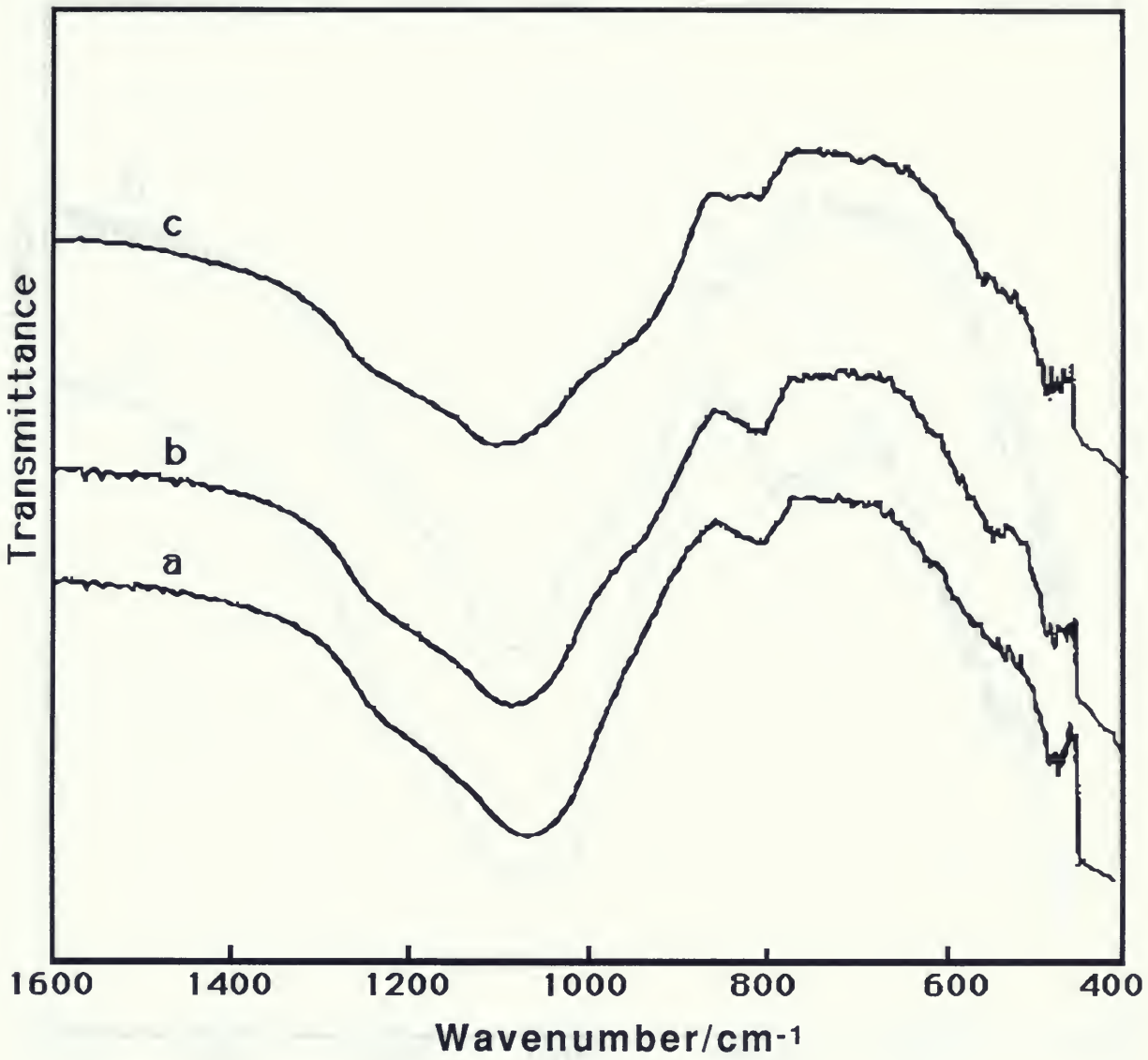

Figure(AI-7) Infrared spectra of CdF_2-K10 reagents dried at 873K,
(a) 1.0 mmol/g
(b) 3.5 mmol/g
(c) 5.0 mmol/g

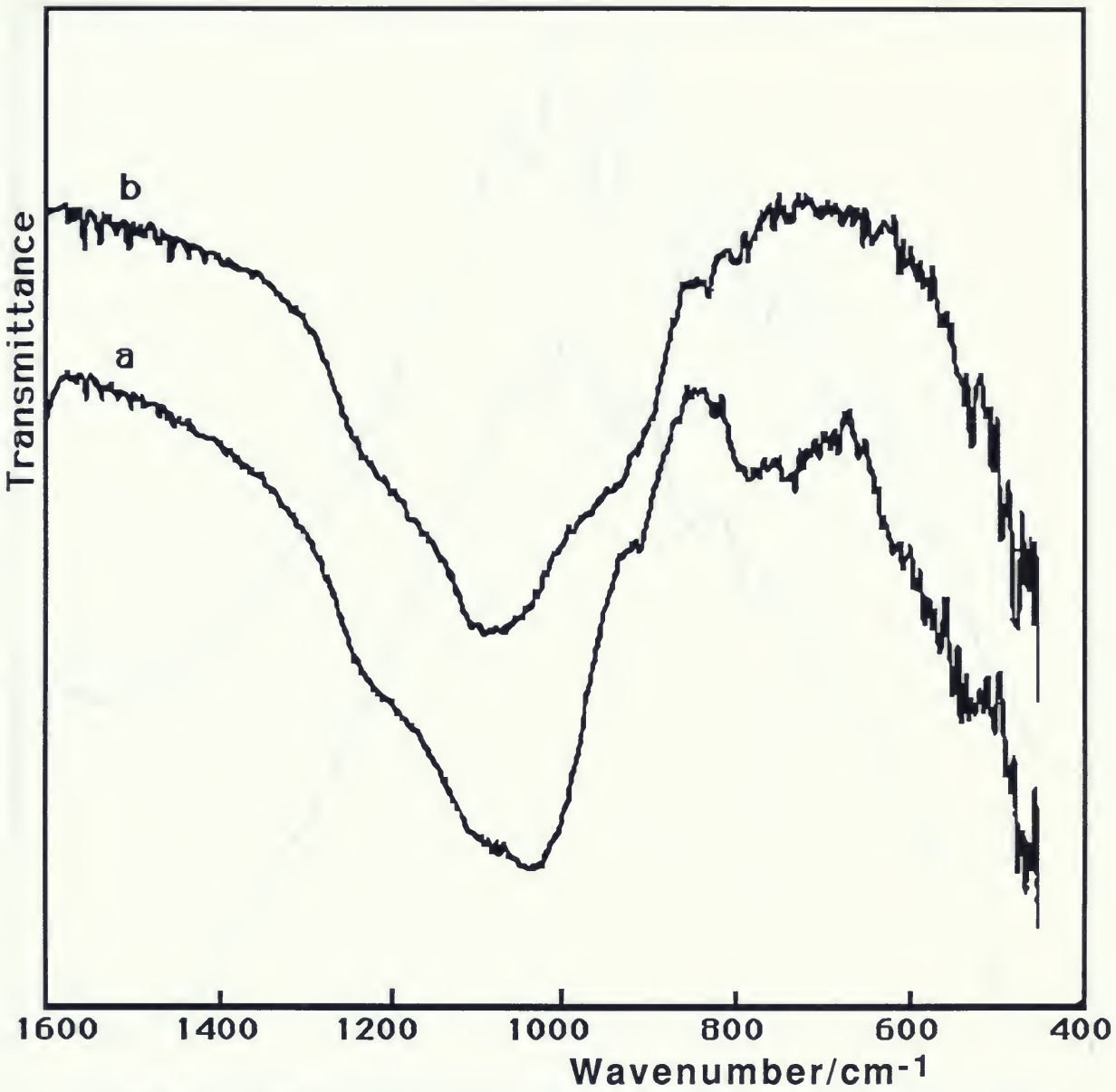

Figure(AI-8) Infrared spectra of 6.5 mmol/g ofCdF2- K10 reagents,

(a) dried at 373K.

(b) dried at 873K.

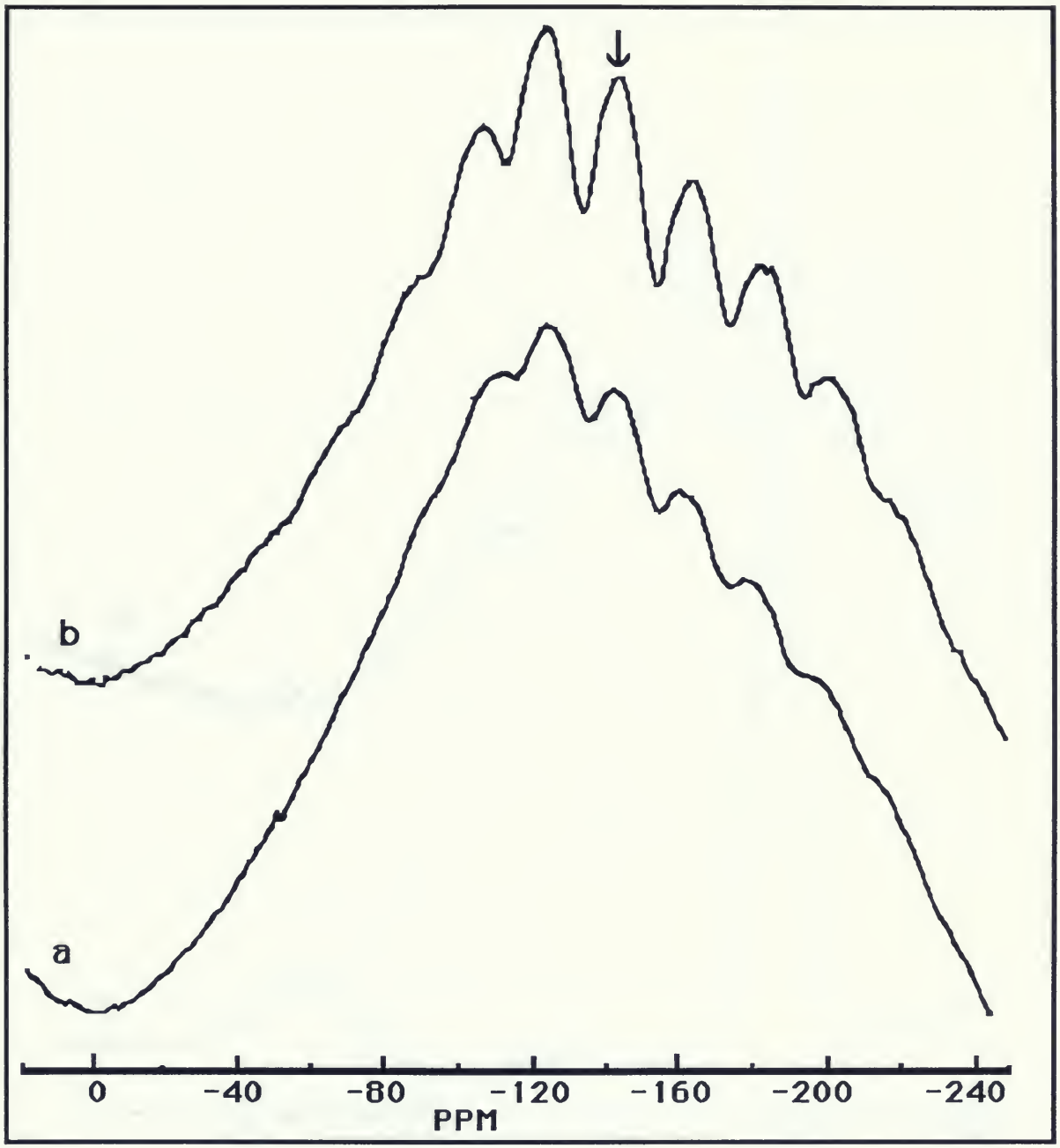

Figure(AI-9) ^{19}F **MAS NMR spectra of** CdF_2**-K10 reagents dried at 573K,**

(a) 3.5 mmol/g.
(b) 5.0 mmol/g.
[arrow points towards central peak]

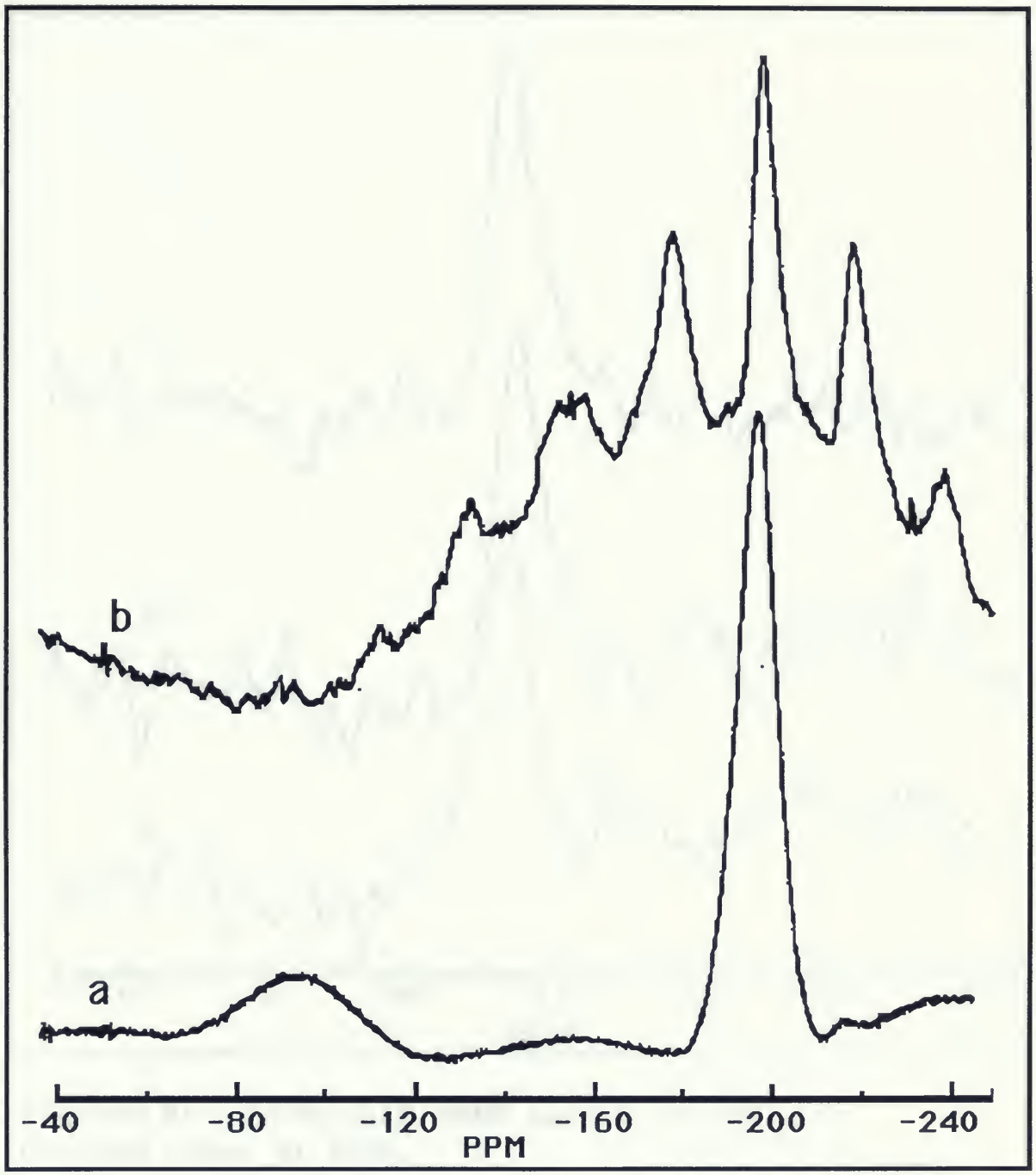

Figure(Al-10) ^{19}F **MAS NMR spectrum of** CdF_2**-K10 reagent compared to the spectrum of** CdF_2**,**

(a) CdF_2
(b) 5.0 mmol/g of CdF_2**-K10 dried at 873K.**

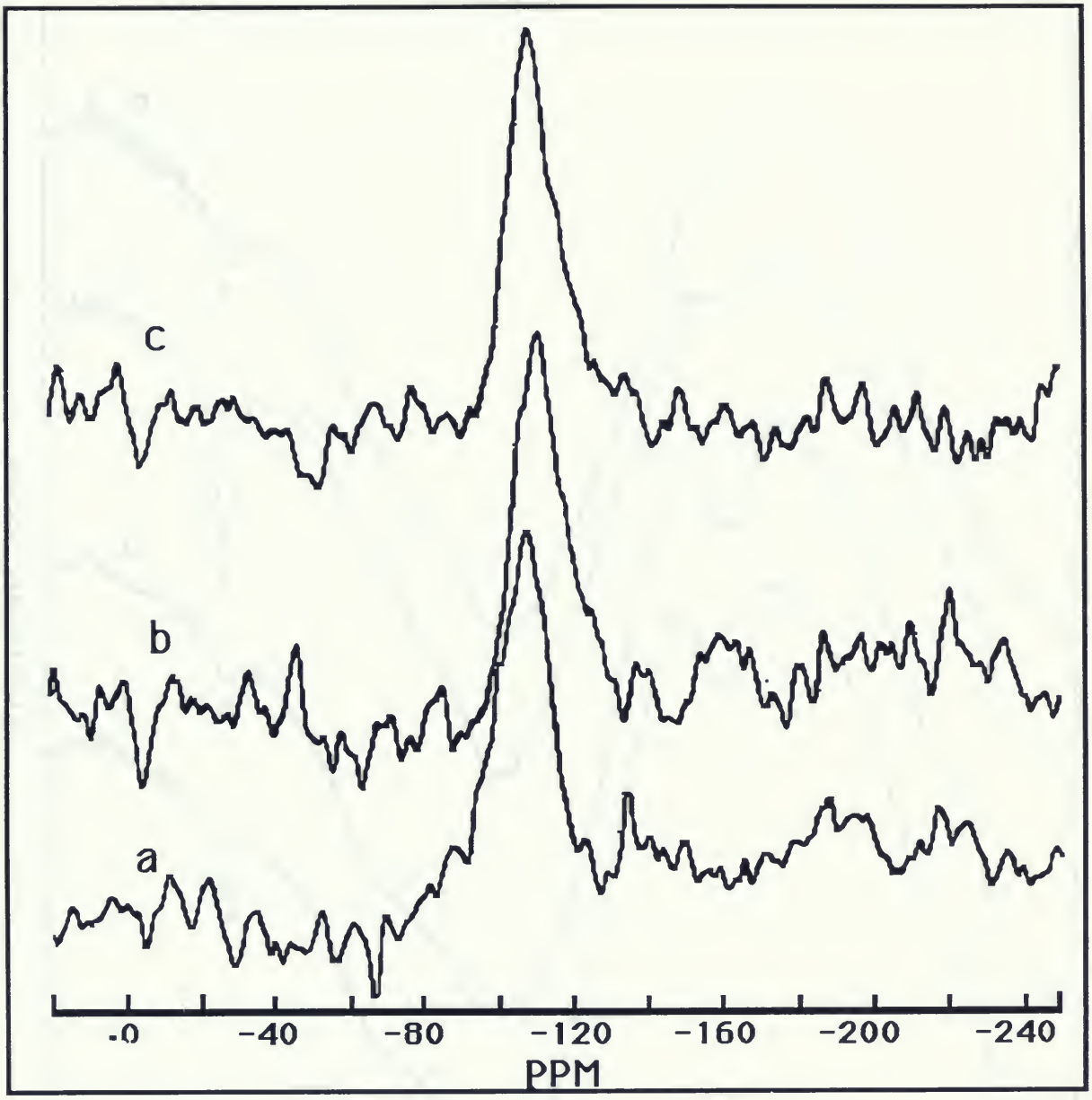

Figure(Al-11)^{29}Si MAS NMR spectra of CdF_2-K10 reagents dried at 873K,

(a) 1.0 mmol/g.
(b) 3.5 mmol/g.
(c) 5.0 mmol/g.

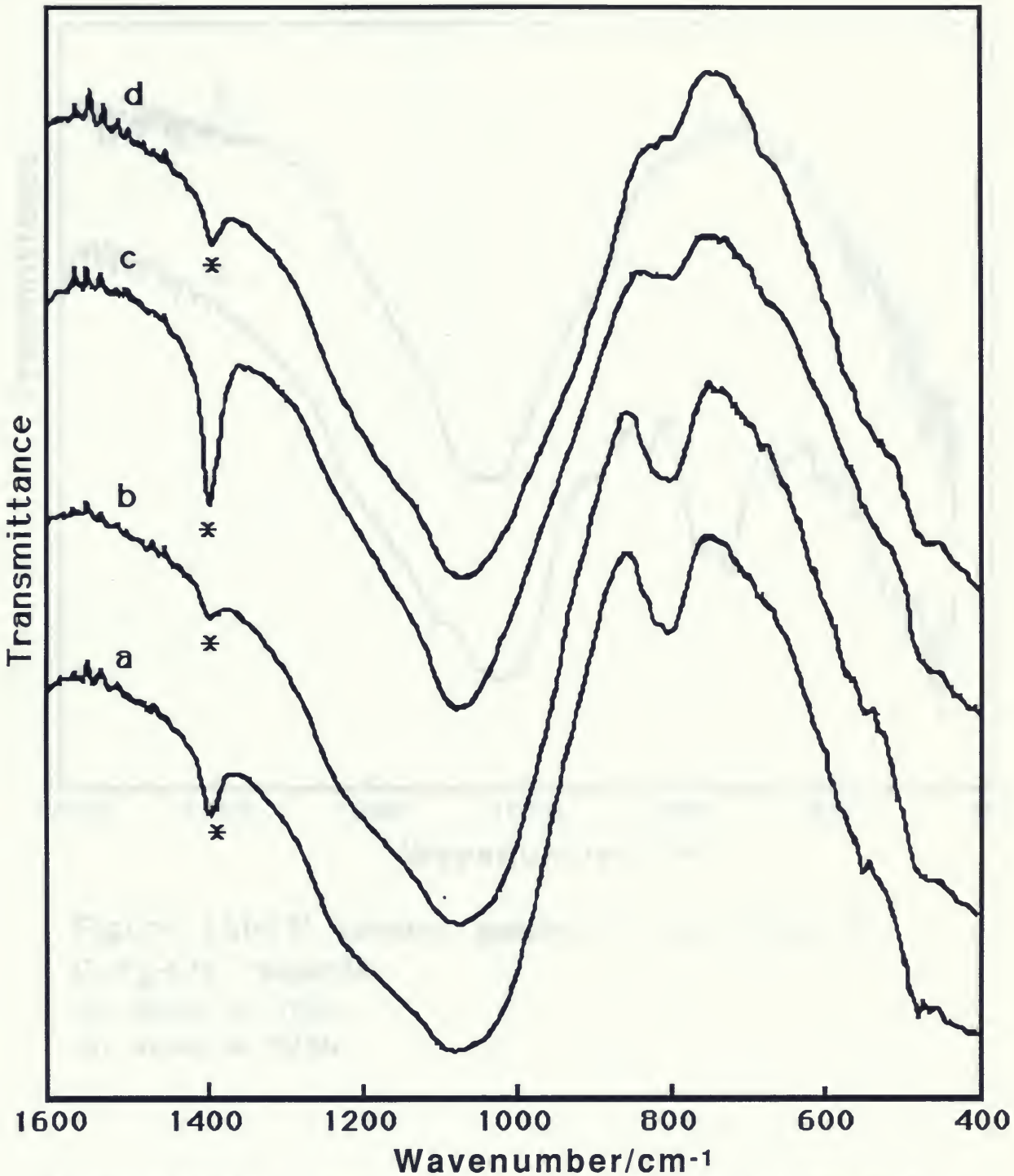

Figure(AI-12). Infrared spectra of CuF_2-K10 reagents dried at 873K,
(a) 0.5 mmol/g (b) 1.0 mmol/g (c)3.5 mmol/g
(c) 5.0 mmol/g (* band due to impurities).

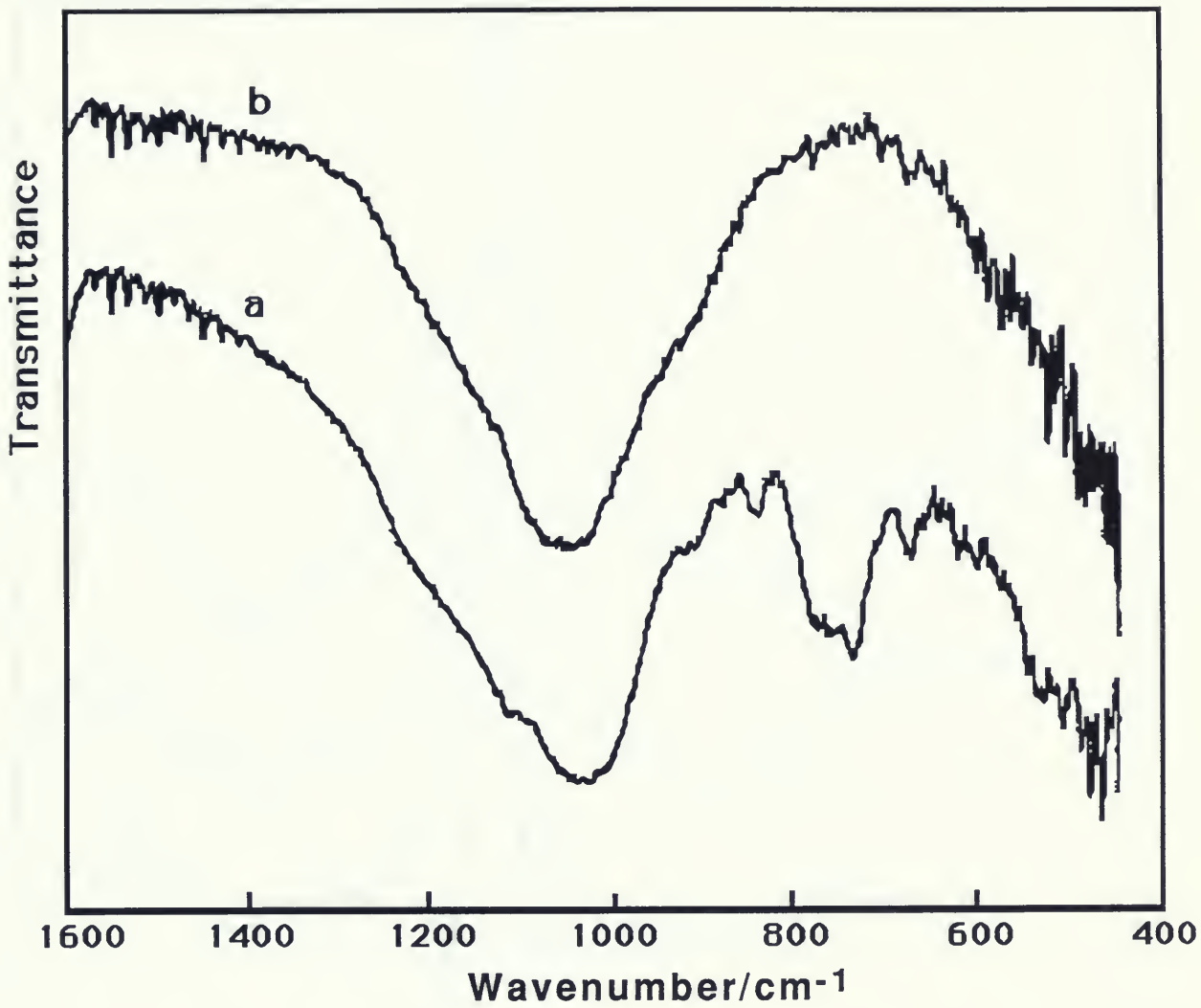

Figure (AI-13) Infrared spectra of 6.5 mmol/g of CuF_2-K10 reagents,
(a) dried at 373K.
(b) dried at 873K

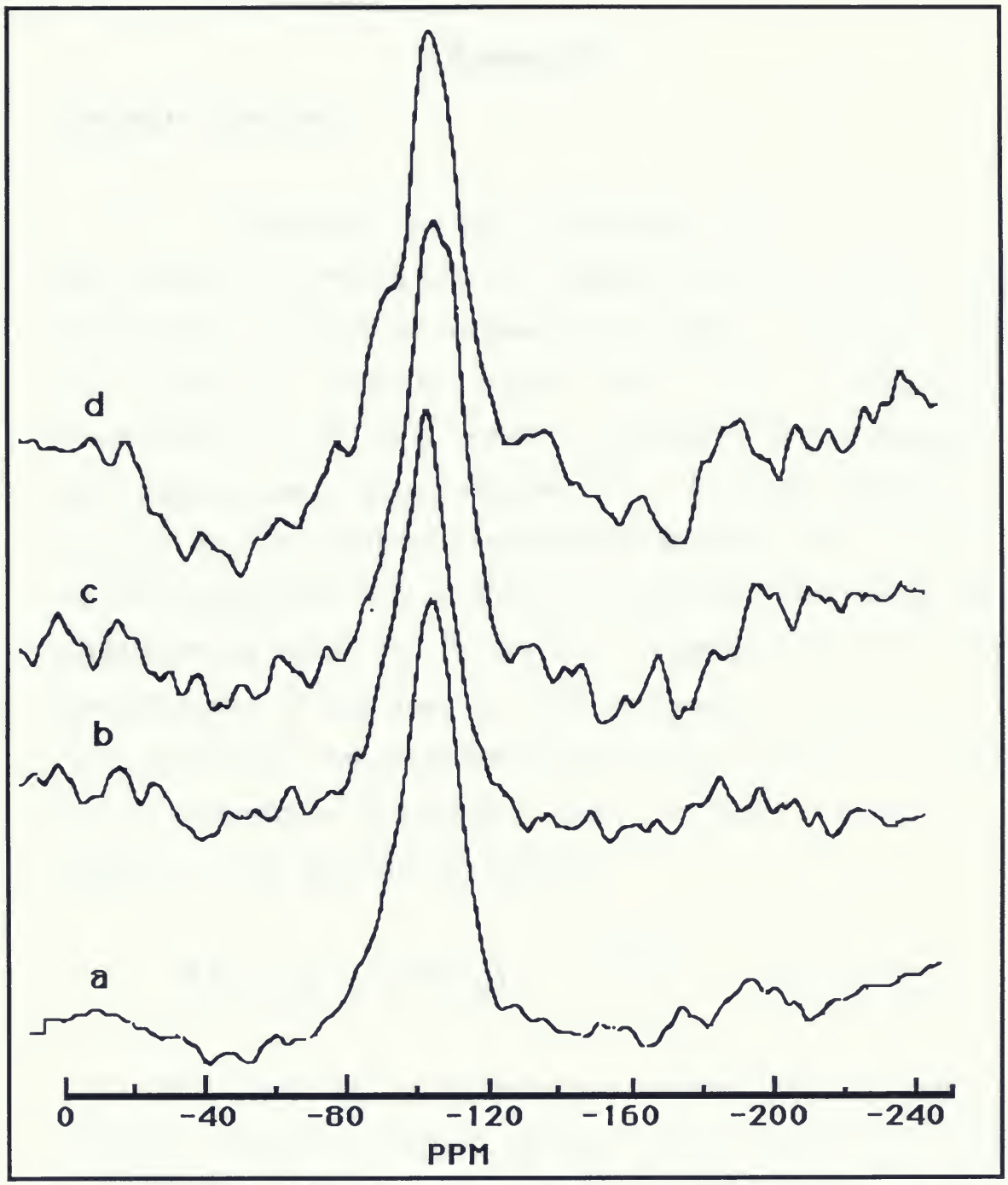

Figure(AI-14) ^{29}Si MAS NMR spectra of CuF_2-K10 reagents dried at 873K.

(a) 0.5 mmol/g
(b) 1.0 mmol/g
(c) 3.5 mmol/g
(d) 5.0 mmol/g

Appendix II

Thermal Analysis

Differential scanning calorimetry (DSC) results for the high loading 5.0 mmol/g MF_2-K10 reagents indicate certain changes taking place as activation temperature increases. The DSC data for this series of reagents (figure AII-1) show a characteristic endotherm at 100-110°C, which is associated with dehydration of the interlayer within montmorillonite K10. A notable difference can be seen for the additional endotherms, at 340°C for CuF_2-K10, at 300°C for CdF_2-K10, and at 400°C for ZnF_2-K10. We believe that the endotherm at 340°C for CuF_2-K10 is associated with the thermal decomposition of the species SiF_6^{2-} to gaseous SiF_4 and possibly CuF_2 or HF [97], and the endotherm at 400°C for ZnF_2-K10 is possibly due to generation of the gaseous $HAlF_4$ component resulting from the reaction of solid AlF_3 and HF gas [98].

$$AlF_3\ (s) + HF\ (g) \xrightarrow{400°C} AlF_4H\ (g)$$

Upon combining the results of i.r. and DSC for high loading (5.0 mmol/g) CuF_2-K10 reagent, we can clearly observe the thermal decomposition of the species SiF_6^{2-}. As it was discussed earlier, the i.r. spectrum of the high loading low temperature dried CuF2-K10 reagent showed a band at 740cm^{-1} due to SiF_6^{2-} complex, then as it is calcined to 600°C this band diminished. A number of attempts were made to trap the gaseous species SiF_4, but the rapid hydrolysis

of the gas by HF and/or residual H_2O to H_2SiF_6 acid [99], prevented the monitoring of pure SiF_4. I.r. spectra (figure AII-2) of the gas trapped in the cell gave very strong bands at 741 cm^{-1} and 480 cm^{-1}, which are presumably due to SiF_6^{2-} of H_2SiF_6 (lit. value 740 cm^{-1} and 483 cm^{-1} ,respectively [84]) (PH analysis of the condensed matter in the cell indicated a strong acidity). An additional weak band at 1072 cm^{-1} corresponds to SiF_4 (lit. value 1070 cm^{-1} [100])

$$2SiF_4\,(g) + 2H_2O(g) \longrightarrow H_2SiF_6 + SiO_2 + 2HF$$

$$SiF_4\,(g) + 2HF\,(g) \longrightarrow H_2SiF_6$$

On pumping out the gas cell the SiF_6^{2-}/H_2SiF_6 bands remained as a deposit on the KBr window of the cell.

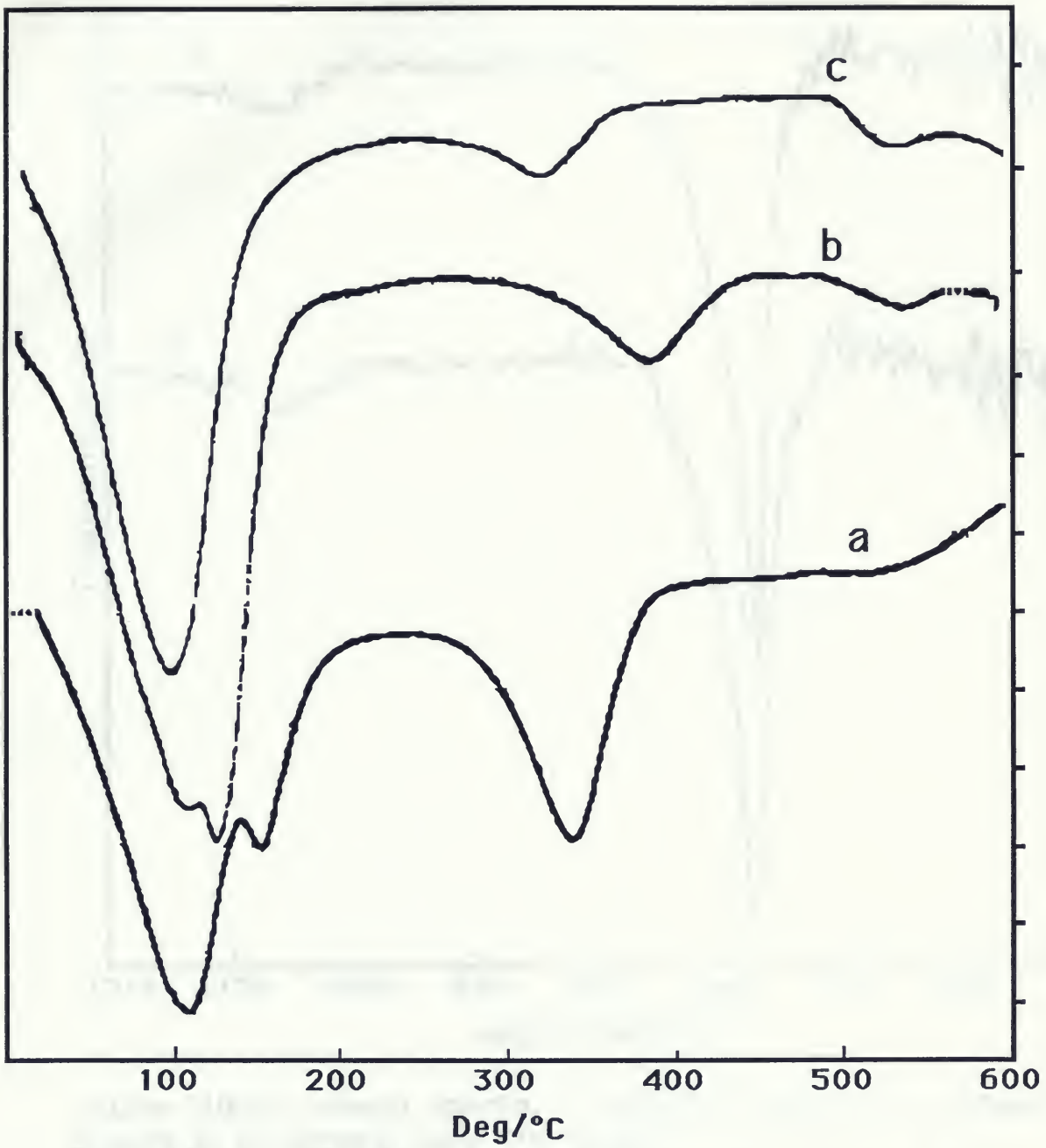

Figure(AII-1) Differential Scanning Calorimetry (DSC) of 5.0 mmol/g
of the reagents

(a) CuF_2-K10
(b) ZnF_2-K10
(c) CdF_2-K10

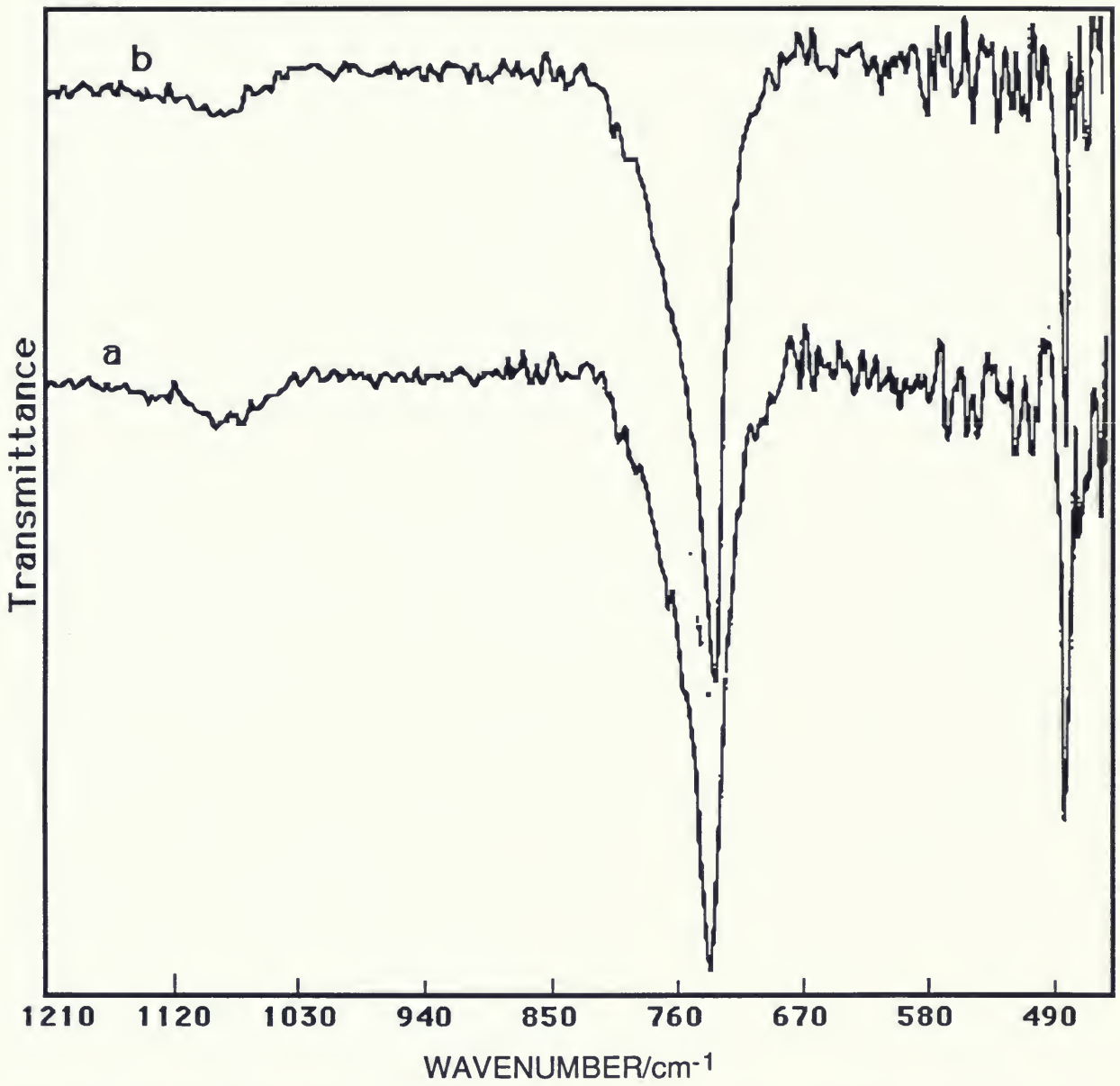

Figure (AII-2). Infrared spectra of collected decomposed gaseous species of 5.0 mmol/g CuF2-K10 reagent.

(a) After 30 mintues of heating the sample.
(b) After 1.0 hour of heating the sample.